The mechanical behaviour of the aortic valve

the mechanical behaviour of the aortic valve

a.a.h.j. sauren

THE MECHANICAL BEHAVIOUR OF THE AORTIC VALVE

THE MECHANICAL BEHAVIOUR OF THE AORTIC VALVE

PROEFSCHRIFT

TER VERKRIJGING VAN DE GRAAD VAN DOCTOR IN DE TECHNISCHE WETENSCHAPPEN AAN DE TECHNISCHE HOGESCHOOL EINDHOVEN, OP GEZAG VAN DE RECTOR MAGNIFICUS, PROF. IR. J. ERKELENS, VOOR EEN COMMISSIE AANGEWEZEN DOOR HET COLLEGE VAN DEKANEN IN HET OPENBAAR TE VERDEDIGEN OP VRIJDAG 19 JUNI 1981 TE 16.00 UUR

DOOR

ALFONS ALOISIUS HENRICUS JOHANNES SAUREN

GEBOREN TE KERKRADE

DISSERTATIE DRUKKERIJ
wibro
HELMOND. TELEFOON 04920-23981

Dit proefschrift is goedgekeurd
door de promotoren:

Prof. Dr. Ir. J. D. Janssen

en

Prof. Dr. R. S. Reneman

Co-promotor Dr. Ir. F. E. Veldpaus

Aan allen die mij hielpen

Aan mijn ouders

Het verschijnen van dit proefschrift werd mede mogelijk gemaakt door steun van de Nederlandse Hartstichting.

CONTENTS

ABSTRACT

In order to gain insight into the factors which govern the mechanical behaviour of the natural aortic valve after closing, a theoretical model has been developed. In developing this model special attention has been paid to aortic valve histology and the mechanical properties of the valve tissues.

Based upon histological observations a valve leaflet is considered as an elastin meshwork reinforced with stiff collagen bundles mainly arranged in one particular direction. The sinus walls consist of smooth muscle cells embedded in a grid of elastin fibres showing no preferred orientation.

From the results of uniaxial tensile experiments the collagen bundles in the leaflets show a stiffening effect and cause a marked anisotropy. The sinus and aortic tissues appear to be much more compliant than the leaflet tissue. The stress-strain curves of the tissues are only slightly sensitive to strain rate. Stress relaxation phenomena were analyzed using a mathematical model. In the leaflets more stress relaxation is found than in the sinus and aortic walls. Predictions based upon the model indicate that on cyclic loading the larger viscous losses have to be expected in the leaflets.

In the theoretical model the influence of the bundle structure on the static, mechanical behaviour of a leaflet in the closed valve was studied. The bundles transmit the pressure load on the membranous parts to the aortic wall. In the presence of the bundles the stresses in the principal directions become nearly the same and equal to the minimum principal stresses as found without bundles. This results in a homogeneous stress distribution without significant shear stresses.

CHAPTER 1

GENERAL INTRODUCTION

1.1. Purpose and scope of the present study

The investigations presented in this study have been performed within the framework of the Eindhoven heart-valve research project[1)] with special reference to the mechanical behaviour of the aortic valve.

The aortic valve is one of the four valves which control the blood flow through the heart[2)]. It is situated at the outlet of the left ventricle and has three leaflets. Behind each leaflet a cavity is present, the so-called sinus of Valsalva. Under normal physiological conditions the closing of the aortic valve starts during the deceleration phase of the aortic volume flow [Bellhouse and Talbot, 1969; Van Steenhoven and Van Dongen, 1979; Van Steenhoven et al., 1981]. A small aortic back flow completes the closure of the valve.

One of the main problems encountered after replacing aortic valves by artificial triple-leaflet-valve prostheses is its limited durability. It is assumed that, apart from tissue degeneration, abnormal hydrodynamical and mechanical factors cause early failure of the prosthesis.

One of the objects of the Eindhoven heart-valve research project is to assess the parameters which govern the stresses in the leaflets of the natural aortic valve. Knowledge of these parameters will contribute to obtain reliable technical specifications for the design and implantation of artificial triple-leaflet-valve prostheses.

The aim of the present study is gaining some insight into the factors which govern the mechanical behaviour of the natural aortic valve after closing. To this end a theoretical model has been

---

1) A description of the purpose and scope of this project is given in Appendix A.

2) An outline of the anatomy of the heart is presented in Appendix B.

developed based upon the extant knowledge about geometry, structural aspects as obtained by histological examination, mechanical material's properties and finally the load to which the valve is exposed. It has been thought the right strategy to restrict the number of parameters taken into account rather than to aim at a sophisticated model, in order to be able to investigate the influence of the factors which are considered to be predominant.

A review of literature reveals that various stress analyses have been performed on theoretical valve models. In nearly all these studies the valve leaflets are considered in the closed position. They range from analytical studies, based upon membrane theory employing simple geometry [Chong et al., 1973; Missirlis and Armeniades, 1976] to sophisticated models using finite-element methods and detailed geometrical data obtained from stereophotogrammetric studies [Cataloglu et al., 1975; Gould et al., 1980]. As to the material's properties, it is mostly linear elasticity, isotropy and homogeneity assumed. Typical of these studies is that the -even macroscopically visible- bundle structure in the leaflets is not explicitly taken into consideration in studying their mechanical behaviour. Moreover, no information could be found on the mechanical significance, if any, of the surrounding regions, i.e. the walls of the sinus cavities and the adjacent portion of the aortic wall. In order to ensure that the relevant features of valve mechanics are studied, these aspects should be investigated before concentrating on detailed modelling of the geometry of the leaflets and nonlinear material properties.

Regarding these considerations, in the present study in particular attention has been paid to the histology of the aortic valve in view of the possible relation to mechanics. In addition, experimental and theoretical investigations of the mechanical properties of the valve tissues were performed. Emphasis was laid on the comparison of the characteristics of the different valve parts (the leaflets as well as the sinus and aortic walls) rather than on a detailed modelling of their properties. For the theoretical modelling of the valve a finite-element model based upon the theory of nonlinear continuum mechanics was developed. Although originally intended to perform static studies of the valve leaflets in the closed configuration, the model can be extended easily to describe the behaviour of the sinus and aortic walls. With respect to the representation of the material's

properties, the model is more or less universal and nonlinear elasticity can be taken into account. An extension to include viscoelastic materials can easily be implemented.

1.2. Contents of the study

In Chapter 2 a description of the anatomy and function of the valve is given. After a description of the valve histology a review of the literature on valve geometry is presented. The load on the valve is briefly discussed and the available data on the mechanical properties of the valve tissue are briefly reviewed. A more detailed survey of material's data is given in Chapter 3, whereas in the same chapter the mathematical model on which the present study is based is discussed. Chapter 4 deals with the constitutive experiments. The results of the model calculations are presented in Chapter 5. Chapter 6 provides the summary and conclusions of the study.

CHAPTER 2
INPUT DATA FOR THE MECHANICAL MODEL OF THE AORTIC VALVE

2.1. *Introduction*

Data on geometry, dimensions, mechanical properties and loads are basic requirements when studying the mechanics of a system. In this chapter a survey is given of the data available on the parameters describing the mechanics of the aortic valve. Before proceeding to this, the anatomy and function of the aortic valve are described in section 2.2. Especially when dealing with a biological system, the structure of its components may provide valuable information on their function and mechanical properties [Wainwright et al., 1976]. In section 2.3 the histology of the aortic valve and its possible relation to valve mechanics is therefore dealt with. The available data on valve geometry and valve loading are presented in sections 2.4 and 2.5, respectively. A review of the literature on the mechanical properties of aortic valve tissue provided a series of experimental investigations. Data on the mathematical description of these properties, however, could not be found in literature. A brief, qualitative description of the results of these experimental studies is given in section 2.6.

2.2. *The anatomy and function of the aortic valve*

The aortic valve, situated at the outlet of the left ventricle, is one of four valves controlling blood flow through the heart (a concise description of the anatomy and physiology of the heart is given in Appendix B). The valve consists of three anatomical entities: three leaflets, three sinus cavities and the aortic ring (fig. 2.1 and 2.2). Two functional areas can be distinguished in each leaflet. The area near the free edge is known as the lunula, thanks to its semilunar shape. When the valve is closed, the outlet orifice of the left ventricle is sealed because the lunulae of adjacent leaflets are

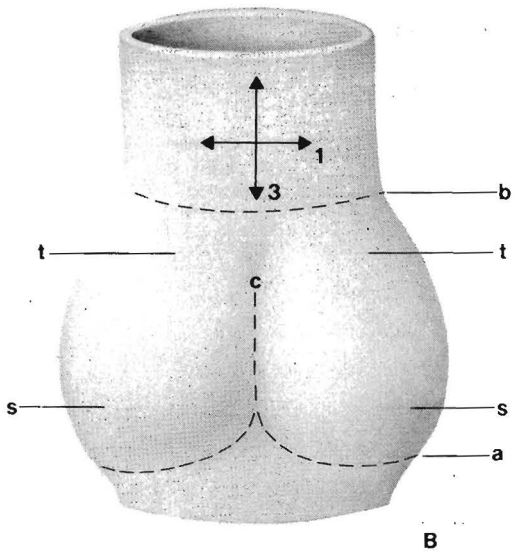

B

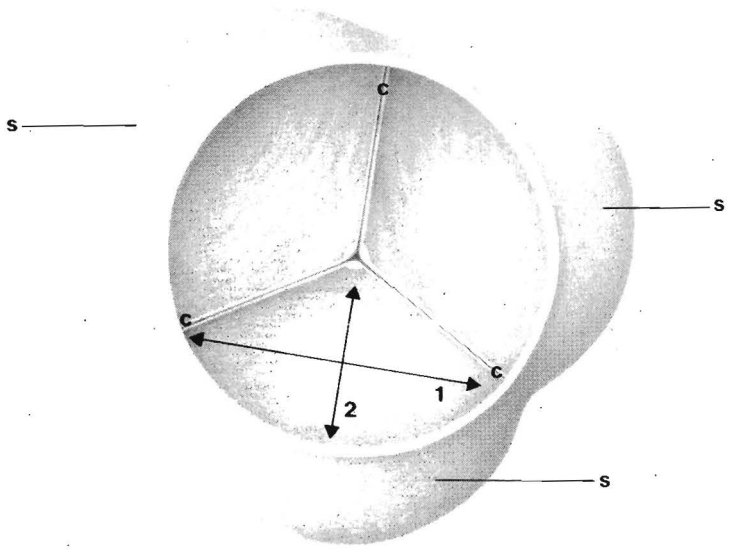

A

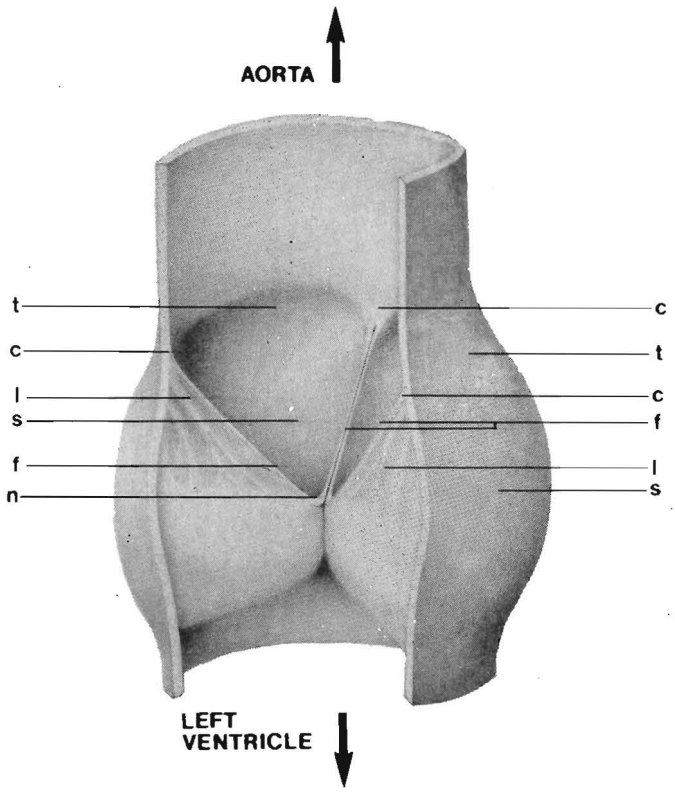

△Fig. 2.2.
Exposure of the aortic valve in the closed configuration after dissection of one leaflet and the corresponding sinus wall. The coronary arteries are not shown.

c: commissure; f: free edge of leaflet; ℓ: lunula; n: node of Arantius; s: sinus wall; t: top of a sinus cavity.

◁Fig. 2.1.
A. The aortic valve in the closed configuration as seen from the aortic side. The coronary arteries (see text) are omitted.
B. Side view of the valve. All elements, lying between the dashed line a (aortic ring) and the circle b in the transversal plane through the sinus tops (t), constitute the aortic valve.

c: commissure; s: sinus wall; t: top of a sinus cavity;
1: circumferential direction; 2: radial direction in the leaflets;
3: axial direction in the sinus and aortic walls.

coincident with each other (fig. 2.1 and 2.2). The remainder of the leaflet surface, not making contact with adjacent leaflets when the valve is closed, is referred to as the load bearing leaflet portion [Mercer, 1973]. Halfway the free leaflet edge there is a thickening, the so-called node of Arantius. The line of attachment of the leaflets to the aortic wall will be referred to as the aortic ring [Missirlis, 1973], although in literature other designations are also used, e.g. annulus fibrosus [Missirlis, 1973] or fibrous coronet [Brewer et al., 1976]. The line of attachment of each leaflet to a sinus forms a U-shaped arch. Consequently, the aortic ring, formed by the three U-arches, is actually a crown-like formation rather than a circular ring. The tops of the arches, where the lunulae of adjacent leaflets merge into the aortic ring, are called commissures. Behind each leaflet the aortic wall expands to form three dilated pouches, the sinuses of Valsalva, the walls of which are considerably thinner than that of the aorta. In two of the three sinuses are located the orifices of the coronary arteries which supply the heart muscle with blood. The two anterior sinuses (and leaflets) are commonly denoted as the right and the left coronary sinus (and leaflet). The third is the non-coronary or posterior sinus (and leaflet) [Silverman and Schlant, 1970].

The term "aortic valve" will be taken to apply to the part of the aortic root consisting of the leaflets and the sinus walls, bounded at the ventricular or inflow side by the aortic ring and at the aortic or outflow side by the circle that is obtained by intersection of the transversal plane through the sinus tops and the aortic wall (fig. 2.1). This definition includes the portions of the aortic wall, that are bounded by this circle and the aortic ring.

Both mechanical and kinematical aspects are involved in valve functioning and differ in importance in the various phases of the cardiac cycle, as will be discussed below. During one cardiac cycle three main phases can be distinguished in valve performance: the opening and closing phases in systole and the diastolic phase during which the valve is closed. In the normal situation valve opening is very fast. The leaflets bulge towards the aorta just before left ventricular ejection begins [Heckman and Ascanio, 1972; Swanson and Clark, 1973]. The valve is completely open when the peak flow in the ascending aorta has reached 75% of its maximum [Van Steenhoven, 1979;

Van Steenhoven et.al., 1981]. As to valve closing, Bellhouse and Talbot [1969] concluded from their model experiments that two phases can be distinguished. The first is the gradual closing of the valve that starts during the deceleration of aortic flow, resulting in about 80% valve closure at the moment of zero flow in the ascending aorta at end-systole. Finally, a small reversed flow completes closure. Similar results were obtained by Van Steenhoven [1979] and Van Steenhoven et al. [1981] in *in vivo* experiments. Moreover, they observed that in the intact animal the valve has already closed by about 10% at the onset of deceleration of ascending aortic flow and that complete closure coincides with maximum backflow in the ascending aorta. Being thin and flexible membrane-like structures, the valve leaflets cannot withstand any significant pressure difference during the opening and first closing phase. During these phases the leaflets may be expected to move with the fluid in an essentially kinematical process governed by the fluid motions. Stresses resulting from pressure-loading, boundary-layer and inertia effects will be insignificant in these phases compared with the stresses to be expected in the second closing phase and during diastole. The coincidence of maximal backflow and complete valve closure [Van Steenhoven, 1979; Van Steenhoven et al., 1981] will inevitably cause peak stresses in the leaflets. In the course of diastole the leaflets have to withstand a slowly varying but none the less considerable pressure load (see section 2.5). Modelling of the valve behaviour during the second closing phase, including the moment of complete closure, is very complex because of its highly dynamical character. The present study will be restricted to investigations of the mechanics of the closed valve in the quasi-static situation in diastole. Insight into the behaviour of the valve in this situation is expected to provide important criteria for the design of a valve prosthesis, that combines an optimum loadbearing function with minimum stresses. Moreover, such a study may serve as a basis for investigations of valve behaviour during the other phases of the cardiac cycle, involving kinematical and dynamical aspects.

2.3. *The histology of the aortic valve*

2.3.1. *Introduction*

When investigating a system consisting of biological tissue, histological data may provide important information for the theoretical modelling as well as the interpretation of experimental results. Information on the occurence and arrangement of different tissue components with their specific properties, facilitates the qualitative interpretation of the results of material experiments as performed on tissue samples (see section 3.2). Moreover, based upon the structure and mechanical properties of the various parts of a biological system one might be able to formulate hypotheses concerning their respective functions. These hypotheses in turn may serve as guidelines for determining how the system components should be schematized in order to develop an appropriate, realistic model of the total system.

Although many histological studies have been performed on both human [Clark and Finke, 1974; Gross and Kugel, 1931; Mohri et al., 1972] and animal [Brewer et al., 1976, 1977; Lyons, 1976] aortic valves, only minor attention has been paid to the possible significance of the various tissue components for the mechanical and kinematical behaviour of the valve. The aim of the work presented here is to contribute to the interpretation of aortic valve histology with respect to the understanding of valve mechanics and kinematics. In order to achieve this, all functional parts of the valve should be considered. Furthermore, reduction of the many detailed findings to a set of relevant data is a necessity for developing a workable valve structure model.

2.3.2. *Material and methods*

Porcine aortic valves obtained from the slaughter house were studied in the relaxed state. The age of the animals was about 4 months. After fixation in formaldehyde the specimens were dehydrated, embedded in paraffin and serially sectioned in the radial and circumferential directions (the definition of these directions is given in fig. 2.1). Following staining with a combination of orcein for the elastin fibres and van Gieson's picrofuchsin for the collagen fibres, the sections (10 μm) were studied by light microscopy. In this study specimens

from 8 animals were investigated. Sections related to the stressed state were obtained from valves fixated in a 0.9% saline/4% formaldehyde solution at a constant pressure difference of 13.3 kPa for about 20 hours. The constant pressure gradient across the valve was maintained by means of a simple set-up consisting of a closed loop containing the valve with ligated coronary arteries, a reservoir with overflow, a supply reservoir and a roller pump. The flow generated by the pump accounted for valve leakage, the surplus of flow being fed back to the supply reservoir.

2.3.3. Results

In the leaflets many macroscopically visible connective tissue bundles are present (fig. 2.3). Originating at the commissures they run circumferentially like the free leaflet margin. Towards the leaflet centre they show many ramifications, centrally forming a dense interwoven network of fine fibres. In addition to these commissural fibres, discrete macroscopically visible bundles, perpendicular to the attachment line, anchor the middle portion of the leaflet to the aortic wall (fig. 2.4). In the aortic wall these bundles diverge into a fibrocartilaginous tissue (fig. 2.5) which forms a U-shaped arch in each sinus as part of the aortic ring. As can be seen in the micrographs (fig. 2.6), the diameter of this arch increases from the commissures towards the bottom of the sinus.

Within the endothelium round the leaflet four different layers are immediately discernable in the load-bearing portion (fig. 2.7). The subendothelial ventricular layer is composed of elastin fibres, oriented in various directions. This layer is continuous with the subendothelial elastic tissue of the ventricle. The second layer consists of a loose connective tissue structure, containing sparse nuclei and a few elastin fibres. This structure is continuous with the loose connective tissue in the attachment line in the aortic wall. The third layer contains the already mentioned coarse bundles of tightly packed collagen fibres. Some elastin fibres are present between these bundles, increasing in number towards the aortic side and passing into a small subendothelial layer of elastin fibres. Close to the attachment to the aortic wall, the middle portions of the unstressed leaflets reveal circumferentially directed

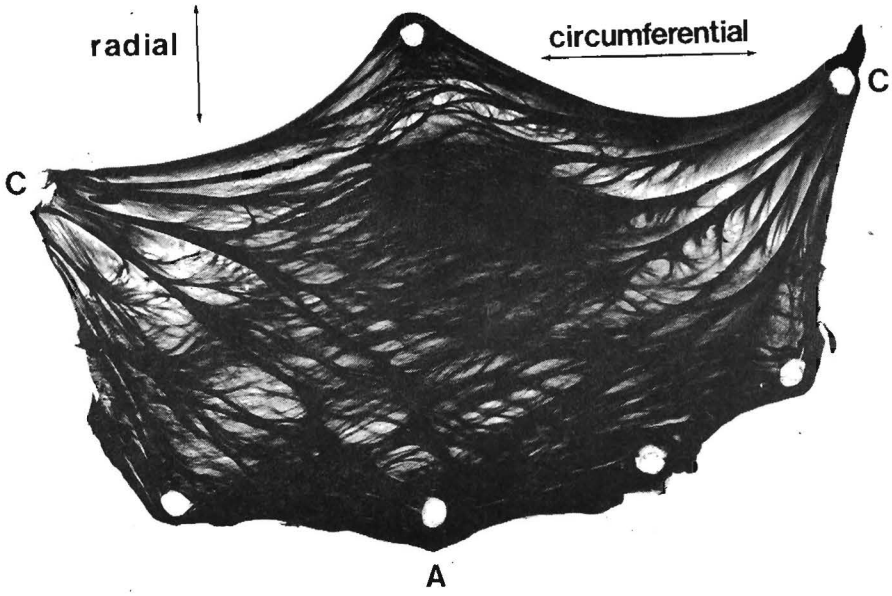

Fig. 2.3.
Porcine aortic valve leaflet showing the typical collagen bundle structure. The leaflet is dissected from the aortic wall along the line C-A-C (van Gieson's picrofuchsin; original magnification x5).

constrictions on the aortic side (fig. 2.4).

The lunulae of the leaflets are much thinner than the load bearing parts (fig. 2.4) and although the same tissue components are present, their arrangement is very irregular at most sites and varies from valve to valve. In some areas only loose connective tissue with a small number of elastin fibres can be seen, while in other areas the cross section of the leaflet consists exclusively of tightly packed collagen fibres of the macroscopically visible commissural bundles.

Fig. 2.8 shows a radial section of a pressure loaded valve. In the load bearing leaflet portion the loosely structured layer has almost vanished. Moreover, this portion shows no significant radial curvature, a phenomenon observed by visual inspection in all stressed valves. Further, it is noted that the constrictions found in the relaxed leaflets have dissappeared in the stressed specimens.

The sinus walls consist of mainly circumferentially arranged smooth muscular tissue embedded in a network of arbitrarily oriented elastin fibres with scattered small collagen fibres (fig. 2.9). These structures are anchored into the fibrocartilaginous aortic ring.

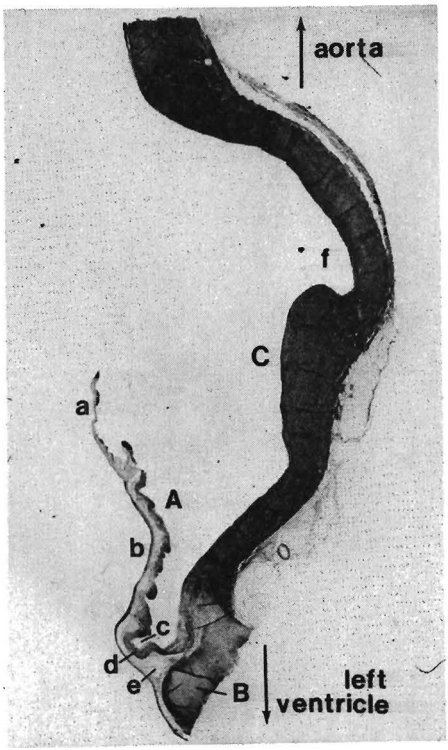

Fig. 2.4.
Radial section through sinus wall and leaflet. Leaflet (A): lunula (a); load-bearing leaflet portion (b); constriction (c); collagen bundles, perpendicular to the line of attachment and anchoring the leaflet to the aortic wall (e). Aortic ring (B) containing fibrocartilaginous tissue. Sinus wall (C) with inlet of coronary artery (f). The wrinkles crossing the sinus wall are artifacts of the sectioning procedure (orcein + van Gieson's picrofuchsin; original magnification x 6).

2.3.4. Discussion

The number and the composition of the observed tissue layers in the leaflets are in fair agreement with similar data, reported by Clark and Finke [1974] and Gross and Kugel [1931] for human leaflets and by Brewer et al. [1977] and Lyons [1976] for canine specimens. The number of the tissue layers observed in the leaflets, unquestionably depends on the resolution of the technique utilized for the examination. Using microscopic techniques of sufficiently high resolution, the four and five layers, as observed by Gross and Kugel [1931] and Clark and Finke [1974] in human specimens, respectively, may appear to contain several sublayers [Missirlis, 1973]. However, in view of the object

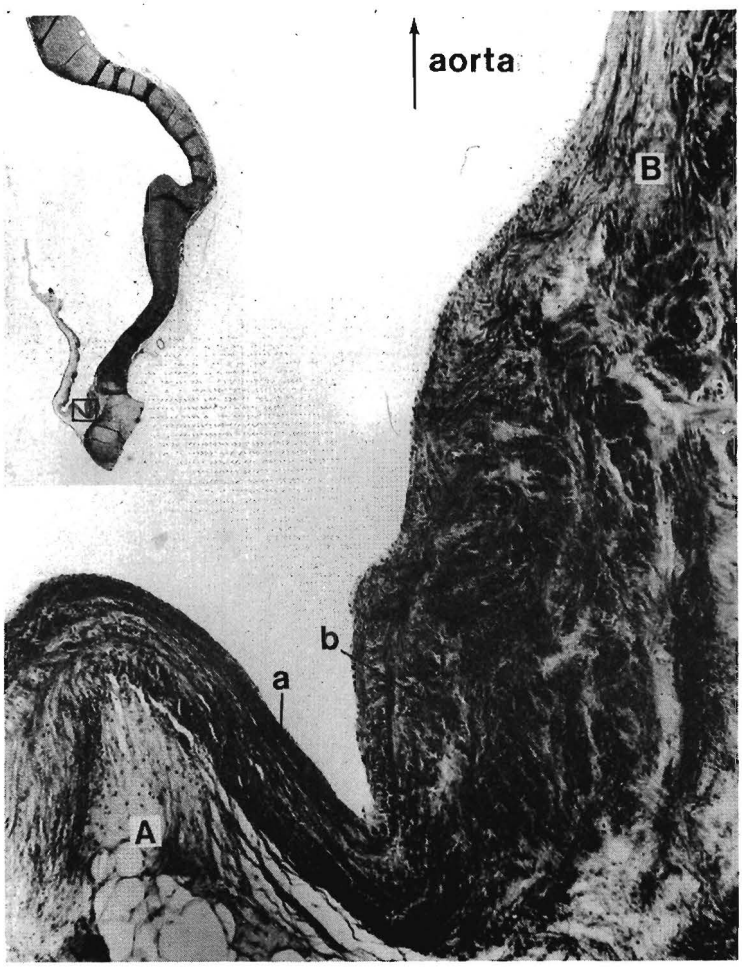

Fig. 2.5.
Detail of radial section through sinus and leaflet (inset) showing collagen bundles (a) perpendicular to the attachment line which anchor the leaflet (A) to the aortic wall (B). In the aortic wall these bundles diverge into the fibrocartilaginous tissue of the aortic ring (b) (orcein + Van Gieson's picrofuchsin; original magnification x 50).

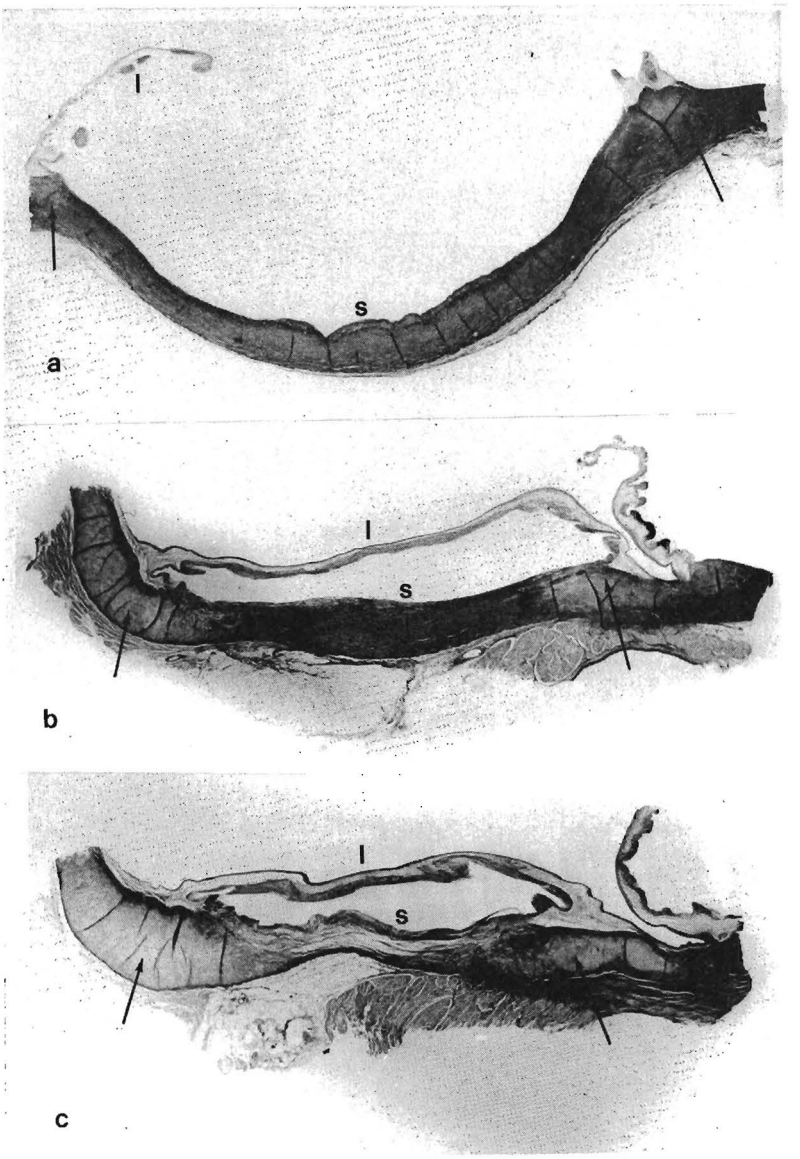

Fig. 2.6.
Circumferential sections through leaflet (l) and sinus (s) at different distances from the bottom of the sinus. The diameter of the fibrocartilaginous structure (arrows) of the aortic ring can be seen increasing from the commissures towards the bottom of the sinus (a-c) (orcein + Van Gieson's picrofuchsin; original magnification x 4).

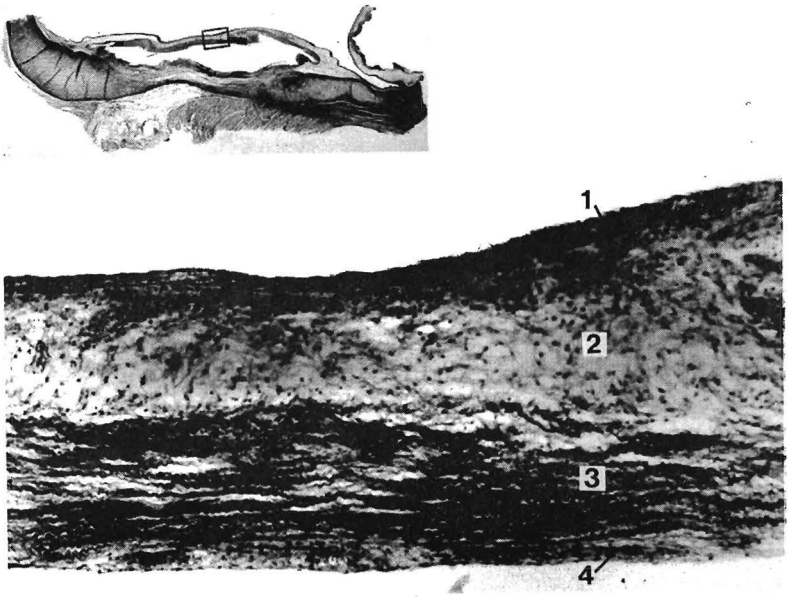

Fig. 2.7.
Detail of circumferential section through the load-bearing portion of an aortic leaflet (inset) showing the layered leaflet structure; 1: elastic layer at the ventricular leaflet side, 2: loose connective tissue; 3: tightly packed collagen bundles; 4: small elastic layer at the aortic leaflet side (orcein + Van Gieson's picrofuchsin; original magnification x 80).

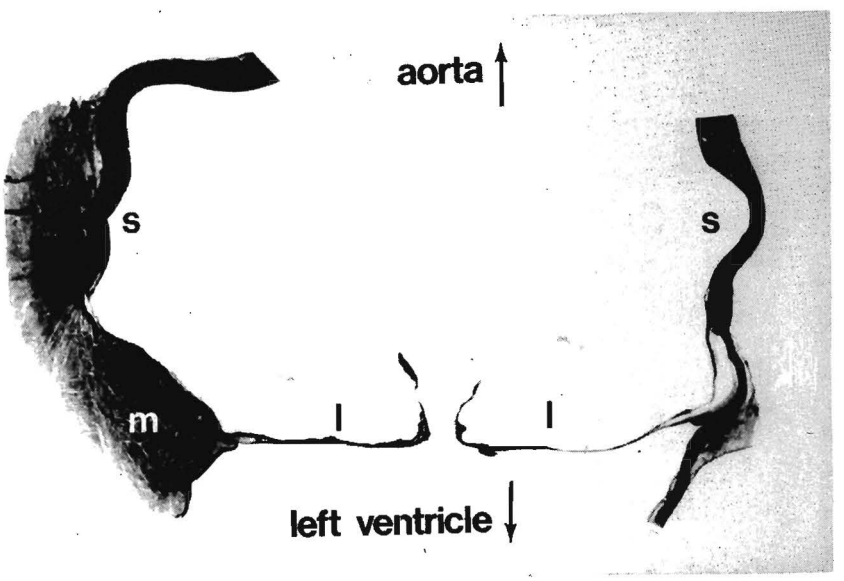

Fig. 2.8.
Radial section through leaflets (ℓ) and sinus walls (s) of a loaded valve, showing the myocardial support (m) of one of the coronary leaflets.

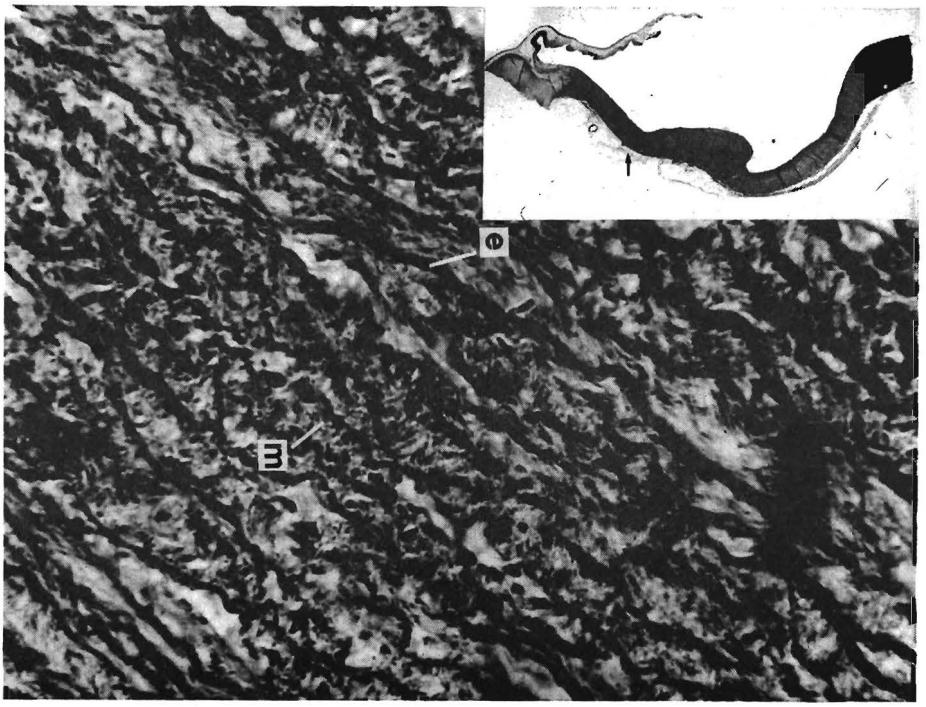

Fig. 2.9.
Detail of radial section through sinus wall (inset). The sinus wall consists of circumferentially arranged smooth muscle (m) embedded in a network of elastic fibres (e) (orcein + Van Gieson's picrofuchsin; original magnification x 300).

of this study, it seems reasonable to think the load-bearing part of the leaflets is composed of three functional layers within the endothelial coverings: a dense layer composed of circumferentially oriented collagen fibres and bundles at the aortic side, a grid of randomly oriented elastin fibres at the ventricular side and, in between, a loosely structured layer. So the load bearing part of the aortic leaflet can be regarded as an elastic grid, reinforced with collagen fibres and bundles. The collagen network transmits the loading of the leaflet to the aortic wall by means of the bundles merging at the leaflet commissures and the collagen bundles, which are perpendicular to the attachment line. In the circumferential direction the relation between load and deformation is mainly expected to exhibit the properties of the collagen bundles. In the radial direction, however, the load-deformation characteristics of the elastic meshwork will be the predominant factor. The anisotropic

characteristics of the leaflet tissue, as found by Missirlis [1973] and Missirlis and Chong [1978], can be explained in this way.

Although there is no unanimity on the importance of the loosely structured layer [Brewer et al., 1977], it is plausible to assume that this structure enables the collagenous layer to move over the elastic layer as has been suggested by Mohri et al. [1972]. Furthermore, the decrease of leaflet thickness with increasing pressure-loading of the valve observed by Clark and Finke [1974] and Swanson and Clark [1974], might result from compression of the loose connective tissue. This could indicate a damping function of the loosely structured layer, that would prevent the impact load on the leaflets from causing vibrations consequent to stopping the back flow on valve closure.

As to the elastic layer, it should be noted that the present study reveals a grid of arbitrarily oriented fibres whereas for human [Mohri et al., 1972] and canine [Lyons, 1976] valve leaflets mainly radially oriented fibres are reported. That does not necessarily mean that the porcine valve has a different structure. A possible explanation for this discrepancy might be found in the fact that the number of layers and sublayers to be distinguished in the leaflet tissue, depends on the examination technique used.

From the composition of the lunulae, showing pronounced collagenous bundles and thin membranous parts in between, the following assumption can be made about their function. While the membranous parts have a sealing function, that of the bundles in the load-bearing leaflet portion is to transmit part of the pressure load on the leaflet to the commissures.

The constrictions, found close to and running parallel with the line of attachment in the middle portion of the unloaded leaflets, have also been observed by others. Mohri et al. [1972] described them as irregular folds composed of circumferentially oriented collagen bundles. Clark and Finke [1974] reported striations on the aortic leaflet side resulting from the macroscopically visible collagen bundles immediately below the endothelium. Because of their particular position and orientation, we think that these constrictions act as hinges, thus reducing bending stresses during leaflet motions. This hinge hypothesis seems consistent with the results of Mercer's [1973] cineangiographic analysis of the movements of the dog's aortic

leaflets and with the observations in model studies on the closing behaviour of the aortic valve, as described by Van Steenhoven and Van Dongen [1979].

In the present study no special attention has been paid to the possible presence of blood vessels in the leaflets. Smith and Taylor [1971] reported the porcine pulmonary and aortic valve vasculature to be relatively insignificant compared with that of atrioventricular valves.

The present observations concerning the aortic ring confirm the crown-like configuration of this structure as described by Gross and Kugel, [1931], Zimmerman [1969] and Brewer et al. [1976]. Its cartilaginous character points to a relatively great stiffness compared with the other parts of the valve. The typical dimensions of the U-arches, constituting the crown, probably bring about the largest flexibility near the commissures and the least at the sinus bottoms and might constitute a stress-reducing mechanism. The bottoms and the extremities of the U-arches can probably move in radial directions. This is supported by the finding that, *in vitro*, the diameters at the ventricular and the aortic side of the closed human valve increase with increasing pressure [Trenkner et al., 1976]. These investigators observed the diameter variations on the aortic side to be the largest. *In vitro*, similar findings were obtained from porcine valves however without evident differences in the behaviour of both diameters. In *in vivo* experiments Thubrikar et al. [1977] observed a 4 to 5 percent decrease of the canine aortic valve diameter at the level of the commissures for a pressure decrease from 13.3 kPa to 10.7 kPa in diastole. During a complete cardiac cycle a variation of about 12 percent was found. The arrangement of the cardiac muscle fibres at the ventricular side of the valve (fig. 2.8) indicates that the bottoms of the U-arches, corresponding to the right and left coronary leaflets, are pulled outward in the radial direction on contraction of the adjacent muscle fibres.

The sinus walls consist of mainly circumferentially arranged smooth muscle cells embedded in a grid of elastic tissue with no special fibre orientation. Collagenous components are almost absent in the sinus walls. As far as the elastic components are concerned, the sinus tissue will probably show hardly any anisotropy whereas it will be rather compliant. The latter assumption is supported by the findings

of Van Renterghem et al. [1979]. In *in vitro* pressure-volume experiments they observed the sinuses of the porcine valve to be about ten times more compliant than the leaflets. It is felt that, in addition to their importance in the hydrodynamical functioning of the aortic valve [Van Steenhoven and Van Dongen, 1979], the sinus walls are also likely to have a mechanical function because of their structural ability of energy storage and/or dissipation. Because of their ability to deform more extensively than the leaflets, the sinus walls could play a significant role in the absorption and/or accumulation of the energy of fluid motion at the moment of valve closure, at the same time reducing the pressure difference across the valve by increasing its volume.

Further investigations as to the specific role of the smooth muscle cells are needed. In the present study their role was not taken into consideration.

2.4. The geometry of the aortic valve

The difficulty in describing the geometry of the aortic valve is illustrated by the paucity of available data. Two types of investigations on valve geometry were found in literature.

One way to determine the geometry is the use of closerange stereophotogrammetry [Karara and Marzan, 1973; Missirlis and Chong, 1978]. This sophisticated method enables the spatial coordinates of a large number of points on a surface to be accurately determined. Photogrammetric studies on silicone rubber casts [Karara and Marzan, 1973] as well as actual valves [Missirlis and Chong, 1978] were reported. These techniques unquestionably present a valuable tool for the acquisition of geometrical data. Thanks to their high degree of accuracy and resolution, enabling small irregularities to be measured, they allow geometries to be determined in detail. Unfortunately, practically no numerical values that could have been used as input data for the present study, could be found in literature.

The determination of a set of characteristic dimensions, from some simplifying but reasonable assumptions on the valve geometry is a different approach. Owing to geometrical irregularities, arising out of differences between similar parts in one and the same valve [Gould

et al., 1976], it is hardly possible to give a description of the valve geometry without such assumptions. It is assumed that the valve has 120° symmetry, the aorta being a cylinder. As to the geometry of the sinus cavities there is no clear unanimity. From the quantities that are used in characterizing the sinus geometry, one is apt to consider it to be spherical. The most detailed investigation of this kind was reported by Swanson and Clark [1974]. The dimensions and geometrical relationships of the human valve as a function of pressure difference across the valve were determined from a series of silicone rubber casts. Reid [1970] concentrated on the sinus cavities of the unloaded human and animal valves, while Sands et al. [1969] compared valves of various species. Data were obtained from quickly frozen specimens at a pressure load of 13.3 kPa. Other comparative studies were reported by Lozsádi and Arvay [1969] and Trenkner et al. [1976]. Fig. 2.10 illustrates the definition of the quantities used in the description of valve geometry. The numerical values reported by the various investigators for the human as well as the porcine valve are stated in Table 2.1. As far as they are available, the values given are applicable to the situation at zero and 13.3 kPa pressure difference across the valve. As can be seen from Table 2.1 the available data are rather poor and certainly not sufficient for a thorough comparison of human and porcine specimens. The use of the definition of the angle α by Swanson and Clark [1974] and Trenkner et al. [1976] is based on their observation that, in diastole, the shape of the load bearing leaflet portion can in essence be considered cylindrical which was confirmed by the findings in the present study.

The thickness of the leaflets was often considered as an important dimension in stress computations. It should be realized that the definition of a mean thickness is actually meaningless in view of the inhomogeneous histological structure of the valve leaflets. The available data on this subject are given in terms of values that have been measured at discrete points or in discrete regions of a leaflet. Swanson and Clark [1974] reported an inverse proportionality between the pressure difference across human leaflets and their thickness. They observed that the thickness at the intersection of the lunulae and the plane of symmetry of the leaflet decreases from 0.48 mm to 0.32 mm when the pressure difference increases from zero to 13.3 kPa. In humans, Sands et al. [1969] found thickness values of 0.67 mm near

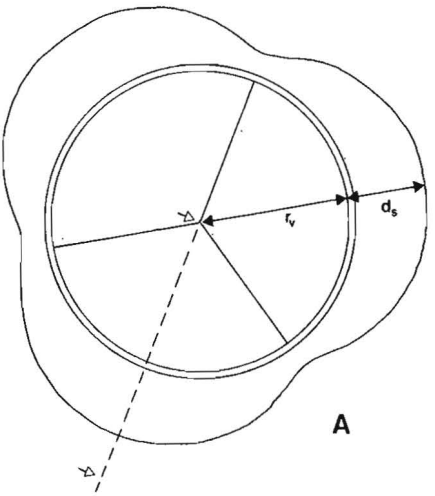
r_v
d_s
A

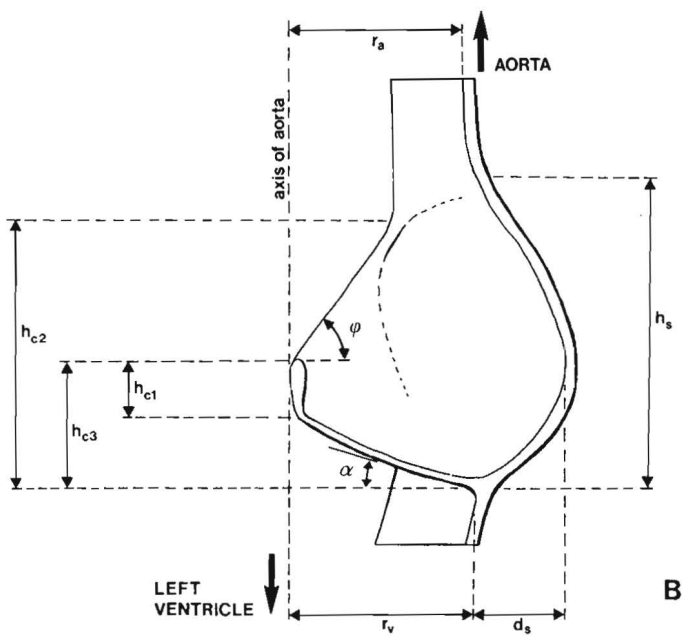
r_a
AORTA
axis of aorta
h_{c2}
h_{c1}
h_{c3}
φ
α
h_s
LEFT
VENTRICLE
r_v
d_s
B

Fig. 2.10.
Definition of the dimensions used for the description of the geometry of the aortic valve.
A. The aortic valve in the closed configuration as seen from the aortic side. The dashed line indicates the plane of symmetry of one leaflet and the corresponding sinus cavity.
B. View in the direction of the arrows in A on one leaflet and sinus cavity after dissection through their plane of symmetry: r_a: aortic valve radius; r_v: ventricular valve radius; h_s: sinus height; d_s: sinus depth; h_{c1}: height of the lunula at the intersection with the plane of leaflet symmetry; h_{c2}: commissural height; the dimension h_{c3} was used only by Sands et al. [1969].

Table 2.1.
Dimensionless quantities at zero pressure difference across the valve, relative to the ventricular valve radius r_v. Dimensions related to the leaflets and sinuses are average for the three leaflets and sinuses. Between parentheses values at 13.3 kPa are given. For the definition of the quantities see fig. 2.10.

	Swanson & Clark [1974]	Sands et al. [1969]		Reid [1970]		Trenkner et al. [1976]		Lozsádi & Arvay [1969]	
	H[1]	H	P[2]	H	P	H	P	H	P
r_a	0.95			0.75	0.69			0.9[3]	1.1[3]
	(1.07)								
h_s	1.74			2	1.32				
	(1.76)								
d_s	0.34			0.70	0.71			0.12	0.12
	(0.46)								
h_{c1}	0.34								
	(0.34)								
h_{c2}	1.46								
	(1.42)	(1.34)	(1.64)						
α	20					19	31		
(degrees)	(22)					(28)	(41)		
ϕ	40					60	55		
(degrees)	(32)	(33)[4]	(28)[4]			(43)	(31)		

1) human; 2) porcine; 3) mean value for loaded and unloaded valve;
4) determined from $\phi = \arctan\{(h_{c2} - h_{c3})/r_v\}$.

the aortic ring and of 0.57 mm near the free edge. In pigs these values amounted to 0.80 and 0.70 mm, respectively. Clark and Finke [1974] reported thickness values ranging from 0.175 to 1.5 mm at various locations in a human valve leaflet at a pressure load of 10.7 kPa. Data on the thickness of the sinus walls could not be found in literature. A study on valve geometry would far exceed the scope of the present investigation. Therefore the available data presented in the foregoing will be used for modelling purposes.

2.5. *The pressure difference across the aortic valve*

The load to be sustained by the closed aortic valve results from the difference between the aortic and left ventricular pressures. Being dependent on a variety of factors, the physiological range of pressures varies with the experimental circumstances and is therefore hard to define. A representative outline of the course of the aortic and left ventricular pressures is given in fig. 2.11. The pressure difference across the valve reaches its maximum at the beginning of diastole, the moment of valve closure. Next it decreases almost linearly during diastole.

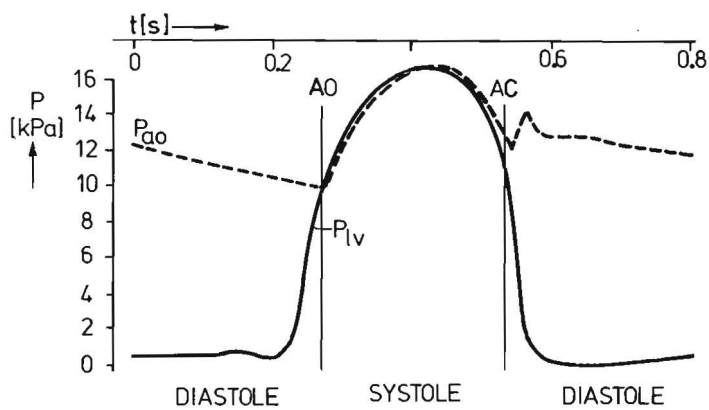

Fig. 2.11.
Representative outline of the aortic (P_{ao}) and left ventricular (P_{lv}) pressures during the cardiac cycle.
AO: aortic valve opens; AC: aortic valve closes.

2.6. *The mechanical properties of aortic valve tissue*

Most studies on the mechanical properties of aortic valve tissue focussed on the leaflet tissue under quasi-static load or strain [Clark and Butterworth, 1971; Mundth et al., 1971; Clark, 1973; Wright and Ng, 1974; Missirlis and Chong, 1978]. The leaflet tissue was found to have highly nonlinear stress-strain characteristics. Moreover the extensibility in the radial direction is much larger than in the circumferential direction. Missirlis [1973] and Van Renterghem et al. [1979] also introduced the sinus and aortic wall properties into their studies, finding them to be much more compliant than the leaflet tissue. Lim and Boughner [1976] demonstrated that the leaflet tissue has viscoelastic properties at low frequencies (frequency range 0.5 - 5 Hz). The above-mentioned investigations will be discussed more extensively in Chapter 3. Nearly all these studies lack mathematical modelling of the mechanical properties of valve tissues. A simple but explicitly formulated mathematical model will therefore be used in the present study, providing a framework for the design of experiments and allowing a concise and more quantitative description of the experimental results. The model chosen in the present study will be discussed in Chapter 3. A description of the experiments performed to test the model for its validity is given in Chapter 4.

CHAPTER 3

THE MECHANICAL PROPERTIES OF AORTIC VALVE TISSUE

3.1. Introduction

As discussed in the previous chapter, in none of the experimental studies published in literature have the mechanical properties of aortic valve tissue been described mathematically. In this chapter various important aspects of the development of a constitutive model are discussed. First, a description is given of the general features of the mechanical behaviour of soft biological tissues (section 3.2). Second, the available data on the constitutive properties of aortic valve tissue are reviewed and classified according to the type of experiment from which the data are obtained (section 3.3). The various models proposed in literature to characterize soft tissues are discussed in section 3.4. Finally the relevant features of the "quasi-linear viscoelasticity law", that has been chosen as a starting point for the present investigation, are explained (section 3.5).

3.2. General features of the mechanical behaviour of soft biological tissues

In general, soft biological tissues mainly consist of collagen and elastin fibres embedded in a mucopolysaccharide structure. The collagen and elastin fibres are commonly thought to be the load-bearing frame of a tissue. Little is known about the mechanical function of the mucopolysaccharide structure. The collagen and elastin fibres differ remarkably as to their mechanical properties. Elastin fibres are able to elongate up to 100% in excess of their relaxed length without irreversible damage [Carton et al., 1962], whereas this upper limit is about 2 to 4% for collagen fibres [Rigby et al., 1959; Rigby, 1964; Abrahams, 1967].

The general shape of the load-elongation curve of a soft tissue sample, that is obtained from a uniaxial tensile test, can be interpreted qualitatively in relation to its histological structure. In the curves obtained from constant-strain-rate experiments four different phases can be distinguished (see fig. 3.1). In the first phase the tissue offers negligible resistance to elongation. Force

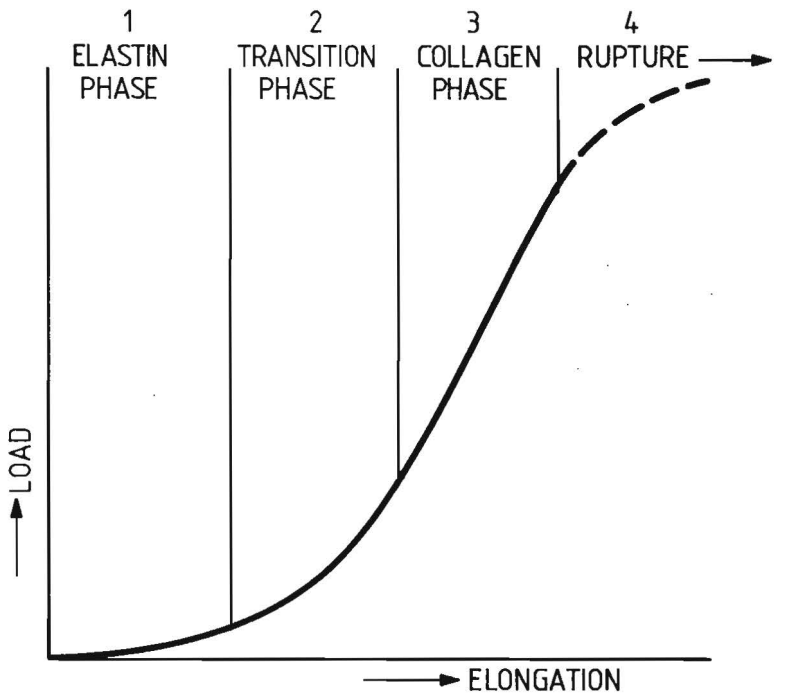

Fig. 3.1.
Typical load-elongation curve for a soft biological tissue in unaxial tension at constant elongation rate.

transmission is provided only by the elastin fibres, so that this phase is often denoted as the elastin phase.
In the second or transition phase gradually more collagen fibres become aligned and uncoiled, thus increasingly contributing to force transmission. In the third or collagen phase all collagen fibres are uncoiled and the slope of the load-elongation curve becomes steep and almost constant, mainly reflecting the material properties of the collagen fibres. In phase 4 the slope of the load-elongation curve becomes less steep and a further increase of the load will finally cause total rupture of the tissue. Whether a specific tissue follows the load-elongation curve as shown in figure 3.1 depends on the structure and quantitative relation of the various tissue components. An additional aspect is that for most soft tissues the load depends not only on the instantaneous elongation but also on the history and

the rate of elongation. Viscoelastic phenomena, such as hysteresis, creep, relaxation and different moduli for different elongation rates have been reported for various soft tissues.

3.3. *A review of literature concerning the mechanical properties of aortic valve tissue*

Only experimental work on the mechanical properties of aortic tissue is reported in literature. In practically none of these studies have viscoelastic phenomena explicitly been taken into consideration. Roughly three types of experiments can be distinguished: the bulge test performed on a valve leaflet, pressurization of an entire aortic root and uniaxial tensile experiments performed on a strip of tissue.

In the bulge test a disc of leaflet tissue forced to bulge under uniform pressure. Assuming that the piece of tissue behaves like a homogeneous thin-walled sphere with uniform thickness during deformation, tension-elongation relationships are derived from pressure-volume curves, using Laplace's law. Mundt et al. [1971] studied the static pressure-volume relations of canine aortic wall and aortic valve leaflets. The leaflet tissue shows the weak elastin phase for pressures up to about 1.33 kPa, while the stiff and almost linear collagen phase is found for pressures exceeding 4 kPa (fig. 3.2a). The aortic wall shows nearly linear characteristics in the pressure range from 0 to 21.3 kPa (fig. 3.2b). Wright and Ng [1974]

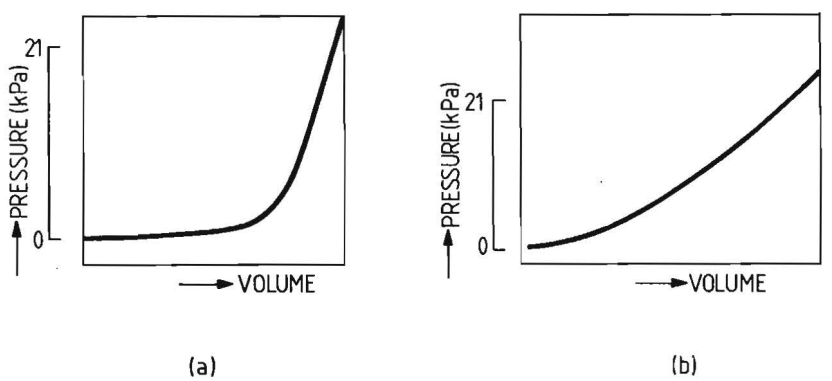

Fig. 3.2.
Pressure-volume curves for (a) a canine aortic valve leaflet and (b) canine aortic wall [Mundt et al., 1971]. No volume units were given.

reported similar studies on human valve leaflets. They measured volume changes due to a 1.67 kPa pressure increase in the ranges 0.13 - 1.80 kPa and 11.66 - 13.33 kPa. In the latter range a significantly less pronounced increase (tenfold) in volume change was found compared to the former for the same increase in pressure. This different behaviour can likely be explained by the elastin and collagen phases in the stress-strain characteristics of the leaflets. Lim and Boughner [1976] studied human aortic valve leaflet samples by applying sinusoidal pressure variations (peak-to-peak ≈ 40 kPa) at frequencies between 0.5 and 5 Hz. Analysis of the results, based upon linear viscoelasticity theory, revealed that the complex modulus and the loss tangent (the definition of these quantities is given in Appendix C) are hardly frequency dependent. The way the specimen in these experiments is loaded looks quite similar to that in the physiological situation. It should be noted, however, that the conditions at the edges are certainly not physiological , which could influence the overall behaviour of the specimen. Moreover, anisotropy and inhomogeneity are not taken into account in interpretating the results. Therefore these methods only provide overall information on the mechanical behaviour of tissue.

A different approach in studying the mechanical properties of the aortic valve has been described by Missirlis [1973] and Missirlis and Chong [1978]. In their experiments an entire aortic root was pressurized. Missirlis [1973] used photographs of the ventricular surface of the valve, on which a random pattern of ink dots was deposited. Strains were determined from the change of distance between neighbouring dots. In the pressure range from 5 to 25 kPa the average radial (see fig. 2.1 for the definition of directions) distension of human valve leaflets was found to be 0.1, the average distension in the circumferential direction being less than 0.02. The aortic ring perimeter remained virtually constant. Missirlis and Chong [1978] performed a similar study on porcine valves. By using a stereophotogrammetric method, the spatial coordinates of a grid of points on the ventricular side of the valve leaflets could be obtained. From these data local strains in various directions were determined as a function of pressure. For an increase of pressure from 0.4 to 16.0 kPa, radial strains from about 0.1 to more than 1.0 and circumferential strains of 0.05 to 0.1 were found in the various

leaflets. The values of the circumferential strains, reported both by Missirlis [1973] and Missirlis and Chong [1978], must be considered with caution because they are in the same order of magnitude as the errors involved in measuring the strains. Changes of the aortic ring perimeter never exceeded 0.1 in the above-mentioned pressure range. In these studies the geometrical and loading conditions approximate very closely the physiological situation. These experiments may therefore be expected to provide reliable data on deformations under (quasi-static) physiological loads, the influence of tissue damage on the measured data being absent. However, the requirements as to instrumentation and in particular regarding data processing are considerable.

The method most frequently used to determine stress-strain characteristics is that of uniaxial tensile experiments on tissue strips. Aortic valvular tissue shows the characteristic load-elongation relationship depicted in fig. 3.1. In order to compare the results of different tissue strips, these characteristics are converted into stress-strain curves. The physiological differences, inherent in the properties of biological tissues, is a major cause of the broad scatter of the data. An additional cause is the diversity of methods and the uncertainties involved in computing stresses and strains. Stress is defined as

$$\sigma = \frac{F}{A} \tag{3.1}$$

where A and F represent the cross-sectional area of the specimen and the load acting on it, respectively. Strictly speaking, the stress definition (3.1) is significant only in the case of a homogeneous distribution of the load over the whole cross-sectional area. Especially in testing leaflet samples it must be doubted whether this is the case because of the obvious inhomogeneous structure and irregular dimensions of the leaflet tissue (see sections 2.3.3 and 2.3.4). For the time being, however, a more precise description of force transmission in these samples does not seem possible. Moreover, stress values will differ according to whether the cross-sectional area is used in the relaxed state or in the stressed state in their computation. In determining the cross-sectional area, Missirlis [1973] measured width and thickness of the mounted specimen at zero load

through a microscope with a calibrated eyepiece. Clark [1973] measured the minimum thickness of the tissue strip during testing, using two cathetometers with a micrometer eyepiece at two different angles. It is unclear what is meant by these "two different angles". Moreover, no information was given about the measurement of the width of the specimen. Missirlis and Chong [1978] measured width and thickness of the specimen, using photographs that were made at known elongations and loads during an experiment. The definition of strain used is

$$\varepsilon = \frac{l - l_0}{l_0} \tag{3.2}$$

where l is the length of the specimen at a given moment and l_0 designates a reference length. The strain definition (3.2) assumes a homogeneous deformation pattern throughout the sample. Here the same remarks apply as those made with respect to the stress definition (3.1). Clark [1973] obtained a reference length by adjusting the length of the jaws" (holding the specimen) "until no buckling or crimping of the tissue was observed". Missirlis [1973] and Missirlis and Chong [1978] determined the reference length optically "at the moment of initial deflection of the load recorder pen", taking care that the specimen was in a slightly slack position at the beginning of the experiment. To eliminate uncertainties, due to a possible inhomogeneous deformation pattern in the tissue samples, Missirlis and Chong [1978] determined strains in two or three sections of a specimen, using the previously mentioned ink-dot method. Their results in fact indicated the deformation pattern to be inhomogeneous. For the radial strips they observed a decrease in the strain values from the aortic ring towards the lunulae, this being diametrically opposed to the results of their whole-valve experiments. As an explanation, they stated that in the whole-valve experiments the leaflets at the "zero" pressure state are lightly compressed, folded or buckled near the lunulae. Consequently, strain values in the leaflet region might not only result from distension but also from unfolding of the leaflet in the radial direction near the lunulae.

Often the experimental results are presented in terms of the tangent moduli in the elastin and collagen phases. They are denoted as the low strain modulus E_l and the high strain modulus E_h, respectively (see fig. 3.3). In this approach the curve is assumed to consist of

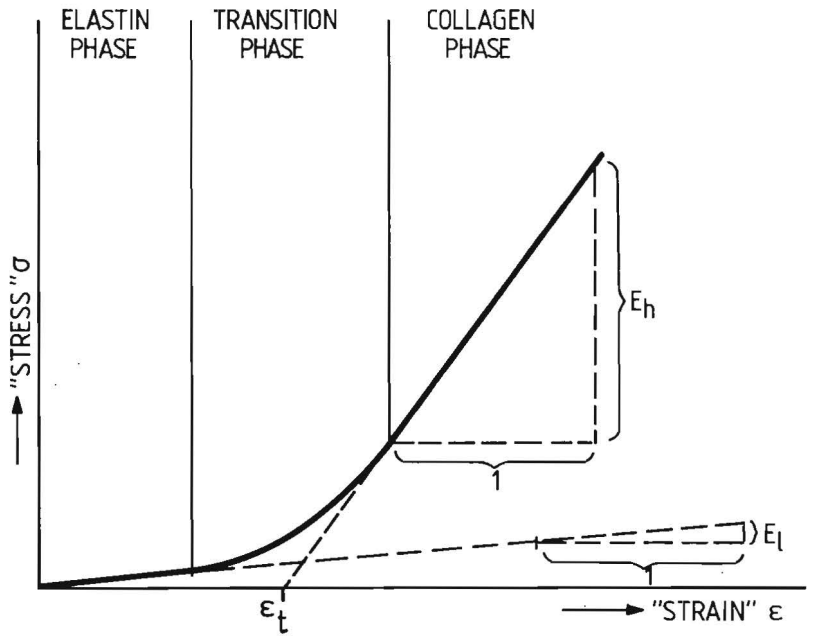

Fig. 3.3.
Definition of the low strain and high strain moduli E_ℓ and E_h, respectively. By ε_t a possible definition of the transition strain is given.

straight portions in the elastin and collagen phases. The ill-defined term "transition strain" is also used by several authors as "the point where the tangent modulus rapidly increases" [Clark and Butterworth, 1971]. Although a more precise definition of this quantity could be formulated in several ways (e.g. by ε_t as shown in fig. 3.3), no such definition was found in literature. The directional designations "transverse" and "circumferential" are used indifferently. Only Missirlis [1973] used "circumferential" in the sense of "parallel with the line of leaflet attachment to the aortic wall" (see fig. 2.1). The data found in literature are summarized in Table 3.1. The highly nonlinear nature of the stress-strain relationships of aortic valve leaflets is emphasized by the great difference between the values of E_l and E_h, found in one study. The marked differences in values of E_h in various directions suggest the existence of significant anisotropy. The compliance of the leaflet

Table 3.1.

Tensile properties of aortic valve tissue. The definitions of E_ℓ, E_h and ε_t are given in fig. 3.3.

	leaflet						sinus				aorta				
	radial			circumferential			axial		circumferential		axial		circumferential		
	E_ℓ [MN/m^2]	E_h [MN/m^2]	ε_t	E_ℓ [MN/m^2]	E_h [MN/m^2]	ε_t	E_ℓ [MN/m^2]	E_h [MN/m^2]	E_ℓ [MN/m^2]	E_h [MN/m^2]	E_ℓ [MN/m^2]	E_h [MN/m^2]	E_ℓ [MN/m^2]	E_h [MN/m^2]	
Clark & Butterworth ['71]*	2.76×10^{-3} – 3.45×10^{-3}	0.17 – 0.69													HUMAN
Clark ['73]	1.12×10^{-2}	1.74	0.24	1.99×10^{-2}	5.98	0.13									
Missirlis ['73]		2.27			3.52		0.10	1.90	0.12	3.54	0.18	2.38	0.24	7.85	
Missirlis & Chong ['78]		1.09	0.60		3.35	0.33									PORCINE
Thubrikar et al. ['78]				0.15	4.7										CANINE
Thubrikar et al. ['80]				0.24	5.2										

* no direction given

tissue in the radial direction is much higher than in the circumferential or transverse directions. Comparison of the data concerning human specimens reveals a broad scatter. Most investigations were performed on leaflet tissue only. Missirlis [1973], however, also incorporated the sinus and aortic walls in his experiments. The data in this table indicate that the behaviour of the human sinus and aortic walls tends to be similar. The sinus tissue appears to be compliant compared with the leaflets and the aortic wall.

In table 3.1 no data on the strength of the leaflet tissue, as reported, for instance by Yamada [1970], are summarized. It is unclear whether such data reflect the proper material behaviour or are governed by edge effects, introduced in the course of preparing and clamping the specimen. Of course, this applies also to other quantities obtained from tensile experiments, which should thus always be considered with caution. However, the relevance of stress-and-strain values at rupture in studying the mechanical properties of a tissue under normal physiological conditions is questionable. This is all the more the case as there are no established criteria which allow a description of the strength of soft tissues in multi-axial-stress situations.

3.4. A brief review of constitutive models for soft tissues

In order to describe the mechanical properties of soft tissues quantitatively, a mathematical framework is needed that is based on a constitutive equation. Such an equation should make it possible to give a concise, well-defined description of the tissue behaviour by using only a few parameters. Likewise it should provide directives for the design of experiments and for data collection. The literature on the subject was reviewed to seek an appropriate model for aortic valve tissue. While making no claim to completeness, this section gives a survey illustrating the variety of constitutive models that have been presented in literature. The demands imposed upon a mathematical model depend largely on the specific aims of the investigation for which the model is used. The mathematical models presented in literature can be roughly divided into two main categories.

Models of the first category try to describe the properties of a

tissue on a macroscopic level, starting from the properties and structure of the microscopic constituent parts. Consequently, their parameters have a distinct physical meaning. Without exception these models are based on the assumption that only the fibrous components transmit forces. The fibre material is always assumed to have linear elastic properties. Lake and Armeniades [1972] proposed a model with a parallel arrangement of elastin fibres and collagen fibril bundles. The elastin fibres were assumed to be of equal length, whereas the lengths of the collagen fibrils were described with a distribution function. Diamant et al. [1972] formulated a mathematical description of the stress-strain curves for rat-tail tendon, modelling a collagen fibre as a zig-zag beam with rigid nodes. Soong and Huang [1973] developed a model to predict tangent moduli of soft tissues and based it on the theory of fibre-reinforced composite materials. They used a stochastic model, formulated in terms of the volume fraction of collagen and elastin fibres and of a "collagen arrival density". Both the collagen and elastin fibres were assumed to be linearly elastic. The collagen arrival density describes the number of collagen fibres participating in force transmission as a function of the overall deformation of the tissue. In this way the nonlinear relation between tangent modulus and strain is introduced. The elastin fibres are assumed to participate in force transmission at all stages of overall deformation of the tissue. Comninou and Yannas [1976] used a long sinusoidal beam and finite-strain beam theory to describe the behaviour of a collagen fibre. A model, not unlike the model proposed by Lake and Armeniades [1972] was presented by Decraemer et al. [1980a]. All these models can only be used for the description of uniaxial stress-strain situations because parallel fibre arrangement is assumed to be present. Lanir [1979] derived biaxial stress-strain relationships for flat tissues. His theory accounts for the different properties of elastin and collagen fibres as well as the degree to which they are interlinked. Material constants and material distribution functions, related to the angular and geometrical nonuniformities of the fibres, are used in the analysis.

The models mentioned thus far concern nonlinear elastic overall properties of soft tissues. Though very useful for gaining insight into the role of the properties and the arrangement of the collagen and elastin fibres with respect to the overall behaviour of the

tissue, they do not take into account viscoelastic phenomena. A linear viscoelastic model for the analysis of the properties of the aortic wall was used by Apter [1964]. Because of the obvious nonlinear characteristics of most soft tissues, this model suffers from a limited applicability when dealing with other tissues. Wijn [1980] developed a nonlinear viscoelastic model for the description of human skin behaviour in the case of small deformations. It consists of fibres with nonlinear viscoelastic properties, viscous effects being accounted for by a linear viscoelastic element.

The constitutive models of the second category are used in the description of tissue behaviour as such, without physical interpretation of the observed phenomena. They are especially useful when the overall mechanical behaviour of biological structures is required in order to formulate specifications, for example, for prosthetic materials.

In some models the elastic properties are described by strain-energy functions [Gou, 1970; Snyder, 1972]. Other investigations describe the elastic stress-strain relationships in terms of polynomial, exponential or power functions [e.g.: Wismans, 1980; Fung, 1967; Kenedi et al., 1975].
Nonlinear viscoelastic properties of soft tissues were described by Viidik [1968] with a model consisting of idealized elements. Three types of elements were used, representing linear elasticity, ideal dry friction and linear viscous friction. Nonlinearly elastic tissue characteristics were simulated by arranging the elastic elements so as to come into subsequent action at various levels of deformation. The result is a discontinuous change in the overall stiffness of the model as a function of deformation. Frisén et al. [1969] developed an alternative formulation of this model. Using a nonlinear continuous function to describe the elastic load-deformation relationship, they ended up with a nonlinear differential equation. Fung [1972] proposed a somewhat similar model, the so-called quasi-linear viscoelasticity law. This model is based on linear viscoelasticity theory, modified so as to describe nonlinear elastic properties by a continuous function. A more comprehensive discussion of this model is presented in section 3.5. Decraemer et al. [1980b] have used Fung's constitutive equation in their fibre model [1980a]. A comparison of the Fung equation with two constitutive equations, derived from

continuum-based theories describing the nonlinear viscoelastic behaviour of polymers, was made by DeHoff [1978]. He showed the equivalence of the two equations to one form of the Fung equation for stress relaxation, whereas different results were predicted for constant-strain-rate tests. In the same way Bingham and DeHoff [1979] characterized the nonlinear viscoelastic properties of the canine anterior cruciate ligament.

In the foregoing some examples were given of the various constitutive models for soft tissues. Two categories were distinguished according to whether the model parameters have a physical meaning or not. Furthermore, a subdivision into elastic and viscoelastic models could be made. It should be noted that nearly all theories discussed in the foregoing are limited to one-dimensional static-strain fields. But, as stated by DeHoff [1978], a constitutive equation that is universally applicable in characterizing soft tissues, should be capable of describing time dependence, anisotropy, nonlinearities and multiaxial stress-strain relationships. In the present state of the art, modelling is confined to one-dimensional strain fields, due to the problems encountered in collecting experimental data on the viscoelastic behaviour of soft tissues under multiaxial loading conditions. In spite of these limitations, one-dimensional constitutive equations are of great value in obtaining insight into tissue behaviour. Besides, they allow quantitative description and may suggest directions for further research. Because of both the obvious nonlinear elastic properties of the valve tissue and the viscoelastic aspects of its behaviour that were to be expected [Lim and Boughner, 1976], a nonlinear viscoelastic model was found suitable for the purpose of the present study. Although desirable, a physical meaning for the model parameters is not strictly necessary. Therefore, the quasi-linear viscoelasticity law proposed by Fung [1972] is chosen.

3.5. The quasi-linear viscoelasticity law

As already stated above the use of a nonlinear viscoelastic constitutive model was considered to be appropriate for the present investigation. The model had to contain a limited number of parameters with values easily determined in experiments. These requirements were met by the so-called quasi-linear viscoelasticity law proposed by Fung [1972]. An additional and important argument in favour of this model were the satisfactory results obtained in describing the behaviour of various soft tissues, such as collagen fibres from rat tail tendon [Haut and Little, 1972], bovine ligamentum nuchae [Jenkins and Little, 1974], cardiac tissue in the passive state [Pinto and Patitucci, 1980], canine aorta [Tanaka and Fung, 1974], rabbit mesentery [Chen and Fung, 1973] and bovine articular cartilage [Woo et al., 1980]. The model is simple, being essentially a modification of linear viscoelasticity theory (a brief outline of linear viscoelasticity theory is presented in Appendix C). In the following pages the essence of the model of Fung will be elucidated.

For a linearly viscoelastic material, the constitutive equation relating stress σ and strain ε [*)] in a one-dimensional strain field can be expressed by the convolution integral:

$$\sigma(t) = \int_{\tau=0}^{t} G(t-\tau) \frac{d\sigma^{(e)}(\varepsilon)}{d\varepsilon} \frac{d\varepsilon}{d\tau} d\tau \qquad (3.3)$$

with $\sigma(t) = 0$ and $\varepsilon(t) = 0$ for $t < 0$,

$G(0) \equiv 1$.

The dependence of stress on both strain and time is separately described by the elastic response $\sigma^{(e)}$ and the reduced relaxation function $G(t)$, respectively. In principle, these two functions can be determined from the stress response $\sigma_{st}(t)$ to a step change of the strain from $\varepsilon = 0$ for $t < 0$ to $\varepsilon = \varepsilon_0$ for $t > 0$ so that

---

*) The choice of the quantities "stress" and "strain" is arbitrary. It should be noted that the theory is equally valid when using other quantities, related to load and deformation, e.g. "force" and "elongation", respectively.

$$\sigma_{st}(t) = G(t)\sigma^{(e)}(\varepsilon_0). \tag{3.4}$$

Because of the definition $G(0) \equiv 1$, the elastic response $\sigma^{(e)}$ can be found from the instantaneous response to step changes with different step magnitudes ε_0 so that

$$\sigma^{(e)}(\varepsilon_0) = \sigma_{st}(0), \tag{3.5}$$

whereas the reduced relaxation function can be determined from

$$G(t) = \frac{\sigma_{st}(t)}{\sigma^{(e)}(\varepsilon_0)} = \frac{\sigma_{st}(t)}{\sigma_{st}(0)} . \tag{3.6}$$

For a linearly viscoelastic material the elastic response $\sigma^{(e)}$ is a linear function of strain. However, as discussed in sections 3.2 and 3.3, the stress-strain relationships of most soft tissues, including aortic valve tissue, are nonlinear. Consequently, a linearly viscoelastic model does not provide a reasonable description of soft-tissue behaviour. To be able to cope with this difficulty, it was proposed by Fung [1972] to represent the elastic response by a nonlinear function of ε. This manipulation is a considerable modification of linear theory, since the use of a nonlinear elastic response makes it impossible to reduce the convolution integral to a differential equation describing the equilibrium of forces within the material. Therefore the convolution integral containing a nonlinear elastic response has in fact to be considered as an empirical formula that has proved to be useful in characterizing the constitutive properties of soft tissues. Although Fung [1972] proposed this concept for soft biological tissues, it is noted that the same approach was already used by Guth et al. in 1946 in describing the results of their experimental work on the stress relaxation of natural and synthetic rubber.

As discussed in Appendix C (section 5), a linearly viscoelastic material will reveal strain-rate sensitivity of σ-ε curves obtained by straining the material at different but constant rates. The stress required to produce a certain strain level will be seen to increase with increasing strain rates. In preliminary constant-strain-rate

experiments with aortic valve tissue we observed, however, a remarkable insensitivity of the load-deflection curves with respect to the strain rate. No significant shift or alteration in shape of these curves was found on varying the strain rate over more than two decades. These observations point in the same direction as the finding of Missirlis [1973] that the high-strain modulus of human aortic valve leaflets is not affected by variation of the strain rate from 0.01 to 0.50 s^{-1}. Similar findings are reported in literature for several other types of soft tissue. Chen and Fung [1973] observed the hysteresis loop of rabbit mesentery to be almost independent of the strain rate within several decades of rate variation. Heart muscle in the passive state has also been found to be insensitive to strain rate [Pinto and Fung, 1973]. The same applies to canine aortic tissue for strain rates, ranging from 0.001 to 1.00 s^{-1} [Tanaka and Fung, 1974] whereas Schwerdt et al. [1980] report the hysteresis loop of human flexor digitorum tendon to be insensitive to the frequency of periodic straining within the range 0.5 to 9 Hz. From dynamical bulge tests on human aortic valve leaflets Lim and Boughner [1976] observed no significant frequency dependence of the loss angle within the range 0.5 - 5 Hz. This means that there will be hardly any variation of the amount of energy dissipation as a function of straining or loading frequency. Energy dissipation is governed by the loss modulus, and is generally a frequency-dependent quantity. In section 4 of Appendix C it is shown that, for a simple linearly viscoelastic model like the standard linear solid, the loss modulus and consequently the amount of energy dissipation will have a maximum at one particular frequency that is determined solely by the relaxation-time constant of the model. Further, it is noted that in characterizing real viscoelastic materials a large number of relaxation-time constants is needed. In these cases fruitful use can be made of a continuous relaxation spectrum (see section 7 of Appendix C). Obviously, the description of many soft tissues requires a loss modulus that shows no sharply defined maximum at one particular frequency, but is rather flat within a certain frequency range. This requirement may be met by choosing a continuous relaxation spectrum like that proposed by Fung [1972] and given below

$$S(\theta)\begin{cases} = \frac{K}{\theta} \text{ for } \theta_1 \leq \theta \leq \theta_2 \text{ (K is a constant)} \\ = 0 \text{ for } \theta < \theta_1 \text{ and } \theta > \theta_2. \end{cases} \tag{3.7}$$

That this approach is not entirely new is shown by the proposal of Neubert [1963] to use a continuous relaxation spectrum of the form: $S(\theta)$ = constant for $\theta_1 < \theta < \theta_2$ and $S(\theta) = 0$ for $\theta < \theta_1$ and $\theta > \theta_2$, in order to describe internal damping in solid materials. The reduced relaxation function of a generalized standard linear solid, having a continuous relaxation spectrum $S(\theta)$, is given by

$$G(t) = \frac{1 + \int_{\theta=0}^{\infty} S(\theta) e^{-\frac{t}{\theta}} d\theta}{1 + \int_{\theta=0}^{\infty} S(\theta) d\theta}, \tag{3.8}$$

whereas, for the storage and loss modulus it applies that

$$E_s(\nu) = C_R\left[1 + \frac{1}{\omega} \int_{\nu=0}^{\infty} \frac{S(\nu)\nu^2}{1+\nu^2} d\nu\right] \tag{3.9}$$

and

$$E_\ell(\nu) = \frac{C_R}{\omega} \int_{\nu=0}^{\infty} \frac{S(\nu)\nu}{1+\nu^2} d\nu, \tag{3.10}$$

where $\nu = \omega\theta$ is a dimensionless frequency, ω denotes the radial frequency and C_R represents the so-called quasi-static stiffness, i.e. the stiffness exhibited by the material under quasi-static load or strain. Substitution of (3.7) into (3.8) to (3.10) inclusive yields

$$G(t) = \frac{1 + K\left\{E_1\left(\frac{t}{\theta_2}\right) - E_1\left(\frac{t}{\theta_1}\right)\right\}}{1 + K \ln\left(\frac{\theta_2}{\theta_1}\right)} \tag{3.11}$$

$$E_s(\nu) = C_R\left\{1 + \frac{K}{2} \ln\left(\frac{1+(\nu_2)^2}{1+(\nu_1)^2}\right)\right\} \tag{3.12}$$

and

$$E_{\ell}(\nu) = C_R K\left\{\arctan(\nu_2) - \arctan(\nu_1)\right\} \qquad (3.13)$$

with: $\nu_{1,2} = \omega\, \theta_{1,2}$

$$E_1(z) = \int_z^{\infty} \frac{e^{-x}}{x}\, dx, \text{ the exponential integral function.}$$

An example of the storage and loss modulus according to (3.8) and (3.9) is given in fig. C8 (Appendix C). The results of an analysis, based upon the reduced relaxation function (3.7), of experimental data obtained from aortic valve tissue are presented in the next chapter.

CHAPTER 4
EXPERIMENTS

4.1. Introduction

In the preceding chapter some of the available data on the mechanical properties of aortic valve tissue were discussed. It appeared that most studies reported in literature were only concerned with the nonlinear elastic properties of the valve leaflets, determined from constant strain rate experiments. Only limited use was made of a mathematical model in analysis and discussion of the results.

In the uniaxial tensile experiments described in the present chapter the mechanical properties of the different valve parts, i.e. the leaflets, the sinus wall and the aortic wall have been dealt with. Tissue strips cut in different directions were investigated. Two aspects of viscoelastic behaviour were examined: the strain rate sensitivity of the stress-versus-strain curves and the relaxation behaviour. In analyzing the relaxation behaviour use was made of the relaxation model proposed by Fung [1972]. The method used for the analysis, is outlined in section 4.2.

During the experiments, care was taken to maintain the applied deformations in the physiological range. To this end the literature on the subject was reviewed (section 4.3). An experimental set-up was developed in which a specimen could be strained at constant strain rates and subsequently kept at a constant elongation (section 4.4). In section 4.5 the test procedure is outlined while the results are presented in section 4.6. Although the stress-versus-strain curves of the various valve parts showed pronounced differences, they were found to be rather insensitive to the strain rate. The relaxation model used proved to be a useful tool in describing the time-dependent material properties (section 4.7).

4.2. Theoretical considerations

In order to give a quantitative description of the relaxation behaviour of the valve tissues, the reduced relaxation function proposed by Fung [1972] (see section 3.5) was used

$$G(t) = \frac{1 + K\left[E_1\left(\frac{t}{\theta_2}\right) - E_1\left(\frac{t}{\theta_1}\right)\right]}{1 + K \ln\left(\frac{\theta_2}{\theta_1}\right)} . \qquad (3.11)$$

with $E_1(y) = \int_{x=y}^{\infty} \frac{e^{-x}}{x} dx$, the exponential integral function.

Strictly speaking, G(t) can only be determined from the load response of the specimen to a step change of the length. As it is physically impossible to realize a true step change, the response to a change in length imposed within a finite time interval t_s (fig. 4.1) was

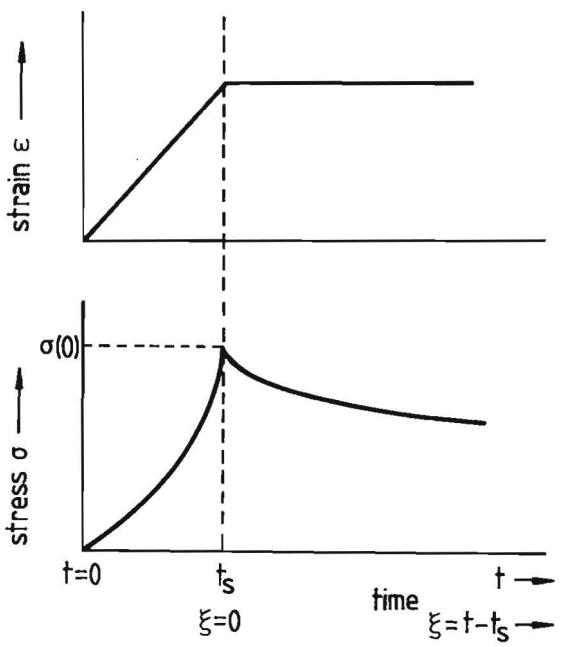

Fig. 4.1.
Time shift used in the analysis of the measurements.

considered. Therefore an "experimental reduced relaxation function" G^* was defined as

$$G^*(\xi) := \frac{\sigma(\xi)}{\sigma(0)} = \frac{1 + K^*\left(E_1\left(\frac{\xi}{\theta_2^*}\right) - E_1\left(\frac{\xi}{\theta_1^*}\right)\right)}{1 + K^* \ln\left(\frac{\theta_2^*}{\theta_1^*}\right)} \tag{4.1}$$

with $\xi := t - t_s \quad \text{for } t \geq t_s$.

In preliminary experiments it was found that the main part of the relaxation took place in the first 100 seconds of $t = t_s$, i.e. for $\xi < 100$ s. In most cases the load decay for $\xi > 100$ s was hardly measurable. The approximation

$$G^*(\xi \to \infty) \simeq G^*(\xi \simeq 120 \text{ s}) \tag{4.2}$$

was therefore assumed to be reasonable. In assessing values of K^*, θ_1^* and θ_2^* the following method was used (see also fig. 4.7): starting from expression (4.1) for the reduced relaxation function and using

$$G^*(\infty) := G^*(\xi \to \infty) = \left(1 + K^* \ln\left(\frac{\theta_2^*}{\theta_1^*}\right)\right)^{-1} \tag{4.3}$$

the constant α and the function $H(\xi)$ are defined as

$$\alpha := \ln\left(\frac{\theta_2^*}{\theta_1^*}\right) \tag{4.4}$$

$$H(\xi) := \frac{G^*(\xi) - G^*(\infty)}{1 - G^*(\infty)} = \frac{E_1\left(\frac{\xi}{\theta_2^*}\right) - E_1\left(\frac{\xi}{\theta_1^*}\right)}{\alpha} . \tag{4.5}$$

If $\theta_1^* << \xi << \theta_2^*$, the following approximation applies

$$\alpha H(\xi) \simeq E_1\left(\frac{\xi}{\theta_2^*}\right) \simeq -\gamma - \ln\left(\frac{\xi}{\theta_2^*}\right), \tag{4.6}$$

where the series expansion of $E_1\left(\frac{\xi}{\theta_2^*}\right)$ has been employed and γ is the Euler's constant. From (4.6) it is seen that $H(\xi)$ can be approximated

by a linear function of $\ell n(\xi)$ in the range $\theta_1^* << \xi << \theta_2^*$. Introducing a scaling factor T with $\theta_1^* << T << \theta_2^*$ and defining

$$X = \ell n\left(\frac{\theta_2^*}{T}\right) - \gamma \tag{4.7}$$

(4.6) can be written as

$$\alpha H(\xi) = -\ell n\left(\frac{\xi}{T}\right) + X. \tag{4.8}$$

Using an interactive computer program, on a visual display the straight portion of the $H(\xi)$-versus-$\ell n(\xi)$ curve was specified by choosing two values ξ_1 and ξ_2 at its beginning and end, respectively (an example of such a plot is given in fig. 4.7a). With the scaling factor T in the range $[\xi_1, \xi_2]$ and using (4.7) and (4.4), the constants θ_2^* and θ_1^* were found from

$$\theta_2^* := T \exp(\gamma + X) \tag{4.9}$$

$$\theta_1^* := \theta_2^* \exp(-\alpha). \tag{4.10}$$

Finally, the value of K^* results from (4.3) and (4.4) together with the assumption (4.2), that is

$$K^* := \left(\frac{1-G^*(\infty)}{G^*(\infty)}\right)\alpha^{-1}. \tag{4.11}$$

4.3. Physiological values of strain

In order to obtain relevant information from the experiments, the load and deformation values should be in the physiological range. As the specimen length is the controlled variable in our experiments, we will mainly discuss strain values as determined under physiological circumstances.

In *in vivo* experiments on dogs Brewer et al. [1977] studied the length variations in the leaflet lunula along its free edge during the cardiac cycle. Using the length in diastole at 10.7 kPa pressure difference across the valve as a reference, they observed a strain of

about 0.02 from the beginning to the end of diastole (fig. 2.11). Between the end of diastole and peak systole a shortening in the same order of magnitude was found. As discussed in section 3.3, Missirlis and Chong [1978] investigated local strains in porcine valve leaflets when pressurizing (16 kPa) an entire aortic root *in vitro*. In the load-bearing leaflet portion they observed strains ranging from 0.05 to 0.1 in the circumferential direction and from 0.1 to more than 1.0 in the radial direction. From *in vivo* experiments on dogs Thubrikar et al. [1980] concluded that the leaflet length of the load-bearing portion in the circumferential direction decreased by about 10% from diastole to systole. Pressure differences across the valve ranged from about 13 kPa to 24 kPa.

In presenting typical stress-strain curves for human aortic and sinus tissue, Missirlis [1973] considered the range between 0.5 and 0.7 as the physiological range of strains (axial and circumferential) in these tissues. In comparison with the data reported by other authors, these values seem rather high. In *in vitro* experiments on pressurized human and porcine valves Trenkner et al. [1976] observed circumferential strains of about 0.4 in the aortic wall at the level of the commissures, the pressure difference across the valve being about 14 kPa. Similar findings were reported by Swanson and Clark [1974] for human valves.

No values for the strain in the axial direction in the aortic wall were given by the above mentioned authors. We therefore performed a simple experiment to get some information on the order of magnitude of these values. Using the set-up described in section 2.3.2, two entire porcine aortic roots in a 0.9% saline solution were pressurized at pressures up to 16 kPa. Pressure increments of about 4 kPa were applied slowly (about 10 seconds per increment) whereupon the pressure was kept constant for several minutes. Using a cathetometer, strains were determined from the changes in distance between two pairs of ink dots deposited at a distance of about 5 mm from each other on the aortic wall in the unloaded situation. The circumferential and axial strains were found to be about 0.4.

From the above-mentioned data it was decided to use strain values of about 0.1 for leaflet strips cut in the circumferential direction.

Strains of 0.4 to 0.5 were imposed when testing radial leaflet strips as well as circumferential and axial strips from the sinus and aortic walls.

Hardly any data could be found in literature on the physiological range of strain rates in the valve tissue. Only Missirlis [1973] gave an estimate of the strain rate to be expected in the leaflets. On the assumption that valve closure takes place within 0.04 seconds and that the strains in the leaflets are about 0.1 he found a strain-rate value of 2.5 s^{-1}.

4.4 Experimental set-up

All specimens used in the experiments were strips approximately 3 mm in width and varying from 10 to 20 mm in length. The average thickness of the leaflet, sinus and aortic strips was, respectively, 0.5, 2.1 and 3.1 mm. They were obtained with a cutter having two parallel razor blades.

The design of the clamping equipment allowed the specimen to be mounted outside the actual experimental set-up (see fig. 4.2). Before mounting the specimen, the aluminium clamps were fixated in a holder. A parallel strip of known dimensions which was part of the holder, kept the jaws at a known distance from one another. On mounting the specimen care was taken to prevent tensile forces in the specimen by ensuring a slack configuration of the tissue strip. The specimen was clamped between jaws with milled surfaces. The two surfaces of each jaw matched each other, the tops of the notches being rounded so as to restrict damage to the tissue. The holder, clamps and specimen were then mounted in the actual testing apparatus. After removal of the holder the elongation of the specimen was continuously measured. An outline of the total experimental set-up is given in fig. 4.3.

Load was measured with a piezoelectrical load cell (Kistler type 9203, measurement error $\leq \pm$ 3% of the actual load value). For the measurement of the elongation of the specimen, i.e. the displacement of the moving clamp, a capacitive displacement-measuring system (Boersma CVM VI; measurement error $\leq \pm$ 2 μm) was used. The displacement of the moving clamp (the lower one, see fig. 4.3) was induced by a electrodynamic exciter (Ling Dynamic, type 200). In the experiments the exciter was controlled by the output signal of a ramp generator. The principle of this device is the conversion of square

pulses produced by an oscillator (Krohn-Hite, model 4100), into analog voltage increments. In this way an analog ramp signal was generated,

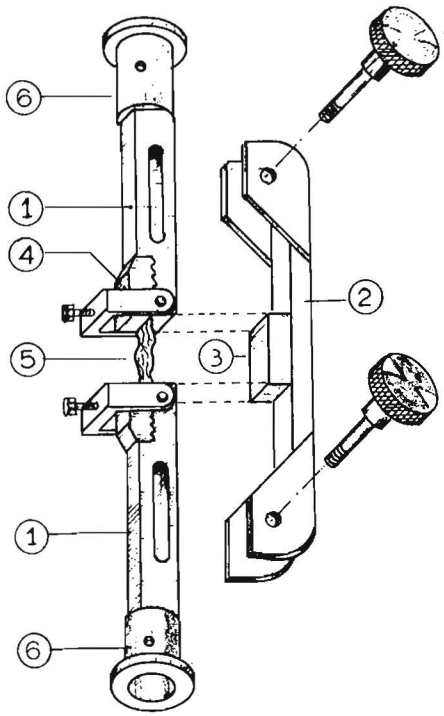

Fig. 4.2.
Clamping equipment used in the experiments.
1: aluminium clamp; 2: brass holder; 3: parallel strip, keeping the end surfaces of the jaws (4) at a known distance when the clamps are fixated in the holder; 5: specimen; 6: tapes for mounting the clamping equipment in the testing apparatus.

the slope of which could be chosen by adjusting the frequency of the pulse generation. The maximum value of the ramp signal was adjusted by setting a comparator to the desired value. Once this value had been reached, the level of the analog output signal was kept constant. The analog signals representing force and elongation were recorded on magnetic tape together with a trigger signal, using an instrumentation recorder (Hewlett-Packard, type 3968A). During an experiment the signals were visualized on the display of an oscilloscope (Tektronix type 7313). After digitizing and pre-processing the signals on a MINC-11 minicomputer, the final analysis of the data was done on a Burroughs B8700 computer.

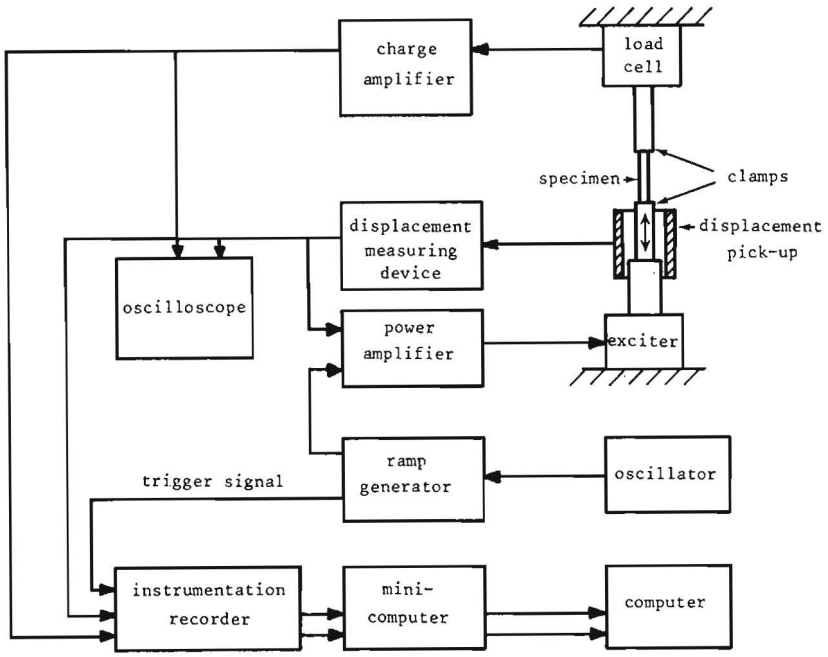

Fig. 4.3.
Outline of the experimental set-up.

4.5. Testing procedure

The experiments were conducted on porcine aortic valve tissue. Prior to a test series the tissue was preserved in a 0.9% saline solution at 10°C. All specimens were tested within 8 hours after death of the animal. The experiments were performed at room temperature, the tissue being kept in a wet condition by physiological saline dripping on it. After mounting as described in section 4.4 the specimen was elongated so that approximately physiological strain values were reached (see section 4.3). During the experiments, the specimen length corresponding to this first elongation was never exceeded. On returning slowly (within about one minute) to the unloaded configuration of the tissue strip, the reference length ℓ_{ref} was determined as the length at which the load was seen to be zero from visual inspection of the force signal displayed on the oscilloscope screen using a high sensitivity.

Subsequently the specimen was "preconditioned" in ten loading and unloading cycles between the reference length and the predetermined elongation level. These cycles were followed by a 120-second rest period.

The meaning of this preconditioning is still rather vague; it is probably required to rearrange tissue structures, which are disturbed during the process of preparing and mounting the specimen. In literature the effects due to the preconditioning process, often are confounded with the actually viscoelastic aspects of the material properties of soft tissues. In previous experiments in our laboratory the preconditioning phenomenon was studied [Rousseau, 1980]. The main requirement for establishing repeatable characteristics was found to be not to exceed the first elongation in subsequent cycles. It was observed that aortic valve tissue is then preconditioned after a series of ten cycles maximum. The preconditioning phenomenon turned out to be insensitive to the rate of loading and unloading.

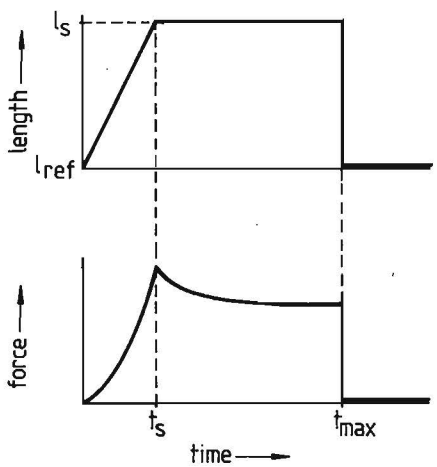

Fig. 4.4.
The specimen length as a function of time and the corresponding load response in one experiment.

After the preconditioning procedure the actual experiments were started. They involved straining of the specimen at a constant velocity of the moving clamp, followed by maintaining the specimen length at a predetermined level ℓ_s (fig. 4.4) for 120 - 140 seconds (see also section 4.2). Between two successive experiments a resting period of 120 - 140 seconds was maintained, with the specimen at the

reference length. All experiments on a specimen were performed within one hour, during which period no significant alterations in the response of the specimen were observed. After a series of experiments, the thickness and width of the specimen, taken out of the clamps, were determined using a microscope with a calibrated eyepiece and a micrometer.

4.6. Results

4.6.1. Introduction

Specimens excised from the non-coronary region of 6 valves were investigated. From the histological observations, discussed in the sections 2.3.3 and 2.3.4, in the different valve parts different mechanical properties were expected. Three tissue strips were therefore taken from each valve: from the leaflet, the corresponding sinus wall and the adjacent portion of the aortic wall. Specimens were cut out of three valves in the circumferential direction, in the three others radial leaflet strips and axial sinus and aortic strips were taken (for the definitions of the directions see fig. 2.1). The circumferential leaflet strips were taken just below the lunula and the radial strips along the line of leaflet symmetry. The circumferential sinus strips were cut at the level of the commissures and the axial strips along the line of symmetry of the sinus. The axial aortic and sinus strips were cut along the same symmetry line. The circumferential aortic specimens were taken just above the top of the sinus wall (fig. 2.1).

The strain definition used in analyzing the results was

$$\varepsilon = \frac{\ell - \ell_{ref}}{\ell_{ref}} , \tag{4.12}$$

where ℓ is the length at a given moment. The stress σ was defined by

$$\sigma = \frac{F}{A} \tag{4.13}$$

where F represents the force on the specimen and A the cross-sectional area of the unloaded specimen, measured after conclusion of the experiments.

4.6.2. The σ-ε characteristics of the various valve parts

Figure 4.5 gives some characteristic σ-ε curves obtained from specimens tested at constant strain rates. In the circumferential direction (fig. 4.5a) there was a remarkable difference between the characteristics of the leaflet tissue on the one hand and the sinus and aortic tissue on the other. The slope of the leaflet curve rapidly increased with increasing strain and became almost constant for strain values greater than 0.05. The curves of the sinus and the aortic tissue were similar. They showed only a slight increase in slope with increasing strain. The slope of the almost linear phase of the leaflet curve was greater by about a factor 30 than the average slope of the curves of the sinus and the aorta. The differences between the characteristics of the specimens cut from one valve in the axial (sinus and aorta) and the radial (leaflet) direction (fig. 4.5b), were less pronounced than the differences when the specimens were cut in the circumferential direction. Nevertheless, the slope of the curve of the radial leaflet specimen shows the most rapid increase with increasing strain. A comparison of the curves in figures 4.5a and 4.5b shows that the stress values needed to produce a certain strain in the leaflet tissue were much lower in the radial than in the circumferential direction. The aortic and sinus tissues showed no pronounced differences in their stress-strain characteristics both in the circumferential and axial directions. The possible relations of these results to the histological observations (section 2.2) will be discussed in the next section.

In most cases the σ-ε curves of the various valve parts were found to be only slightly sensitive to the strain rate $\dot{\varepsilon}$. The force needed to produce a certain strain, showed a relatively slight increase with increasing strain rate. The experiments in which the highest rate sensitivity was observed, are shown in figure 4.6.

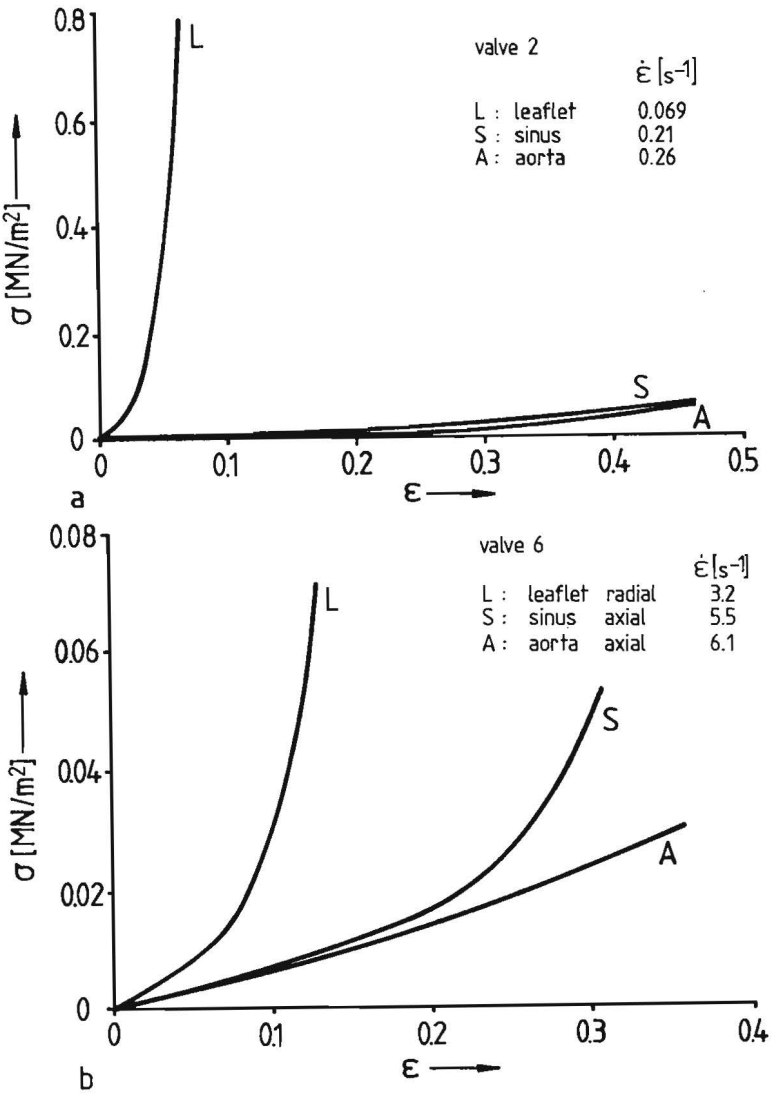

Fig. 4.5.
Stress-strain characteristics of the various parts of one valve: a: circumferential direction; b: axial (radial) direction. Note the different scaling factors in a. and b.

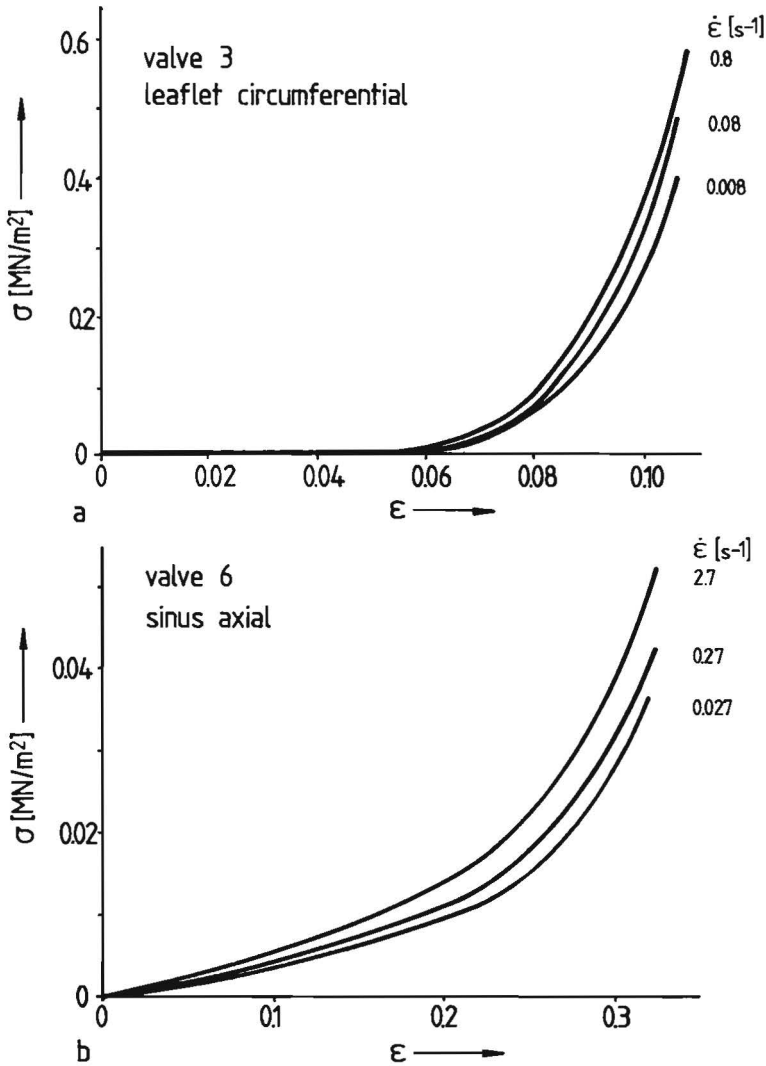

Fig. 4.6.
Stress-strain characteristics for different constant strain rates:
a: leaflet circumferential; b: sinus axial.

4.6.3. The relaxation behaviour of the various valve parts

In all the specimens tested, relaxation phenomena were observed when the length of the specimens was kept fixed after a certain amount of stretch had been applied.

The relaxation phenomena were analyzed by determining the parameters K^*, θ_1^* and θ_2^*, using the method outlined in section 4.2,

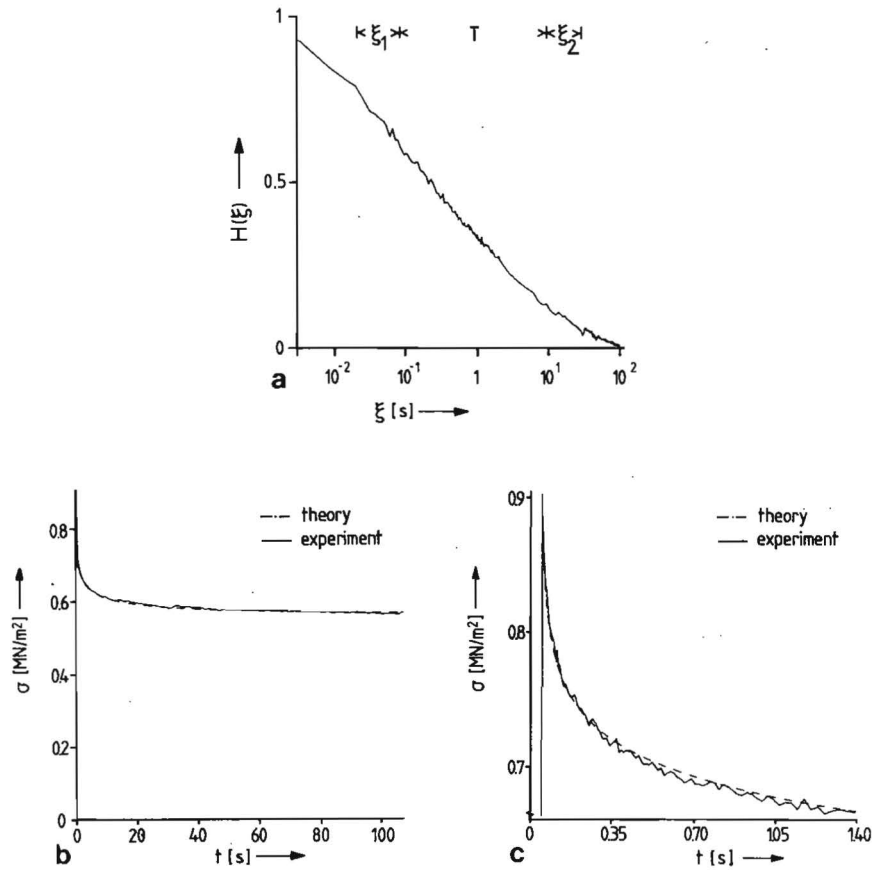

Fig. 4.7.
a. H(ξ) as defined by (4.5) and calculated from measurement data.
b. Experimental and theoretical relaxation curves over 100 seconds.
c. Zoom plot of the first 1.4 seconds of fig. 4.7b.

Table 4.1.
Relaxation parameters K^*, θ_1^* and θ_2^* according to (4.1) as obtained in 13 experiments on tissue strips from the various valve parts and cut in different directions. The mean values of 3 series of measurements in one experiment are given (unless otherwise stated). The numbers in italics represent the average of the means. Between parentheses the total range covered by the individual values is stated.

Valve part and direction	θ_1^*(s)	θ_2^*(s)	K^*	G^*(120s)	rise time t_s (ms)	Valve
Leaflet circumferential	0.0005	128	0.0804	0.499	59	1
	0.0026	36	0.0610	0.631	51	2[1]
	0.0025	67	0.0852	0.534	74	3
	0.0019	*77*	*0.0755*	*0.555*		
	(0.0003 - 0.0035)	*(32-133)*	*(0.0575 - 0.0877)*	*(0.489 - 0.633)*		
Leaflet radial	0.0004	30	0.0859	0.517	116	4[1]
	0.0001	76	0.0894	0.578	57	6[2]
	0.00025	*53*	*0.0877*	*0.548*		
	(0.0001 - 0.0007)	*(24 - 76)*	*(0.0827 - 0.0894)*	*(0.495 - 0.578)*		
Sinus wall circumferential	0.0320	386	0.0367	0.742	244	3
	(0.0144 - 0.0488)	*(259 - 493)*	*(0.0358 - 0.0384)*	*(0.732 - 0.755)*		
Sinus wall axial	0.0007	17	0.0448	0.688	108	4
	2.9×10^{-5}	68	0.0445	0.611	45	5
	0.0001	36	0.0584	0.580	63	6
	0.0003	*40*	*0.0492*	*0.626*		
	(2.4×10^{-5} - 0.0007)	*(14 - 140)*	*(0.0426 - 0.0602)*	*(0.574 - 0.688)*		
Aortic wall circumferential	0.0002	187	0.0395	0.646	94	2
	0.0006	51	0.0525	0.628	120	3
	0.0004	*119*	*0.0460*	*0.637*		
	(0.0001 - 0.0007)	*(45 - 190)*	*(0.0380 - 0.0546)*	*(0.620 - 0.655)*		
Aortic wall axial	0.0012	22	0.0334	0.752	88	5
	3×10^{-5}	182	0.0228	0.737	68	6
	0.0006	*102*	*0.0281*	*0.744*		
	(2.7×10^{-5} - 0.0014)	*(15 - 204)*	*(0.0220 - 0.0340)*	*(0.730 - 0.756)*		

[1] only two series of measurements available; [2] only one series of measurements available.

and the theoretical and experimental findings were compared. From 30 sets of ξ_1, ξ_2 and T-values (see section 4.2), chosen in the ranges indicated in figure 4.7a, the following mean values and standard deviations (between parentheses) were found in this particular case (valve 2, circumferential leaflet strip): $\theta_1^* = 0.0029$ s (0.0004), $\theta_2^* = 37$ s (4), $K^* = 0.0624$ (0.0016). The agreement between the experimental and theoretical curves is demonstrated in figures 4.7b and c.

Relaxation data, obtained from measurements on 13 specimens, are listed in Table 4.1. The values of t_s ranged from 50 to 250 milliseconds. The order of magnitude of the θ_1^* values was 10^{-2} s for

the sinus in the circumferential direction and 10^{-3} s for both the leaflets in the circumferential direction and the aortic wall in the axial direction. θ_1^*-values in the order of magnitude of 10^{-4} s were observed for the radial direction in the leaflets and in the other valve parts in both directions. The values of θ_2^* showed no tendencies which allowed for a differentiation as to valve part and direction. The θ_2^*-values were in the order of magnitude of 10 to 100 s, the actual values showing a broad scatter.

As to the long-term relaxation behaviour ($G^*(\xi=120s)$), a difference was seen between the leaflet tissue and the other valve parts. Within some 120 seconds of a certain elongation with a high strain rate being applied, the load on both the radial and the circumferential leaflet strips showed a decrease of some 45% of its initial value at $\xi = 0$. For the strips of the aortic and sinus walls this decrease ranged from about 25% to 37%. This difference was also reflected by the values of K^*. For the leaflet tissue they ranged from about 0.061 to 0.089, whereas for the other valve parts values were found, ranging from 0.023 to 0.058.

4.7. Discussion

4.7.1. The σ-ε characteristics

The strains used in the experiments in the present study are summarized in Table 4.2. These data show that the used strain values were within the physiological ranges (see section 4.3).

Table 4.2.
Ranges of the maximum strains used in the experiments.

Leaflet		Sinus		Aorta	
radial	circumf.	axial	circumf.	axial	circumf.
0.18 - 0.47	0.07 - 0.11	0.34 - 0.59	0.49	0.42 - 0.57	0.41 - 0.49

The σ-ε characteristics, shown in figure 4.5, agree fairly well with the assumptions based upon the histological structure (section 2.3.4). To produce a certain strain, a considerably larger stress is required in the leaflets than in the aortic and the sinus walls which was

expected from the high elastin content in the latter. The characteristics of the leaflet tissue show a directional dependency, reflecting the stiffening function of the mainly circumferentially oriented collagen bundles. Already at small strains the slope of the circumferential σ-ε curves becomes steep and approximates the value reported for collagen fibres [Haut and Little, 1972] as will be seen in the following. The radial σ-ε curves show much more the typical three-phase characteristic as outlined in fig. 3.1. The increase of their slope with increasing strain can be explained by the fact that the collagen bundles are not exactly oriented in the circumferential direction, thus gradually more contributing to force transmission with increasing strain. However, even the largest slopes of the radial curves are much smaller than those of the circumferential σ-ε characteristics. In the present investigation no marked differences were observed between the σ-ε characteristics of tissue strips, taken in different directions from the aortic and sinus walls. This is in agreement with the histological observation that there is no preferred orientation of the elastin fibres in the sinus wall.

In all valve parts the stress at a given strain was only slightly influenced by the strain rate. A hundredfold increase of the strain rate resulted in an increase of the stress in a circumferential leaflet strip and an axial sinus strip of 50 (at $\varepsilon = 0.1$) and 40% (at $\varepsilon = 0.3$), respectively (fig. 4.6). In the greater part of the experiments significantly less variations in stress were found when the strain rate was varied over two decades or more. These observations indicate that the aortic valve tissue is rather insensitive to the strain rate.

Fig. 4.8 shows the largest slopes of the σ-ε curves measured in the present investigations. In Table 4.3 they are tabulated together with similar data for porcine and human specimens as reported by Missirlis and Chong [1978] and Missirlis [1973], respectively. The circumferential leaflet specimens exhibit the largest slope, 20 to 40 MN/m^2, at relatively small strains ($\varepsilon \approx 0.1$). These values are about a factor 10 larger than the corresponding values found in the literature (Table 4.3). The values found in the present work agree rather well with the value of 45 MN/m^2, determined from the data of Haut and Little [1972] as the average slope of the σ-ε curves of collagen fibres. This indicates that the circumferential leaflet

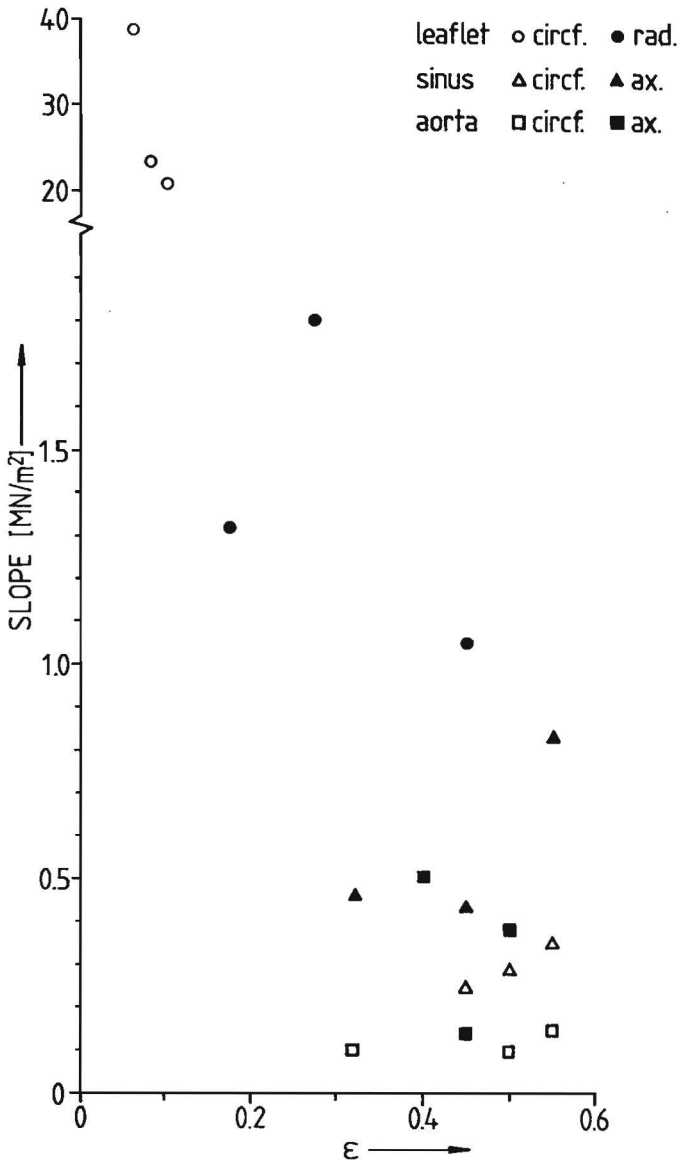

Fig. 4.8.
Maximum slopes of the measured σ-ε curves (note the change of the scaling factor on the vertical axis).

specimens exhibit mainly the properties of the collagen bundles as was expected from the histological observations (section 2.3.4). The leaflet tissue is much more compliant in the radial direction. The slopes of the σ-ε curves agree fairly well with similar data in literature (Table 4.3). The curves for the sinus and aortic tissues

Table 4.3.
Slopes (MN/m^2) of the σ-ε curves of aortic valve tissues.

	leaflet		sinus		aorta		
	circf.	radial	circf.	axial	circf.	axial	
this work[1)]	20 - 40	1.0 - 1.8	0.5 - 0.65	0.4 - 0.8	0.1 - 0.15	0.1 - 0.5	porcine valve
Missirlis & Chong [1978][2)]	3.35	1.09					porcine valve
Missirlis [1973][2)]	3.52	2.27	0.12	0.10	0.24	0.18	human valve

[1)] the corresponding strains are given in fig. 4.8; [2)] no strains given.

show no evident directional dependency with respect to their slopes. From Table 4.3 it is seen that the slopes of the sinus curves, found in the present work, are a factor 4 to 8 larger than those reported for human sinus tissue [Missirlis, 1973]. Our values for the aortic wall agree fairly well with similar data on human aortic tissue. Hass [1942] reported a tangent modulus (slope of the σ-ε curve) of 0.3 MN/m^2 for elastic tissue, isolated from the human aortic wall. The values in Table 4.3 for the intact aortic wall as well as the sinus wall indicate that the characteristics of these tissues are mainly governed by their elastic components.

Despite the similarities of the trends which can be seen in our results and the data in literature, the discrepancies between the numerical values are often substantial. This applies especially to the leaflet tissue. A comparison of the σ-ε curves as such of aortic leaflet tissue, obtained in the present investigation, with similar data in literature reveals considerable differences (figs. 4.9 and 4.10). Apart from the "physiological spread", these differences may result from such factors as uncertainties involved with the

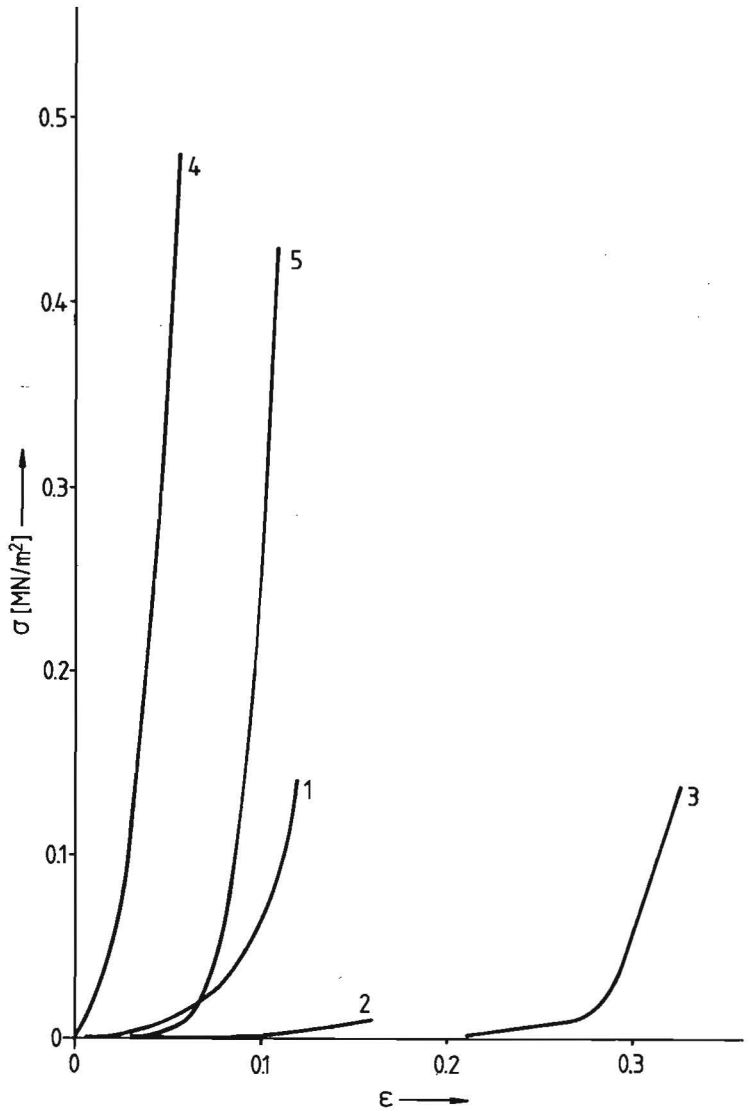

Fig. 4.9.
σ-ε characteristics of circumferential aortic leaflet specimens. 1: Missirlis [1973], human valve; 2: Clark [1973], human valve; 3: Missirlis and Chong [1978], porcine valve; 4: this study; valve 2 ($\dot{\varepsilon}$ = 0.069 s^{-1}); 5: this study, valve 3 ($\dot{\varepsilon}$ = 0.008 s^{-1}).

definitions of stress and strain (see also section 3.3) and clamping effects.

The stress definition used,

$$\sigma = \frac{F}{A} \quad (F: \text{force; } A: \text{cross-sectional area}) \tag{3.1}$$

is significant only if the force F leads to a homogeneous stress

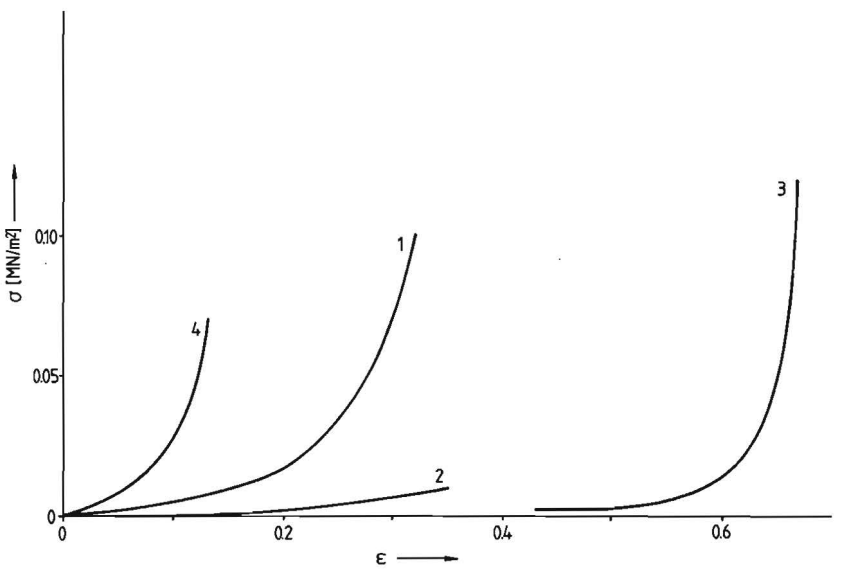

Fig. 4.10
σ-ε characteristics of radial aortic leaflet specimens.
1: Missirlis [1973], human valve; 2: Clark [1973], human valve; 3: Missirlis and Chong [1978], porcine valve; 4: this study, valve 6 ($\dot{\varepsilon} = 3.2\ s^{-1}$).

distribution over the cross-sectional area A. It is questionable whether this applies when testing leaflet strips, taking into account their coarse bundle structure. Moreover, the effect on the σ-ε characteristics of cutting bundles in preparing the specimen is not known. Another source of uncertainty involved in the computation of stresses is the cross-sectional area. In the present investigation the cross-sectional area was computed using the mean thickness and width as determined from measurements at 5 to 8 positions in the unloaded specimen after performing all experiments on that specimen. In the leaflet and sinus specimens standard deviations of 10% of these mean values were observed. The stress values should therefore be considered with caution.

The strain values computed according to the definition

$$\varepsilon = \frac{\ell - \ell_{ref}}{\ell_{ref}} \tag{3.2}$$

depend strongly on the reference length ℓ_{ref}. In earlier investigations on aortic valve tissue [Sauren and Van Hout, 1979] it was observed that a permanent elongation always resulted from the first stretch. This elongation was in the order of magnitude of 5 to 10% of the length at which the load-measuring device showed application of load on the specimen. In the present experiments the reference length was determined after applying an initial elongation (see section 4.5). In this way the permanent elongation contributed to the reference length and thus was accounted for in the strain computations.

Finally it is noted that, in consequence of the inhomogeneous tissue structure as well as clamping effects, the strain in a segment away from the clamped ends is likely to differ from the end-to-end strain, as was observed, for instance, by Pinto and Patitucci [1980] in rabbit papillary muscle.

4.7.2. The relaxation behaviour

At first sight, the values of θ_1^* for the leaflet tissue in the circumferential and radial directions differ by one order of magnitude. The higher values are observed in the circumferential direction. In view of the broad scatter in the θ_1^*-values in the radial

direction, however, more experiments are needed to decide whether this parameter is direction-dependent. The values of $G^*(\infty)$ reveal no pronounced differences. In any case, the directional dependence of the viscoelastic behaviour of the leaflet tissue is negligible in comparison with that of the elastic behaviour found in the constant strain rate experiments. This could point to a negligible importance of the collagen-bundle structure with respect to the time-dependent behaviour of the leaflet tissue.

Among the different valve parts, the leaflets tend to reveal the greatest relaxation. This might be explained as follows. Considering the histological structure of the leaflets on the one hand and the sinus and aortic wall on the other, two marked differences can be observed. The leaflet tissue contains many more collagenous components and there is a loosely structured layer in this tissue. As was stated before, the collagenous components are not very likely to govern the time-dependent behaviour. The presence of the loosely structured layer, however, might allow a repositioning of the collagenous and elastic fibre networks with respect to each other as well as a rearrangement of fibres within each network. In addition to fluid movements between the fibres, these two mechanisms might account for the more pronounced relaxation observed in the leaflets.

As to the values of θ_1^* for the sinus and the aortic tissue, it should be noted that for the sinus wall only one experiment on a circumferential strip was available and that the values for the axial strips show a broad scatter. It is therefore difficult to decide from the available data whether the sinus and aortic tissues show evident differences in their time-dependent behaviour with respect to each other as well as to the directions.

Relaxation parameters, as found in literature for different tissues and in the present work for aortic valve tissue, are summarized in Table 4.4. The parameter values for the different tissues vary greatly. The values for canine aorta, reported by Tanaka and Fung [1974], are most suitable for a comparison with the data for the aortic and sinus walls found in the present investigation. The order of magnitude of the K^* values for canine aorta agree remarkably well with that of the values for the porcine sinus and aortic walls found in the present study.

The θ_1^*-values, on the contrary, differ significantly. For the

Table 4.4.
Relaxation parameters as found in literature for various tissues and in the present study for aortic valve tissue.

	θ_1^*(s)	θ_2^*(s)	K^*	t_s (ms)	tissue	
Chen and Fung [1973]	1.7352×10^{-5}	1.8693×10^{4}	0.02657	-	rabbit mesentery	
Tanaka and Fung [1974]	0.367	434	0.0424	-	arch circf.[1]	canine aorta
	0.431	451	0.0311	-	arch axial	
	0.260	192	0.0399	-	prox.thor.[2] circf.	
	0.137	93.9	0.0297	-	prox.thor.axial	
Woo et al. [1980]	0.006	8.38	2.02	250	articular cartilage	
Pinto and Patitucci [1980]	0.015	1058	0.093	100	rabbit papillary muscle	
	0.020	3151	0.081	100	cat papillary muscle	
this study[3]	0.0019	77	0.0755	61	leaflet circf.	porcine aortic valve
	0.00025	53	0.0877	86	leaflet radial	
	0.0320	386	0.0367	244	sinus circf.	
	0.0003	40	0.0492	72	sinus axial	
	0.0004	119	0.0460	107	aorta circf.	
	0.0006	102	0.0281	78	aorta axial	

[1] circumferential; [2] proximal thoracic; [3] average values of the means in Table 4.1 are given.

canine aortic arch and the proximal thoracic aorta these values were reported to be in the order of magnitude of 10^{-1} s, whereas values of 10^{-4} s were found for the sinus and aortic walls. The simplest explanation for this difference is that these values reflect the actual differences in the time-dependent properties of these tissues. Apart from this possibility they might be due to different rise times used in performing the experiments. As discussed in section 6 of Appendix C, the longer the rise time, the less relaxation will be observed during the phase of constant elongation. Unfortunately, data on the rise times used by Tanaka and Fung [1974] are not available.

As to the θ_2^*-values, no clear trends are observed. In the case of the canine aorta as well as the porcine aortic valve they show a wide spread. In this regard some remarks have to be made on the method

used to determine the θ_1^* and θ_2^* values. As stated by equation (4.10), θ_1^* can be determined only if θ_2^* is known, so inaccuracies in θ_1^* will, at least partly, be governed by those in θ_2^*. This is a disadvantage of the method followed in the present study. It should be noted, however, that the parameters θ_1^* and θ_2^* correspond to experiments where the specimen length is not a step function of time. Thus θ_1^* and θ_2^* are only approximations of the parameters θ_1 and θ_2 which describe the response to a true step change in the length. Because of the approximative character of θ_1^* and θ_2^* the advantage of the simplicity in their determination was considered to outweigh the above-mentioned disadvantage.

Assuming linearly viscoelastic properties, Lim and Boughner [1976] determined the loss angle ϕ in human aortic valve leaflets by applying sinusoidal pressure variations at frequencies between 0.5 and 5 Hz. This loss angle ϕ governs the description of the viscous losses during sinusoidal straining. From the definition of the loss angle (see also section 3 of Appendix C)

$$\phi = \arctan\left(\frac{E_\ell}{E_s}\right) \tag{4.12}$$

and using (3.9) and (3.10) for the storage and loss modulus E_s and E_ℓ, respectively, an indication as to the frequency-dependent behaviour of the aortic valve tissue can be obtained. Figure 4.11 illustrates the ϕ values for the aortic valve tissues computed in this way together with the values reported by Lim and Boughner [1976]. In the calculations the following relaxation-parameter values were chosen as being representative

	$\theta_1^*(s)$	$\theta_2^*(s)$	K^*
Leaflet	10^{-3}	10^{2}	0.08
Sinus and aortic wall	10^{-4}	10^{2}	0.04

The ϕ-values for the leaflet tissue, predicted by the present relaxation model, are twice as large as those reported by Lim and Boughner [1976]. Comparison of the predicted values for the leaflets on the one hand and the sinus and aortic walls on the other, indicates that the largest viscous losses are to be expected in the leaflet

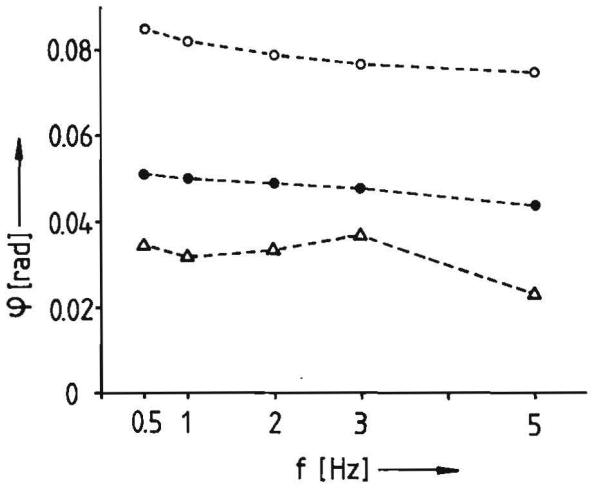

Fig. 4.11.
The loss angle ϕ as predicted by the relaxation model used in the present study and measured values, reported by Lim and Boughner [1976].
o porcine leaflet: $\theta_1^* = 10^{-3}$ s; $\theta_2^* = 10^2$ s; $K^* = 0.08$.
• porcine sinus and aortic walls: $\theta_1^* = 10^{-4}$ s; $\theta_2^* = 10^2$ s; $K^* = 0.04$.
Δ human leaflet [Lim and Boughner, 1976].

tissue. This is consistent with the greater stress relaxation in the leaflets as observed in our experiments. It should be noted, however, that a proper investigation of the frequency-dependent behaviour should include sinusoidal-straining experiments in order to test these conclusions.

The general conclusions to be drawn from the foregoing are: The elastic properties of the different valve parts differ considerably. In the physiological strain range the sinus and aortic tissues show a maximum tangent modulus (slope of the stress-strain curve) in the order of magnitude of 0.1 MN/m^2, regardless from the direction (circumferential or axial) in which the specimens are taken. This value is in reasonable agreement with data found in literature for human specimens (Table 4.3). The mechanical properties of the leaflet tissue show a distinct directional dependence (anisotropy). In the circumferential direction, i.e. the direction of preferred orientation

of the collagen bundles, the leaflet tissue reflects mainly the bundle properties, resulting in tangent-modulus values of 20 to 40 MN/m^2. In the radial direction values ranging from 1.0 to 1.8 MN/m^2 are found. The latter values agree fairly well with comparable data in literature (Table 4.3). The tangent-modulus values, found in the present study for circumferential specimens, are about a factor 10 higher than similar data reported in literature for human as well as porcine specimens. The stress-strain curves of the aortic valve tissues appear to be only slightly sensitive to strain rate.

The relaxation model used has proven to be a useful tool in describing the relaxation behaviour of the different valve parts. In the leaflet tissue more stress relaxation is observed than in the sinus and aortic tissues. Predictions based on the mathematical model indicate that in the leaflets greater viscous losses have to be expected than in the sinus and aortic walls. This aspect should be investigated further. It is likely to be of importance as to valve functioning in dynamical situations as, for instance, at the moment of valve closure.

CHAPTER 5

A THEORETICAL MODEL OF THE AORTIC VALVE

5.1. Introduction

The main objective of the present study was to gain insight into the general features of the mechanical behaviour of the natural valve. A review of the literature on this subject (section 5.2) showed that almost all studies dealt mainly with the stress analysis of the leaflets in their closed configuration whereas no attention was paid explicitly to their bundle structure (see sections 2.3.3 and 2.3.4). Furthermore no clear information was encountered on the importance of the sinus and aortic walls.

The development of the present model, as described in section 5.3, was prompted by the consideration that these aspects should be studied before modelling leaflet geometry and material properties in detail. It was assumed that in the situation, in which the valve is closed and subject to an approximately time-independent pressure-load, the bundles in the leaflets are of specific importance in the transmission of forces. In exploring the function of these bundles, detailed modelling of the mechanical properties of the leaflet tissue as well as the boundary conditions is of minor importance. For instance, the time-dependence of the mechanical properties does not seem to be very relevant in such an investigation. This will not apply when studying dynamic phenomena, as in the valve-closing process. Leaving this subject to future research, the present study focussed on the function of the collagen-bundle structure in the leaflets in their closed configuration.

The results of the model calculations corroborated the hypothesis that the bundle structure in the leaflets has a distinct mechanical function (section 5.4). In section 5.5 the results are discussed. Suggestions as to further investigations are made in Chapter 6.

5.2. Review of the literature on stress analysis of the aortic valve

The stress analyses which were found in literature, were static and dealt with the load-bearing leaflet portion in the closed configuration.

Chong et al. [1973] using membrane theory, analyzed the valve leaflets. The leaflets were assumed to be attached to a rigid cylinder representing the aortic wall. From measurements on silicone rubber casts of closed human valves (the pressure difference across the valve was not given) they concluded that a valve leaflet could be closely approximated by a surface with two constant principal radii of curvature. With a ratio of radii of curvature, R_{radial} / $R_{circumferential}$, ranging from 0.6 to 0.9 (for the definition of the directions see fig. 2.1), their model predicted that the highest stresses would occur in the radial leaflet direction, contrary to the findings in other investigations (e.g. Gould et al., 1980). This discrepancy can be explained by the fact that the geometrical data obtained by Chong et al. [1973] are essentially different from the data used by others [Swanson and Clark, 1974; Trenkner et al., 1976] who found the load-bearing leaflet portion to be approximately cylindrical, with the slighter curvature in the radial direction. The latter findings were confirmed by our own observations on pressurized valves (see fig. 2.8).

Another analytical stress analysis of the valve leaflets, based upon membrane-shell theory, was reported by Missirlis and Armeniades [1976]. Their work centred on the influence of leaflet geometry on the computed stress values. Using two geometries, a sphere and an ellipsoid of revolution, with zero displacements at the boundaries, they found that small changes in geometry brought about considerable changes in the stress values. The need for realistic geometrical data was therefore emphasized by the authors. The stress analysis of Gould et al. [1973] also emphasized the importance of leaflet geometry. Employing a thin-shell finite-element model and assuming small deformations and linearly elastic and isotropic material properties, they analyzed different leaflet geometries: an elliptical paraboloid, a paraboloid of revolution and a sphere. Their conclusions were similar to those of Missirlis and Armeniades [1976].

Also using a thin-shell finite-element model, Cataloglu et al. [1975] compared the results of geometrically linear shell theory with the results of finite deformation shell theory. In both cases linear elasticity, isotropy and homogeneity were assumed. In addition, two different valve models were used. One model contained only the load-bearing leaflet portion. At the boundaries, i.e. along the aortic

ring and the coapting edge (the line between the lunula and the load-bearing leaflet portion), they suppressed displacements but allowed rotations. The other model involved the leaflet, the aortic ring and the sinus wall, using the above mentioned boundary conditions at the coapting edge. No information was given on boundary conditions in the sinus region or on whether the material properties of the aortic ring and the sinus wall were different from those of the leaflets. Geometrical data obtained from photogrammetric studies were used for both models. It was observed that the linear theory predicted higher maximum stresses and higher normal displacements than the geometrically nonlinear theory. Besides, in both theories, incorporation of the aortic ring and the sinus wall resulted in slightly higher values for the maximum stresses and considerably higher values (40 - 50%) for the normal displacements in the leaflets. From these findings the authors surmised that "the increased curvatures, produced by the pressure loading, distort the geometry to a more efficient load-resisting configuration and, therefore, the linear analysis is conservative". Moreover, it was concluded that in a stress analysis of the valve only the leaflets had to be taken into consideration. As a continuation of the above-mentioned study and using the same geometrically linear thin-shell finite-element model, Gould et al. [1980] observed the maximum principal stress resultants to be oriented mainly in the circumferential direction. Maximum stresses were found near the centre of the load-bearing leaflet portion.

Chong and Missirlis [1978] presented a stress analysis of the leaflets of one porcine valve, based on a modification of membrane stress theory. Modifications were made to model the leaflets as inhomogeneous, non-linearly elastic and orthotropic membranes with the radial and circumferential directions as main directions for orthotropy. Geometrical data and strains, occurring under static pressure loading, were obtained from stereo-photogrammetric studies on a pressurized, entire valve. From these data the corresponding radial and circumferential stresses were calculated using the nonlinear stress-strain characteristics as determined in uniaxial tensile experiments on specimens cut out of another valve in the corresponding directions (Missirlis and Chong [1978]; see also section 3.3). The calculated radial stresses were considerably larger than the

circumferential stresses. The areas of highest stress concentrations were found near the node of Arantius (see fig. 2.1) while a progressive increase of radial stresses was observed from the aortic ring towards this node.

The literature review reveals that the stress analyses performed deal mainly with the valve in the static, closed situation. Besides, these studies centre on the leaflets alone, considering them to be attached to a rigid, cylindrical wall representing the aorta. Only Cataloglu et al. [1975] considered the aortic ring and the sinus wall too, in one of their models. Unfortunately, the data on material properties and boundary conditions employed in modelling the aortic ring and the sinus wall, were inadequately described. Owing to the lack of these data it is difficult to judge their conclusion that these valve parts do not necessarily have to be included in analyzing the mechanical properties of a valve.

As to the material properties, homogeneity, linear elasticity and isotropy were assumed by most authors. Only Chong and Missirlis [1978] employed inhomogeneity, orthotropy and nonlinear elastic properties in their study.

Most of the analyses were based on geometrically linear membrane or thin-shell theories (i.e. allowing only small deformations). Only Cataloglu et al. [1975] compared the results obtained with a linear and a nonlinear thin shell theory. They concluded the linear theory to be appropriate because it yielded conservative results and the calculations were cheaper and less time-consuming.

With respect to the geometrical descriptions used, the studies can be divided into those using idealized geometries [Chong et al., 1973; Missirlis and Armeniades, 1976; Gould et al., 1973] and studies using detailed geometrical data obtained from photogrammetric studies [Cataloglu et al., 1975; Gould et al., 1980; Chong and Missirlis, 1978].

5.3. Description of the model

5.3.1. Introduction

In developing the present valve model the following considerations served as directives: None of the studies which were found in literature has taken into account explicitly the possible mechanical

function of the collagenous bundle structure in the valve leaflets (see sections 2.3.3 and 2.3.4). Furthermore, the mechanical role of the other valve parts, i.e. the aortic ring, the sinus walls and the adjacent portion of the aortic wall, remains rather vague. It is felt to be premature to put considerable effort into detailed modelling of the geometry and the material properties of the leaflets alone, so long as the importance of the above-mentioned aspects to the general features of mechanical behaviour of the valve is not known.

The finite element model, used in the present work, was meant to explore the general features of the mechanics of the closed valve. Special attention was paid to the bundle structure in the leaflets. The model is based upon the theory of nonlinear continuum mechanics. It is therefore capable of representing geometrical nonlinearities. This was considered to be of importance because relatively large deformations were expected to occur which considerably influence the equations of equilibrium. Although linearly elastic material properties were assumed in the present investigations, nonlinearly elastic or viscoelastic properties can also be implemented in the model without drastic modifications. Both membrane and cable elements were used in modelling the leaflets. Because the leaflets are thin, flexible structures having no bending stiffness, membrane rather than shell elements seemed appropriate in describing the elastin layer. The cable elements represented the collagen bundles. An extensive treatment of the theory of general continuum mechanics as well as the numerical methods used in the calculations, would far exceed the scope of the present study. Therefore, only a brief outline of the theory and the derivation of the properties of the elements used, is presented in Appendix D. A more extensive treatment of the elements is given by De Wilde [1981].

5.3.2. Geometry

The valve geometry was assumed to have 120° symmetry. In defining the geometry, the characteristic dimensions at zero pressure difference across the valve as reported by Swanson and Clark [1974] and summarized in Table 2.1 (see also fig. 2.10), were used. Modelling the aorta as a cylinder, the ventricular and aortic valve radii r_v and r_a were both assigned a value of 13 mm [Sands et al., 1969;

Swanson and Clark, 1974]. Since the radial curvature of the leaflets in the loaded configuration is negligible (see section 2.4), the load-bearing leaflet portion was schematized by a segment of a cone. The axis of the cone was coincident with the plane of leaflet symmetry and thus intersected the axis of the aorta. From observations on valves, fixated in the closed situation at a pressure load of about 13 kPa, we found that point B was situated about halfway up the commissural height (fig. 5.1) on the aortic wall, where the load-bearing leaflet portion merges into the lunula. Given the position of this point, the top of the cone and the angle α, the cone was fully defined. The top of the cone was chosen so that the radius of curvature of the load-bearing leaflet portion along EA ranged from 3.3 r_v to 3.6 r_v.

5.3.3. Material properties

No detailed modelling of the material properties was attempted. For the purpose of the present exploratory investigation, linearly elastic properties were considered to be appropriate. The numerical values actually used in the calculations are given in the sections 5.4.2 and 5.4.3.

5.4. Some results of model calculations

5.4.1. Introduction

As discussed in section 5.3.1, the main purpose of the calculations with the valve model was to find out about the mechanical function of the leaflet bundle structure. Therefore calculations were performed on a leaflet with and without a simplified bundle structure. Some of the results of these calculations are presented and discussed in section 5.4.2.

5.4.2. A simple model incorporating the bundle structure

In the model used to study the effects of bundle structure on the mechanical behaviour of a valve leaflet, the aorta was represented by a rigid cylinder. Therefore all displacements of the leaflet at the intersection of the leaflet and the aorta (the aortic ring) were suppressed, but rotation of the leaflet was still possible at this intersection. Because of the leaflet symmetry, the model incorporated

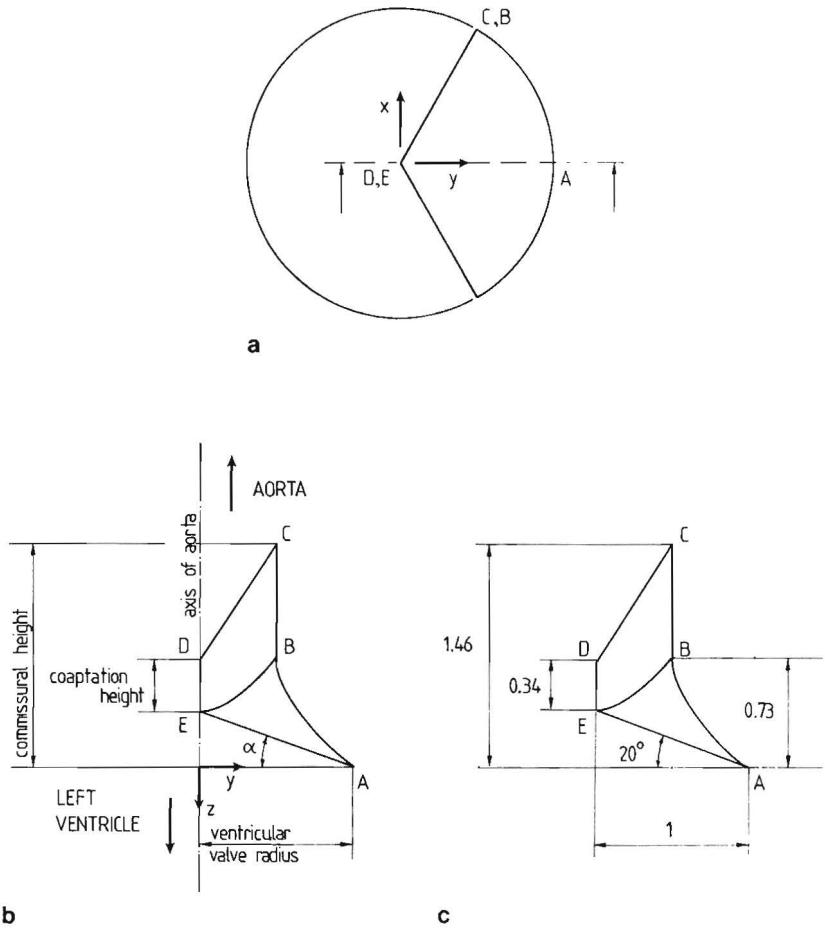

Fig. 5.1.
Outline of the geometry of the leaflet model.
a. View on the closed valve from the aortic side (the sinuses are omitted.
In figs. 5.1b and 5.1c the view (in the direction of the arrows in fig. 5.1a) of one half of the leaflet, dissected along its plane of symmetry (AED), is shown.
b. Nomenclature of the dimensions.
c. Dimensionless values related to the ventricular valve radius and used in the leaflet model.
EDCB: lunula, EAB: load-bearing leaflet portion; ABC: aortic ring; AE: generator of the cone; EB: coapting edge; C: commissure.

only one half of the leaflet with the usual boundary conditions applying at the line of symmetry. The leaflet points lying on the axis of the aorta (i.e. on the line DE, fig. 5.2) were allowed to translate along this axis only. In the lunula (surface BCDE, fig. 5.2) forming part of one of the planes of 120° valve symmetry, displacements perpendicular to this plane were suppressed.

Modelling of the bundle structure was based upon the histological observation, discussed in Chapter 2. In order to limit the number of elements (the total number of elements was 72), the bundle structure was simplified. In the load-bearing leaflet portion six bundles were situated. They ran circumferentially in the main, as illustrated in fig. 5.2. In the lunula two bundles ran from the commissures C (see also fig. 2.3) to the line DE. Along the line BE (transition from the load-bearing portion to the lunula) a bundle was situated as well.

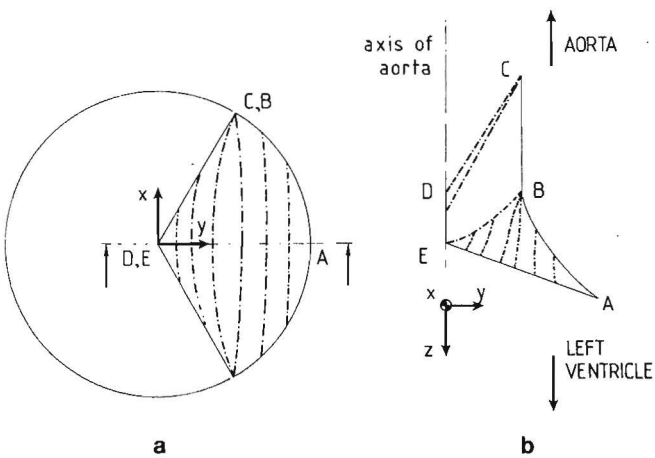

Fig. 5.2.
The modelling of the leaflet bundle structure. The dashed lines represent the bundles.
a. The bundles as seen from the aortic side.
b. View (in the direction of the arrows in fig. 5.2a) of one half of the leaflet.
EDCB: lunula; EAB: load-bearing leaflet portion; ABC: aortic ring; EB: coapting edge; C: commissure.

The bundle material was assigned a tangent modulus of 45 MN/m^2, as reported for collagen fibres [Haut and Little, 1972], while for the membranes a value of 1.5 MN/m^2 was applied as reported for elastin fibres [Carton et al., 1962]. As can be seen from Table 4.3, these values are in the order of magnitude of the results of our own experiments on the properties of the leaflet tissue in the circumferential and radial directions, respectively. The bundles and the membranes were assumed to be incompressible. The diameter of the circular cross-sectional area of the bundles as well as the thickness of the membranes were taken as 0.4 mm. The leaflet was loaded at a uniform pressure.

The behaviour of the leaflet was calculated with and without bundles. In order to prevent excessive deformations in the latter case and to facilitate the comparison between both situations, in all calculations a pressure load of 0.133 kPa was used instead of the physiological value of 13.3 kPa.

Owing to the presence of the bundles the displacements in the z-direction (towards the left ventricle, see fig. 5.2) showed a sixfold decrease at line DE. Figure 5.3 illustrates the reaction forces on the leaflet with and without bundles. At the aortic ring (ABC in fig. 5.2) the presence of the bundles resulted in an increase in the forces at their points of attachment to the ring and a reduction in the forces on the membranous parts in between (line section A'BC). Along the part AA' of the aortic ring no bundles were attached to the aortic ring. Here the effect of the bundles was a rotation rather than a reduction of the reaction forces so that their direction became more perpendicular to the aortic ring. This could explain the presence of collagen bundles perpendicular to the aortic ring, anchoring the middle portion of the leaflet to the aortic wall as was observed in the histological investigations (see section 2.3.3, figs. 2.4 and 2.5).

The influence of the bundles on the stresses in the load-bearing leaflet portion can be illustrated in a representative manner by considering the stress distribution along the line of leaflet symmetry AE and the line BF (fig. 5.4). The line BF is chosen because it is directed nearly circumferentially and because at point F maximum stresses were found without bundles. The principal stresses along AE and BF as well as those in the bundles (at the intersections

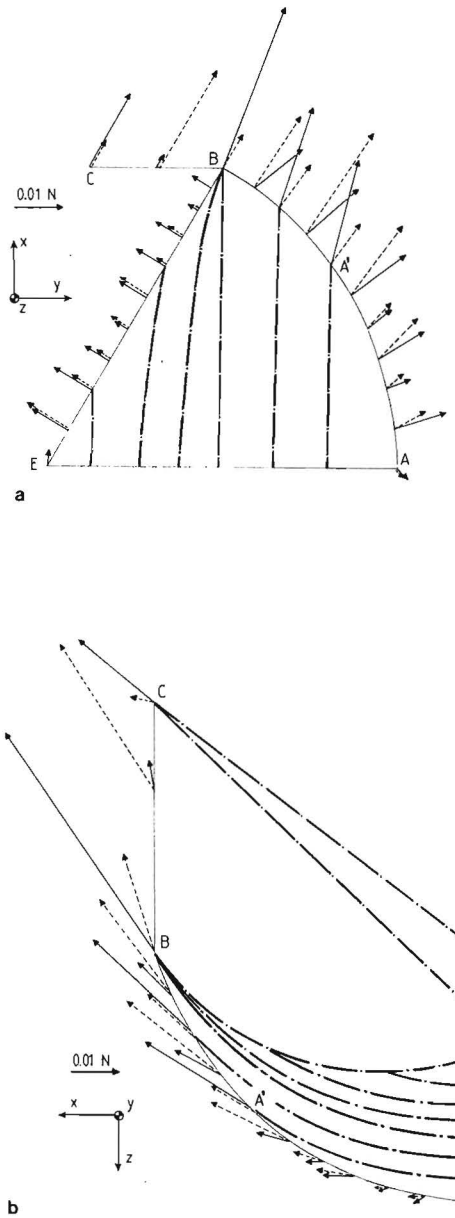

Fig. 5.3.
Reaction forces on the load-bearing leaflet portion.
a. Projection in the (xy) plane.
b. Projection in the (xz) plane.
—·—bundle; ——▶ reaction force with bundles;
- - - -▶reaction force without bundles.

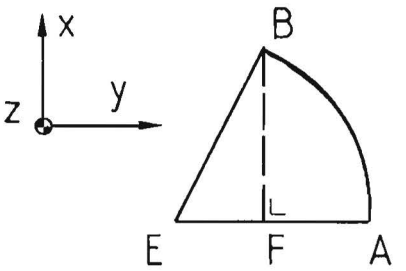

Fig. 5.4.
Illustration of the lines EA and BF in the load-bearing leaflet portions along which stress distributions were considered.

of these bundles with line AE) are given in fig. 5.5. The maximum principal stresses -with and without bundles- were encountered in the circumferential direction.

The bundles were found to have a pronounced influence on the stress distribution in the leaflet. Due to the presence of the bundles, the maximum principal stress values were reduced almost to the level of the minimum principal stresses, the values of the latter remaining almost unchanged in comparison with the situation in which bundles were absent. In the absence of bundles, compressive stresses were found in the vicinity of B (fig. 5.5). These compressive stresses were negligibly small compared with the tensile stresses. In the presence of bundles, compressive stresses were absent in the membranes, whereas in the bundle along BE (fig. 5.2) relatively low compressive stresses were observed near E (fig. 5.5). Thus the main effect of the collagen bundles on the stress distribution in the membranes was a smoothing of the stress distribution throughout the load-bearing leaflet portion. Because the stresses in the principal directions were nearly the same, almost coinciding, as they did, with the radial and circumferential directions, shear stresses were negligible.

In order to investigate the influence of the stiffness of the membranes on the stress distribution, the situation without bundles was investigated with the membranes having a tangent modulus of 4.5 and 9 MN/m^2 (a respectively threefold and sixfold increase in their

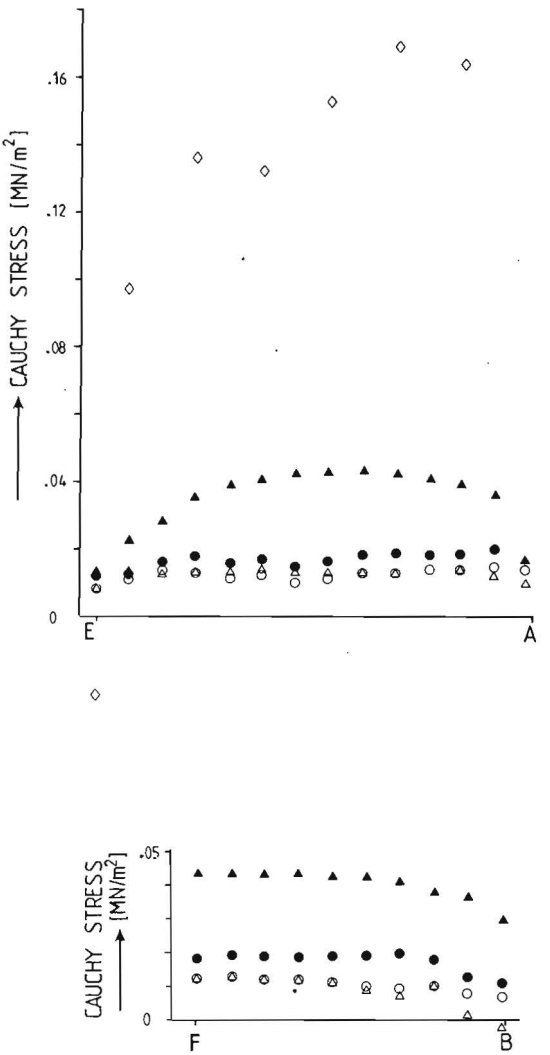

Fig. 5.5.
The stress distributions along EA and BF (see fig. 5.4) and the stresses in the bundles at the intersections with AE.
o● principal stresses with bundles,
Δ▲ principal stresses without bundles,
◇ stresses in bundles.
Solid and open symbols represent maximum and minimum stresses, respectively.

stiffness with respect to the situation discussed in the foregoing). In the latter case the displacements in the z-direction (towards the left ventricle) were about the same as in the situation with bundles, discussed above, while they were twice as large in the first-named. The effect of the stiffness of the membranes on the stress distribution was negligible.

5.5. Discussion and conclusions

The results of the investigations on the function of the bundle structure in the leaflets reveal that the bundles are of considerable importance in the stress distribution in the leaflets. They bring about a more homogeneous stress distribution and reduce the shear stresses in the membranous parts. The assumption, based upon the histological observations (section 2.3.4), that the bundles transmit the load on the membranous parts to the aortic wall, is confirmed. At the points where several bundles come together at the aortic wall (B and C, fig. 5.2), stress concentrations are to be expected. It is concluded that the anisotropy of the leaflet tissue found in the tensile experiments (see Chapter 4), can be modelled by taking the bundle structure explicitly into account. We are convinced that realistic and workable modelling of the bundle structure is one of the principal requirements if we are to arrive at an accurate and reliable model for the analysis of the mechanical behaviour of the natural aortic valve.

In the present model the aortic wall is assumed to be rigid. Therefore, no conclusions can be drawn on the influence of the stiffness of the surrounding structures on the stresses in the leaflets. This aspect needs further investigation.

CHAPTER 6

SUMMARY AND CONCLUSIONS

The present study was performed within the framework of an interdisciplinary research project on the aortic valve. This project was prompted by the fact that biological valve prostheses have a limited life span. Apart from tissue degeneration, abnormal hydrodynamical and mechanical factors were recognized as an important cause of valve failure. The aim of the project is the determination of the parameters which govern the stresses in the leaflets of the natural aortic valve. Better insight into these parameters may improve the technical specifications for the design and implantation of artificial triple-leaflet valve prostheses.

The present investigation was conducted to study the mechanical behaviour of the leaflets of an aortic valve in its closed configuration. For the design of a theoretical model, the histological structure and the mechanical properties of valve tissue were investigated.

Histological sections of porcine valves were studied by light microscopy. The valve leaflet appeared to have a triple-layered structure: a dense layer composed of mainly collagen fibres and bundles, oriented in one particular direction, at the aortic side, a grid of randomly oriented elastin fibres at the ventricular side and, in between, a loosely structured layer. The sinus walls consist of mainly circumferentially arranged smooth muscle cells embedded in a grid of elastic tissue with no special fibre orientation. The attachment of the leaflets to the sinus walls is constituted by the aortic ring, a crownlike fibrocartilaginous structure containing large amounts of collagen fibres.

The mechanical properties of the leaflets as well as the sinus and aortic walls were investigated *in vitro* in uniaxial tensile experiments. Tissue strips, taken in different directions from the various valve parts, were stretched with constant strain rates and subsequently kept at a constant, stretched length. Care was taken not to exceed the physiological strain ranges. Considerable differences

were found between the stress-strain curves of the leaflet tissue on the one hand and the sinus and aortic tissues on the other. These differences can be explained qualitatively by their different histological structures.

In the leaflet-tissue strips, cut in the direction of the collagen bundles (circumferential direction), a considerably higher stress is required to produce a certain strain than in the specimens taken perpendicularly to the bundles (radial direction). The tangent moduli in the circumferential direction are by more than a factor 10 higher than in the radial direction. In the sinus and aortic walls no pronounced differences were observed between the stress-strain curves of tissue strips taken in two perpendicular directions. These tissues appeared to be much more compliant than the leaflet tissue. Their tangent moduli are by a factor 2 or to 10 smaller than the corresponding values for the radial leaflet specimens. The characteristics of the leaflet tissue clearly reflect the stiffening function of the collagen bundle structure. The high compliance of the sinus and aortic walls is consistent with their high elastin content. The insensitivity of their characteristics to direction can be explained by the random character of the fibre orientation.

In almost all specimens a hundredfold increase of the strain rate resulted in a relatively slight increase of the stress at a given strain. This indicates a small strain-rate sensitivity of the stress-strain curves.

After applying a certain strain with a constant, high strain rate the stress in the leaflet specimens decreased by 37 to 50% of its maximum value during the constant-length phase of the experiments. In the sinus and aortic strips this decrease ranged from 25 to 37%. The long-term relaxation behaviour of the specimens showed no distinct dependence on the direction in which they were cut. More experimental data are needed to decide whether this applies to the short-term behaviour as well. The stress relaxation in the specimens was analyzed using a mathematical model. Predictions based upon this model indicate that on cyclic loading the viscous losses in the leaflets are relatively large as compared to the losses in the sinus and aortic walls. This might be a relevant aspect of the mechanical properties of the valve in dynamic situations and hence should be further investigated.

The mechanical significance of the bundle structure in the leaflets of the closed valve was studied in a theoretical model. With and without bundles the principal stress directions in the membranous parts were almost coincident with the circumferential and radial directions. Without bundles maximum principal stresses occurred in the circumferential direction. The effect of the bundle structure appeared to be twofold. The bundles transmit the pressure load on the membranous parts to the aortic wall. At the same time they cause a more homogeneous stress distribution in these parts by reducing the maximum principal stress values to the level of the minimum principal stresses. The values of the latter remain almost unchanged in comparison with their values in the case without bundles. Because with bundles the stresses in the principal directions become nearly the same, shear stresses are negligibly small.

As the ultimate goal is to determine the parameters which govern the stresses in the leaflets of the natural valve as well as to obtain specifications for the design and implantation of artificial triple-leaflet valve prostheses, several aspects remain to future research.

With the present model of the leaflet as a basis, the model of the bundle structure could be refined, for instance, by varying the cross-sectional areas of the bundles and introducing cross-links between them. The bundles originating at the commissures (C in figs. 2.3 and 5.2) are relatively thick in the neighbourhood of these commissures, but towards the central portion of the leaflet they branch out to form a meshwork of thinner bundles (fig. 2.3). The influence of leaflet geometry on the stress distribution should be studied when the bundle structure is present.

However, extension of the present model to include a deformable aortic ring and sinus and aortic walls seems more conducive to enlarging our insight into the general features of natural valve mechanics. Moreover, from the results of such investigations it could be decided whether these valve parts, at least when the valve is closed, are of critical importance with respect to the stresses in the leaflets.

At a final stage of development of the model attention should be centred on the dynamic and kinematic aspects involved in the processes

of valve closure and aperture. Such investigations should include the time-dependence of both the load on the valve and the mechanical properties of the valve tissue. In the present study the mechanical properties were studied in one-dimensional stress-strain situations. An extension to include the mechanical tissue behaviour in two-dimensional stress-strain situations might therefore seem a logical subsequent step. We believe, however, that a further investigation of the viscous losses in the leaflets versus those in the sinus and aortic walls, be it in one-dimensional stress-strain situations, will be of more importance for the development of a realistic model of the valve.

Parallel with the development of the valve model attention should be paid to the assessment of criteria which can be used in judging the admissibility of stresses with respect to the life span of the valve. Although actually indispensable for the final evaluation of stress analyses, untill now such criteria have not been established for biological tissue, as far as we know.

APPENDIX A
THE PURPOSE AND SCOPE OF THE EINDHOVEN HEART-VALVE RESEARCH PROJECT

The present study falls within the framework of the Eindhoven heart-valve research project, which was itself prompted by the limited life span of biological, triple-leaflet valve prostheses. Apart from eventual tissue degeneration, abnormal hydrodynamical and mechanical conditions were recognized as the possible major contributing factors to valve failure. It is assumed that such failure is due to higher local stresses in the leaflets of the prosthesis compared to the natural valve. The ultimate goal of the present research is twofold:

(i) to determine by means of theoretical and experimental modelling, the parameters which govern the stress in valve leaflets, and

(ii) to formulate technical specifications for the design and implantation of artificial triple-leaflet valve prostheses whose function and life span are much nearer the optimum.

The research philosophy is based on the view that observation of natural aortic valve behaviour gives insight into the relevant parameters. This research can be performed in experiments with an analogue model as well as *in vivo* experiments. It is hoped that from the resulting insight, specifications can be derived for artificial valves. The project has four main topics:

(i) Hydrodynamic behaviour of the aortic valve

The aim is to describe the interaction between flow pattern and cusp motion. The main subject has been the investigation of the closing mechanism of the aortic valve. To this end experiments with an analogue model were performed to find a physical one [Van Steenhoven and Van Dongen, 1979]. Furthermore the valve closure was studied in animals [Van Steenhoven et al., 1981]. Currently this research programme focusses on leaflet instabilities.

(ii) Dynamic behaviour of the aortic valve

The purpose is to study the relationship between movement of the valve components on the one hand and the pressures in and across the valve leaflets on the other. These relationships are formulated in terms of valve compliance. Static and dynamic valve compliances are determined from *in vitro* [Van Renterghem et al., 1979] and *in vivo* experiments, respectively.

(iii) Mechanical behaviour of the aortic valve

The aim of this programme is to correlate the pressure difference across the valve to the local stresses within the valve components. To achieve this, valve histology [Sauren et al., 1980] and the mechanical properties of the valve tissue have been closely studied with the ultimate aim of developing a theoretical model of valve mechanics.

(iv) Application to valve prostheses

In order to apply such basic information to better design of heart-valve prostheses, the natural stress-reducing mechanisms must be translated into design specifications [Van Steenhoven et al., 1979a].

APPENDIX B

A BRIEF OUTLINE OF THE ANATOMY AND PHYSIOLOGY OF THE HEART

Only a concise description of the anatomy and physiology of the heart is given here. Comprehensive treatises on these subjects can be found in textbooks on physiology and anatomy (e.g.: Guyton, 1981; Gray, 1980).

The heart has four cavities, the left (LA) and right (RA) atria and the left (LV) and right (RV) ventricles (Fig. B1). The atria and

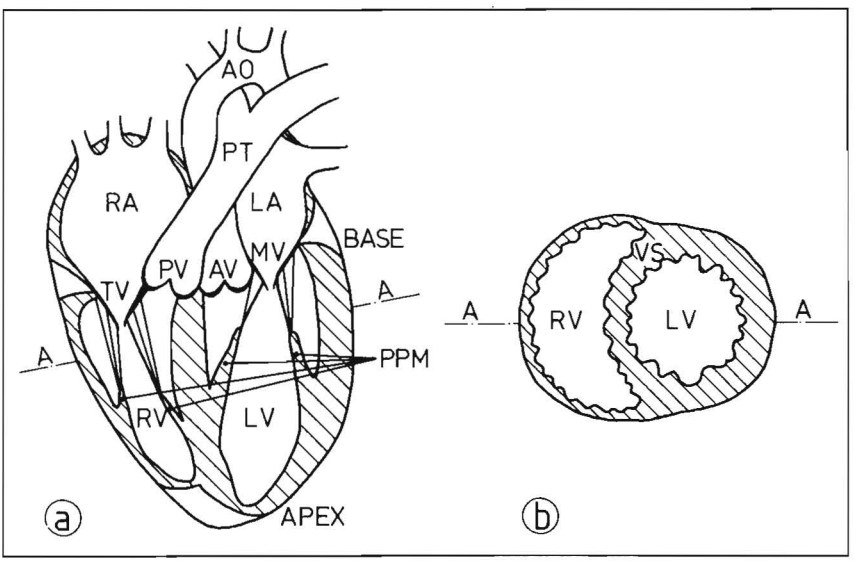

Fig. B1.
Diagram of the heart [Arts, 1978]:
a. Section of the heart in the sagittal plane.
   RA = right atrium, LA = left atrium, RV = right ventricle,
   LV = left ventricle, TV = tricuspid valve, MV = mitral valve,
   PV = pulmonary valve, AV = aortic valve, PT = pulmonary trunk,
   AO = aorta, PPM = papillary muscles.
b. Cross-section of the ventricle in a plane which is indicated as AA in a.
   VS = ventricular septum.

the ventricles are separated by the atrial and ventricular (VS) septa.

The systemic veins collect the blood from the systemic circulation and lead it into the right atrium. The pulmonary veins conduct the reoxygenated blood from the lungs into the left atrium. The right atrium is connected to the right ventricle by way of the tricuspid valve (TV), whereas the left atrium is connected to the left ventricle over the mitral valve (MV). The leaflets of the mitral and tricuspid valves are connected by the chordae tendineae to a number of papillary muscles (PPM) that emanate from the ventricular walls. The pulmonary valve (PV) is situated between the right ventricle and the pulmonary trunk (PT). The aortic valve (AV) connects the left ventricle and the aorta (AO). The heart valves are situated in the basal plane. The inlet valves to the ventricles (the tricuspid and mitral) are also called the atrio-ventricular (A-V) valves, and the outlet valves from these cavities (the pulmonary and aortic) are also known as the semilunar valves.

Under normal conditions the human heart contracts and relaxes about once a second. The cardiac cycle comprises a period of contraction, systole, together with a period of relaxation, diastole. There is a delay of more than one tenth of a second between contraction of the atria and the ventricles. This delay enables the atria to fully discharge into the ventricles before they start to contract.

During the cardiac cycle the following phenomena occur. Blood flows into both atria in the course of systole and diastole. This raises the pressures in the atria. Because of this rise and the decreasing pressure in the relaxing ventricles, the mitral and tricuspid valves open early in diastole and the ventricles are filled. This filling is completed by contraction of the atria (atrial systole).
Thereupon, the ventricles contract, followed by commencement of ventricular systole. The atrio-ventricular valves then close, partly as a result of the increased pressure in the ventricular cavities. In this phase of the cardiac cycle the ventricular volumes remain constant because all valves are closed. This phase is therefore known as the isovolumic contraction phase. Next the pulmonary and aortic valves open because the right and left ventricular pressures are greater than those in the pulmonary trunk and aorta, respectively. The ejection phase has started. At the end of this phase the outflow ceases and the semilunar valves close as a result of the relaxation

of the heart. The ventricular volumes are again constant, while ventricular pressures rapidly decrease. This phase is called the isovolumic relaxation phase. As a consequence of complete relaxation filling of the atria is completed and diastole starts again.

APPENDIX C
LINEAR VISCOELASTICITY

1. Introduction

This appendix contains a brief outline of linear viscoelasticity theory. Only those elements that are indispensable for proper understanding of the "quasi-linear viscoelasticity law" proposed by Fung (1972) will be discussed. Of the numerous material functions that might be used in describing the behaviour of linear viscoelastic materials, only the elastic response, the reduced relaxation function, the complex modulus and the relaxation spectrum will be introduced. The physical meaning of these functions will be illustrated with a few examples. A more extensive treatment of this matter can be found in textbooks on viscoelasticity (e.g. Lockett, 1972; Christensen, 1971).

2. Reduced relaxation function and elastic response

The constitutive equation relating stress σ and strain ε [*)] in a linear viscoelastic material under uniaxial stress/strain can be written in a general form as:

$$p_0\sigma + p_1\frac{d\sigma}{dt} + p_2\frac{d^2\sigma}{dt^2} + \ldots + p_m\frac{d^m\sigma}{dt^m} = \tag{2.1}$$

$$= q_0\varepsilon + q_1\frac{d\varepsilon}{dt} + \ldots q_n\frac{d^n\varepsilon}{dt^n} ,$$

i.e. a linear differential equation with constant coefficients. In order to formulate the response $\sigma(t)$ to an arbitrary strain history $\varepsilon(t)$ we take the Laplace transform [**)] of (2.1):

---

*) The symbols σ and ε denote quantities related to load and deformation respectively. Whether they have to be interpreted as force or stress and elongation or strain depends on the scaling of the coefficients p and q in (2.1).

**) In the subsequent the Laplace transform $\int_0^\infty f(t)e^{-st}dt$ of a function f(t) will be denoted by $f_L(s)$; s and t are complex and real variables respectively.

$$(p_0+p_1s+p_2s^2+\ldots+p_ms^m)\ .\ \sigma_L(s) = (q_0+q_1s+\ldots+q_ns^n)\varepsilon_L(s) \qquad (2.2)$$

or, in a more manipulable form, if $p_0+p_1s+\ldots+p_ms^m \neq 0$,

$$\sigma_L(s) = E_L(s)\varepsilon_L(s);\ E_L(s) = \frac{q_0+q_1s+\ldots+q_ns^n}{p_0+p_1s+\ldots+p_ms^m}\ . \qquad (2.3)$$

By means of back transformation of (2.3) into the time domain we will derive a specific formulation of $\sigma(t)$ as a function of $\varepsilon(t)$ and some material functions. First we consider the response to a unit-step change of the strain at t=0. This can be derived by substitution of $\varepsilon_L(s) = \frac{1}{s}$ into (2.3), resulting in

$$\sigma_{Lu.st.}(s) = \frac{1}{s}\,E_L(s). \qquad (2.4)$$

By solving $E_L(s)$ from (2.4) and substituting the result into (2.3) we can write the stress response to an arbitrary strain history as

$$\sigma_L(s) = \sigma_{Lu.st.}(s)\ s\ \varepsilon_L(s) \qquad (2.5)$$

and, after applying inverse Laplace transformation, as

$$\sigma(t) = \int_{\tau=0}^{t} \sigma_{u.st.}(t-\tau)\frac{d\varepsilon(\tau)}{d\tau}d\tau\ . \qquad (2.6)$$

The functions $G(t)$ and $\sigma^{(e)}(\varepsilon)$, defined by

$$G(t) = \frac{\sigma_{u.st.}(t)}{\sigma_{u.st.}(0)}\ , \qquad (2.7)$$

$$\sigma^{(e)}(\varepsilon) = \sigma_{u.st.}(0)\varepsilon \qquad (2.8)$$

are called the *reduced relaxation function* and the *elastic response*, respectively. From these definitions it is seen that

$$G(0) = 1 \qquad (2.9)$$

and that $\sigma^{(e)}(\varepsilon)$ is a linear function of ε. Differentiation of (2.8) yields

$$\sigma_{u.st.}(0) = \frac{d\sigma^{(e)}(\varepsilon)}{d\varepsilon} \tag{2.10}$$

By substituting (2.7) and (2.10) into (2.6) we obtain

$$\sigma(t) = \int_{\tau=0}^{t} G(t-\tau)\frac{d\sigma^{(e)}(\varepsilon)}{d\varepsilon}\frac{d\varepsilon(\tau)}{d\tau}\,d\tau \ . \tag{2.11}$$

This states that the stress response, dependent as it is both on strain and time, can be formulated with a convolution integral. The two dependencies then emerge explicitly in terms of the functions $\sigma^{(e)}(\varepsilon)$ and $G(t)$.

Because of the linearity of the differential equation (2.1) it can be shown that the response to a step change of the strain at t=0 with magnitude ε can be stated as

$$\sigma_{st}(t,\varepsilon) = \varepsilon\ \sigma_{u.st.}(t) \ . \tag{2.12}$$

By using (2.7) and (2.8) this can be rewritten as

$$\sigma_{st}(t,\varepsilon) = \sigma^{(e)}(\varepsilon)\ G(t) \ , \tag{2.13}$$

showing that both the reduced relaxation function G(t) and the elastic response $\sigma^{(e)}(\varepsilon)$ can be deduced from the stress response to a step change of the strain.
With G(0) = 1, equation (2.13) shows that

$$\sigma_{st}(0,\varepsilon) = \sigma^{(e)}(\varepsilon) \ , \tag{2.14}$$

i.e. the elastic response at a certain value ε is identical with the instantaneous stress response to a step change of the strain with that same value ε. Partial integration of (2.11), after some manipulation gives,

$$\sigma(t) = \sigma^{(e)}\big(\varepsilon(t)\big) + \int_{\tau=0}^{t} \sigma^{(e)}\big(\varepsilon(t-\tau)\big)\frac{dG(\tau)}{d\tau}\,d\tau \tag{2.15}$$

with $\varepsilon = 0$ for $t \leq 0$ and $\sigma^{(e)}(0) = 0$.

In general $G(\tau)$ will be a monotonously decreasing function so that $\frac{dG(\tau)}{d\tau}$ is negative. Consequently (2.14) and (2.15) tell us that the stress at time t is equal to the instantaneous response to the strain at that time, decreased by a history-dependent amount.

3. Complex modulus

A useful material function for describing the constitutive behaviour in the frequency domain is the so-called complex modulus. In defining this function we use the function $E_L(s)$ in (2.3) as a starting point. For a further investigation of $E_L(s)$ we take the Fourier transform*) of (2.1):

$$\sigma_F(\omega) = \bar{E}(\omega)\varepsilon_F(\omega) \tag{3.1}$$

thus introducing the frequency-like parameter ω. $\bar{E}(\omega)$ is a complex function of ω and is called the *complex* or *dynamic modulus* of the viscoelastic material. Writing $\bar{E}(\omega)$ in terms of its real and imaginary parts yields

$$\bar{E}(\omega) = E_s(\omega) + iE_\ell(\omega) = |\bar{E}|e^{i\phi} \tag{3.2}$$

$$\text{with } |\bar{E}| = \sqrt{E_s^2 + E_\ell^2}\ ;\ \cos\phi = \frac{E_s}{|\bar{E}|}\ ;\ \sin\phi = \frac{E_\ell}{|\bar{E}|}\ ;\ 0 \le \phi \le \frac{\pi}{\ell}\ .$$

---

*) The Fourier transform of a function f(t) (t is a real variable) is defined as

$$f_F(\omega) = \int_{-\infty}^{\infty} f(t)e^{i\omega t}dt$$

where ω is a real variable. In most cases where f(t) has a physical meaning, it applies that $f(t) = 0$ if $t < 0$. Then the Fourier transform

$$f_F(\omega) = \int_{0}^{\infty} f(t)e^{i\omega t}\,dt$$

can be considered the equivalent of the Laplace transform $f_L(s)$ under the formal substitution $s = -i\omega$.

$E_s(\omega)$ and $E_\ell(\omega)$ are called *storage modulus* and *loss modulus*, respectively, while $\phi(\omega)$ is referred to as the *loss angle*, and $\tan\phi(\omega)$ is the *loss tangent*.

Another, equivalent, way to introduce the complex modulus, moreover one which is more convenient for illustrating its physical significance, is the following. Imposing a strain on the material varying sinusoidally with time is mathematically simulated by substituting

$$\bar{\varepsilon}(t) = \mathrm{Re}\{\varepsilon_o e^{i\omega t}\} \quad (\varepsilon_o \text{ is a real number}) \tag{3.3}$$

into (2.1). The steady state response then will take the form

$$\sigma(t) = \mathrm{Re}\{\bar{\sigma} e^{i\omega t}\} \quad (\bar{\sigma} \text{ is a complex variable}). \tag{3.4}$$

From (2.1), (3.3) and (3.4) it follows that

$$\frac{\bar{\sigma}}{\bar{\varepsilon}} =: \bar{E}(\omega) \ . \tag{3.5}$$

For the energy per unit volume to be supplied to a material undergoing a one-dimensional deformation $\varepsilon(t)$, it will generally apply that

$$W_t = \int_{\tau=0}^{t} \sigma(\tau)\dot{\varepsilon}(\tau)d\tau \ . \tag{3.6}$$

Expressing ω in terms of the period time T

$$\omega = \frac{2\pi}{T} \ , \tag{3.7}$$

in the case of a sinusoidally varying strain, described by (3.3), it is found after some manipulation that

$$W_t = \tfrac{1}{2}\,\varepsilon_0^2\left(\tfrac{1}{2}E_s\{\cos(4\pi\tfrac{t}{T}) - 1\} + E_\ell\{2\pi\tfrac{t}{T} - \tfrac{1}{2}\sin(4\pi\tfrac{t}{T})\}\right) \tag{3.8}$$

In deriving this expression the identities $\cos\phi = E_s/|\bar{E}|$ and $\sin\phi = E_\ell/|\bar{E}|$ have been employed.

This expression states that the amount of dissipated energy resulting from cyclic loading and unloading of a linear viscoelastic material

can be described in terms of the strain amplitude and the complex modulus. If we consider a time interval equal to a multiple of T so that

$$t = kT \quad (k \text{ is a positive integer})$$

it is found that the supply of energy governed by the storage modulus E_s, vanishes and that

$$W_{kT} = \pi k \varepsilon_0^2 E_\ell(\omega) \ , \tag{3.9}$$

i.e. the energy dissipated in a whole number of periods can be described fully in terms of the strain amplitude and the loss modulus. The storage modulus accounts for the elastic energy storage.

4. Example

In the examples which follow, the theory presented in the preceding sections will be elucidated. Use will be made of the standard linear solid, a spring-and-dashpot model (fig. C1), consisting of a parallel

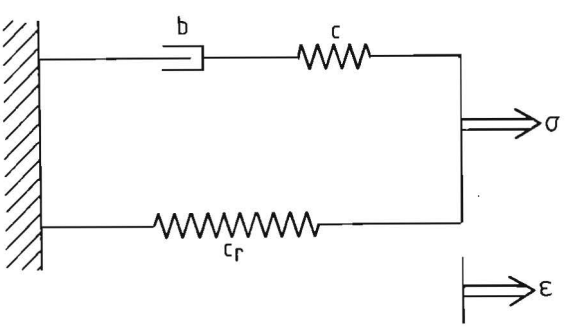

Fig. C1.
Standard linear solid.

arrangement of a spring element (spring constant c_r) and a spring-dashpot series connection (spring constant c, damping constant b). The behaviour of the spring is described by

$$\sigma = c\varepsilon \tag{4.1}$$

and of the dashpot by

$$\sigma = b\dot{\varepsilon} \ . \tag{4.2}$$

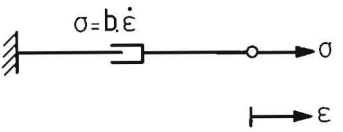

①

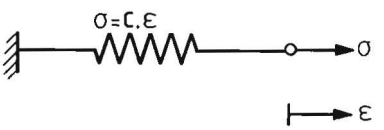

②

Fig. C2.
Linear dashpot (1) and spring element (2) and their constitutive equations.

Reduced relaxation function and elastic response

The differential equation relating stress σ and strain ε for the standard linear solid is given by

$$\sigma + \theta\frac{d\sigma}{dt} = c_r\varepsilon + \theta(c+c_r)\frac{d\varepsilon}{dt} \ , \tag{4.3}$$

where θ is the relaxation time constant, defined by

$$\theta = \frac{b}{c} \ . \tag{4.4}$$

The response to a unit-step change of the strain at t=0 (σ=0, ε=0 for t<0) is found to be

$$\sigma_{u.st.}(t) = c_r + ce^{-\frac{t}{\theta}} . \tag{4.5}$$

For the reduced relaxation function the definitions given in (2.7) and (2.8) yield

$$G(t) = \frac{c_r + ce^{-\frac{t}{\theta}}}{c_r + c} \tag{4.6}$$

and for the elastic response

$$\sigma^{(e)}(\varepsilon) = (c_r+c)\varepsilon . \tag{4.7}$$

From (4.6) we define

$$G(\infty) := G(t\to\infty) = \frac{c_r}{c_r+c} \tag{4.8}$$

and

$$\frac{c}{c_r+c} =: 1 - G(\infty) . \tag{4.9}$$

With (4.8) and (4.9) the reduced relaxation function can be written as:

$$G(t) = G(\infty) + \{1-G(\infty)\}e^{-\frac{t}{\theta}} \tag{4.10}$$

Complex modulus

From the Laplace transform of the unit-step response, given by (2.4), the following expression is found for the complex modulus,

$$\bar{E}(\omega) = i\omega\sigma_{Lu.st.}(\omega) \tag{4.11}$$

where use is made of s = iω. Substitution of the Fourier transform of the unit-step response (4.5) for the standard linear solid into (4.11) leads to

$$\bar{E}(\nu) = c_r + \frac{c\nu^2+ic\nu}{1+\nu^2}$$

or

$$E_s(\nu) = c_r + \frac{c\nu^2}{1+\nu^2} \; ; \; E_\ell(\nu) = \frac{c\nu}{1+\nu^2} \tag{4.12}$$

with $\omega\theta =: \nu$, a dimensionless frequency parameter.

By using (4.7) to (4.9) inclusive these quantities may be written as

$$E_\ell(\nu) = \nu \frac{1-G(\infty)}{1+\nu^2} \frac{d\sigma^{(e)}}{d\varepsilon} \tag{4.13}$$

and

$$E_s(\nu) = \frac{d\sigma^{(e)}}{d\varepsilon} - \frac{1}{\nu} E_\ell(\nu) \; . \tag{4.14}$$

These equations illustrate that for an elastic material, for which $G(\infty) = 1$ applies, the loss modulus vanishes and the storage modulus equals the well-known (tangential) elastic modulus $\frac{d\sigma^{(e)}(\varepsilon)}{d\varepsilon}$. From (3.9) we know that maximal energy-dissipation on sinusoidal straining will occur at the frequency ν_e, i.e. the solution ν from $\frac{dW_{kT}}{d\nu} = 0$ or $\frac{dE_\ell}{d\nu} = 0$. For the standard linear solid using (4.13) we have

$$\nu_e = 1. \tag{4.15}$$

Further we note that

$$\lim_{\nu\to\infty} E_s(\nu) = \frac{d\sigma^{(e)}}{d\varepsilon} \tag{4.16}$$

and

$$\lim_{\nu\downarrow 0} E_s(\nu) = G(\infty)\frac{d\sigma^{(e)}}{d\varepsilon} \tag{4.17}$$

Fig. C3 shows an example of the loss and storage modulus for a standard linear solid.

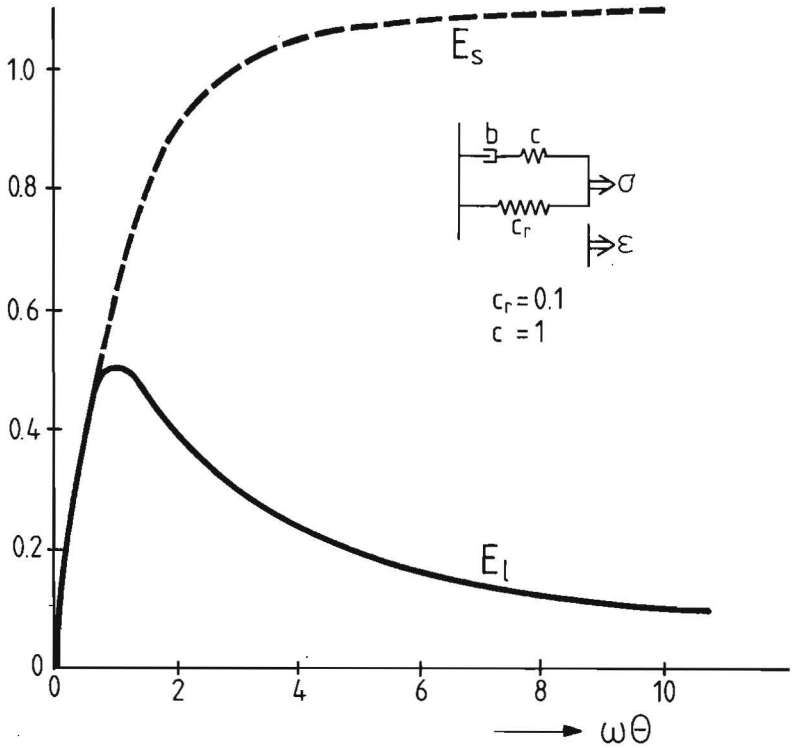

Fig. C3.
Loss and storage modulus for a standard linear solid.

5. σ-ε *Characteristics for different constant strain rates*

In determining σ-ε relations of a viscoelastic material it should be taken into account that the stress required to produce a certain strain, will depend not only on the strain level but also on the strain history. Consequently, on subsequently straining a viscoelastic material at different but constant strain rates, different σ-ε curves will be found. The stress response for a constant-strain-rate test is derived from the convolution integral (2.11) using (4.7), (4.10) and

$$\begin{aligned} &\varepsilon(t) = 0,\ \sigma(t) = 0 \quad \text{for } t < 0 \\ &\varepsilon(t) = vt \qquad\quad \text{for } t > 0 \end{aligned} \tag{5.1}$$

where the strain rate v is a constant. This yields

$$\sigma(t) = \frac{d\sigma^{(e)}}{d\varepsilon} v\theta\left(G(\infty)\frac{t}{\theta} + \{1-G(\infty)\}\{1 - e^{-\frac{t}{\theta}}\}\right). \tag{5.2}$$

Elimination of t by writing $t = \frac{\varepsilon}{v}$ leads to the following expression for σ explicitly formulated in terms of ε and v

$$\sigma(\varepsilon,v) = \sigma^{(e)}(\varepsilon)\left(G(\infty) + \frac{v\theta}{\varepsilon}\{1-G(\infty)\}\{1 - e^{-\frac{\varepsilon}{v\theta}}\}\right). \tag{5.3}$$

From this equation it follows immediately that the response at low strain rates is given by

$$\sigma(\varepsilon,v\to 0) = G(\infty)\sigma^{(e)}(\varepsilon). \tag{5.4}$$

Using $e^{-\frac{\varepsilon}{v\theta}} \approx 1 - \frac{\varepsilon}{v\theta}$ for $v \to \infty$, the response at high strain rates is found to be

$$\sigma(\varepsilon,v\to\infty) = \sigma^{(e)}(\varepsilon) \tag{5.5}$$

From (5.4) and (4.17) we conclude that $G(\infty)\frac{d\sigma^{(e)}}{d\varepsilon}$ can be considered the "quasi-static" stiffness of the material, i.e. the stiffness exhibited by the material under quasi-static loading or straining. In fig. C4 these results are illustrated for a standard linear solid with arbitrarily chosen values of c, c_r and θ.

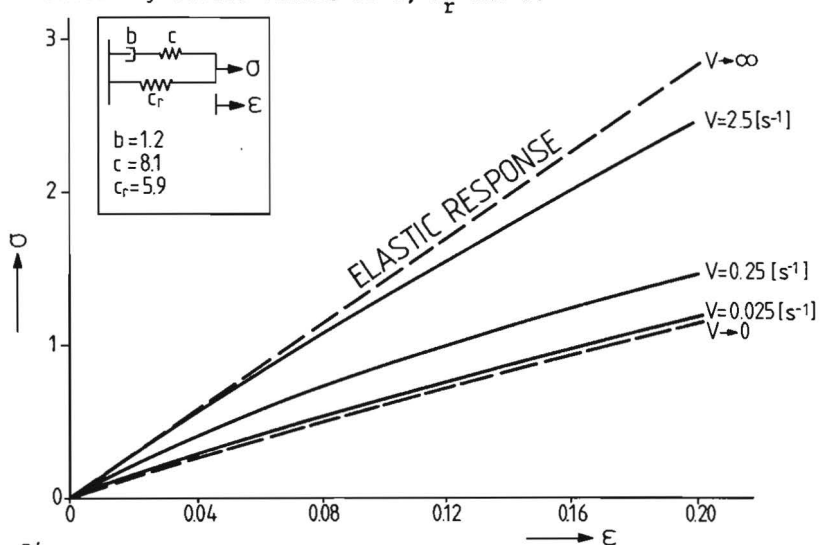

Fig. C4.
σ-ε curves of a standard linear solid obtained for different values of the strain rate v.

6. Stress response to a step-like strain history

In section 2 it was shown that the elastic response and the reduced relaxation function can be determined from the stress response to a step change of the strain. However, it is impossible to realise a true step change in an experiment. The best one can hope for is to succeed in performing a step-like strain history, as outlined in fig. C5.

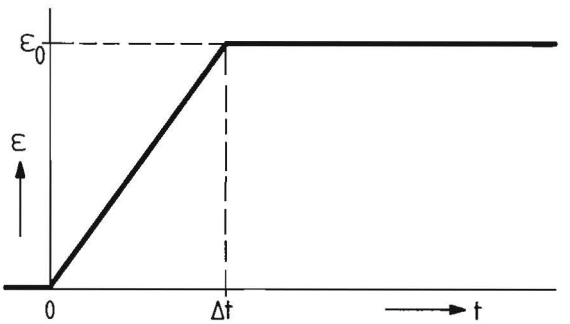

Fig. C5.
Step-like strain history.

If $\varepsilon(t) = 0$ and $\sigma(t) = 0$ for $t < 0$, the stress response is found from (2.11) to be

$$\sigma(t) = \int_{\tau=0}^{x} G(t-\tau)\frac{d\sigma^{(e)}}{d\varepsilon}\frac{d\varepsilon}{d\tau}\,d\tau \quad \text{for } t > 0 \tag{6.1}$$

with $x = t$ for $t \leq \Delta t$

$x = \Delta t$ for $t \geq \Delta t$.

For $t \leq \Delta t$, substitution of (4.7) and (4.10), of course yields (5.2) with $v = \varepsilon_0/\Delta t$, while for $t \geq \Delta t$ it applies that

$$\sigma(\varepsilon_0,t) = \sigma^{(e)}(\varepsilon_0)\left[G(\infty) + \{G(t)-G(\infty)\}\frac{\theta}{\Delta t}\{e^{\frac{\Delta t}{\theta}} - 1\}\right]. \tag{6.2}$$

From this equation it follows immediately that

$$\sigma(\varepsilon_0,\ t\to\infty) = \sigma^{(e)}(\varepsilon_0)G(\infty) \tag{6.3}$$

i.e. maintaining a constant strain level over a long period of time

will result in a stress response that is independent of the way in which this strain level is reached.

Another relation that can be deduced from (6.2) is

$$\sigma(\varepsilon_0,t) = \sigma^{(e)}(\varepsilon_0)G(t) \quad \text{for } \Delta t \ll \theta. \tag{6.4}$$

Fig. C6 shows an example of the response of a standard linear solid to the strain history of fig. C5 for different values of Δt and one value of ε_o (i.e. for different constant strain rates). It is seen that the larger the period Δt, the more relaxation has taken place during the straining phase ($t < \Delta t$). Only if $\Delta t \to 0$, i.e. a step change of the strain, stress relaxation will fully develop during the constant strain phase.

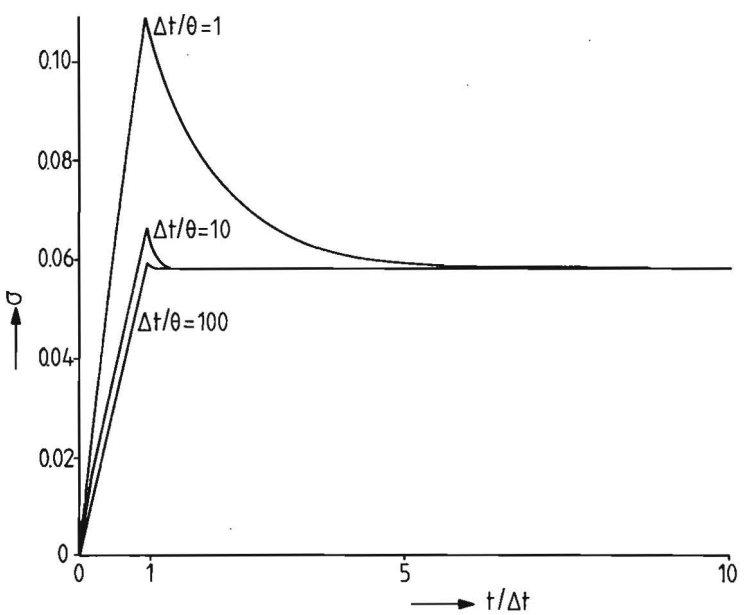

Fig. C6.
Stress response of a standard linear solid to the strain history shown in fig. C5 for different values of Δt and one value of ε_0.

7. Relaxation spectrum

In the foregoing examples the standard linear solid was used to illustrate some characteristics of linear viscoelastic materials. An adequate description of real materials, however, would in general require the use of quite a large number of standard linear solids. The formulation of the constitutive relations for such large spring-and-dashpot models becomes rather tedious. Moreover, because of the large number of model parameters involved, these models soon proof to be hardly suitable for the description of the behaviour of real materials. Where a large number of spring-and-dashpot models would be required, advantageous use can be made of the "relaxation spectrum", which will be introduced in this section. The reduced relaxation function and the complex modulus will also be formulated in terms of this spectrum.

Consider a model made up of a large number (N) of standard linear solids (SLS) shown in Fig. C7. For the total stress σ acting on the model it applies that

$$\sigma = \sum_{i=1}^{N} \sigma^{(i)} \tag{7.1}$$

where $\sigma^{(i)}$ is the contribution of the i-th SLS to the total stress.

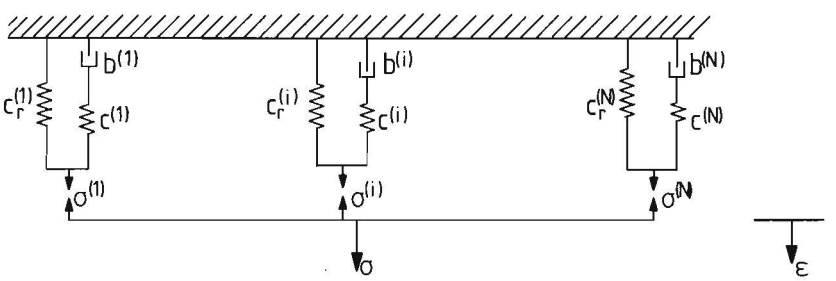

Fig. C7.
Model made up of a parallel arrangement of N standard linear solids.

Further, we will denote the relaxation time constant, the reduced relaxation function and the elastic response of the i-th SLS by $\theta^{(i)}$, $G^{(i)}(t)$ and $\sigma^{(e)}{}^{(i)}(\varepsilon)$, respectively. Because of the parallel arrangement,

the relation between the strain ε of the total model and the strain $\varepsilon^{(i)}$ of the i-th SLS will be

$$\varepsilon = \varepsilon^{(i)}. \tag{7.2}$$

First we derive an expression for the reduced relaxation function. Bearing in mind the definition

$$G(t) = \frac{\sigma_{u.st.}(t)}{\sigma_{u.st.}(0)} \tag{2.7}$$

we formulate the unit-step response for the total model

$$\sigma_{u.st.}(t) = \sum_{i=1}^{N} \sigma^{(i)}_{u.st.}(t). \tag{7.3}$$

Substitution of (4.7) to (4.9) inclusive into (4.5) yields for the contribution $\sigma^{(i)}_{u.st.}(t)$ of the i-th SLS to the total response:

$$\sigma^{(i)}_{u.st.}(t) = \left(G^{(i)}(\infty) + \{1-G^{(i)}(\infty)\}e^{-\frac{t}{\theta^{(i)}}}\right)\frac{d\sigma^{(e)}{}^{(i)}}{d\varepsilon} \tag{7.4}$$

yielding

$$\sigma_{u.st.}(t) = \sum_{i=1}^{N} \left(G^{(i)}(\infty) + \{1-G^{(i)}(\infty)\}e^{-\frac{t}{\theta^{(i)}}}\right)\frac{d\sigma^{(e)}{}^{(i)}}{d\varepsilon} \tag{7.5}$$

As the behaviour of the total model will not be affected by the arrangement of the composing SLS, an arrangement is chosen so that

$$\theta^{(i)} \geq \theta^{(j)} \quad \text{for } i > j.$$

Further, we define the discrete quantities

$$\Delta\theta^{(i)} := \frac{\theta^{(i+1)} - \theta^{(i-1)}}{2}, \tag{7.6}$$

$$\gamma^{(i)} := \frac{G^{(i)}(\infty)}{\Delta\theta^{(i)}} \cdot \frac{d\sigma^{(e)}{}^{(i)}}{d\varepsilon}, \tag{7.7}$$

$$\kappa^{(i)} := \frac{1-G^{(i)}(\infty)}{\Delta\theta^{(i)}} \cdot \frac{d\sigma^{(e)}{}^{(i)}}{d\varepsilon}. \tag{7.8}$$

Combining (7.5) to (7.8) inclusive we get the total response

$$\sigma_{u.st.}(t) = \sum_{i=1}^{N} \left(\gamma^{(i)} + \kappa^{(i)} e^{-\frac{t}{\theta^{(i)}}}\right)\Delta\theta^{(i)}. \tag{7.9}$$

Increasing the number of the constituting SLS ($N\to\infty$) and assuming $\Delta\theta^{(i)} \to 0$ for $N \to \infty$ we arrive at an expression for $\sigma_{u.st.}(t)$ in integral form

$$\sigma_{u.st.}(t) = \int_{\theta=0}^{\infty} \{\gamma(\theta) + \kappa(\theta) e^{-\frac{t}{\theta}}\} d\theta. \tag{7.10}$$

Next we define the *quasi-static stiffness*

$$C_R := \int_{\theta=0}^{\infty} \gamma(\theta) d\theta \tag{7.11}$$

and the *relaxation spectrum*

$$S(\theta) := \frac{\kappa(\theta)}{C_R}. \tag{7.12}$$

With these definitions the unit-step response of the model, now consisting of an infinite number of SLS, can be written as

$$\sigma_{u.st.}(t) = C_R\left(1 + \int_{\theta=0}^{\infty} S(\theta) e^{-\frac{t}{\theta}} d\theta\right) \tag{7.13}$$

which, for the reduced relaxation function, yields

$$G(t) = \frac{1 + \int_{\theta=0}^{\infty} S(\theta) e^{-\frac{t}{\theta}} d\theta}{1 + \int_{\theta=0}^{\infty} S(\theta) d\theta}. \tag{7.14}$$

The expression for the complex modulus is derived in the following manner: the Fourier transform of the constitutive relation for the i-th SLS is given by

$$\sigma_F^{(i)}(\omega) = \bar{E}^{(i)}(\omega)\varepsilon_F^{(i)}(\omega), \tag{7.15}$$

$\bar{E}^{(i)}(\omega)$ being the complex modulus of the i-th SLS. Using (7.1), (7.2) and (7.15), the equivalent relation for the total model is found to be

$$\sigma_F(\omega) = \{ \sum_{i=1}^{N} \bar{E}^{(i)}(\omega) \} \varepsilon_F(\omega) \tag{7.16}$$

from which the complex modulus of the total model is found to be given by

$$\bar{E}(\omega) = \sum_{i=1}^{N} \bar{E}^{(i)}(\omega). \tag{7.17}$$

Replacing ω by ν and using (4.12) we have for the complex modulus of a SLS

$$\bar{E}^{(i)}(\nu) = \left(\frac{G^{(i)}(\infty) + \{1-G^{(i)}(\infty)\}\{(\nu^{(i)})^2 + i\nu^{(i)}\}}{1 + (\nu^{(i)})^2} \right) \frac{d\sigma^{(e)(i)}}{d\varepsilon} \tag{7.18}$$

By the same method as used for the derivation of expression (7.14) for the reduced relaxation function, we get for the complex modulus in terms of the relaxation spectrum

$$\bar{E}(\nu) = E_s(\nu) + iE_\ell(\nu) \tag{7.19}$$

with $E_s(\nu) = C_R \left[1 + \frac{1}{\omega} \int_{\nu=0}^{\infty} \frac{S(\nu).\nu^2}{1+\nu^2} d\nu \right]$; $E_\ell(\nu) = \frac{C_R}{\omega} \int_{\nu=0}^{\infty} \frac{S(\nu)\nu}{1+\nu^2} d\nu$.

In fig. C8 an example is given of the loss and storage modulus corresponding to a relaxation spectrum $S(\theta) = \frac{K}{\theta}$ for $\theta_1 < \theta < \theta_2$ and zero elsewhere. The specific property of this spectrum, proposed by Fung [1972] for the description of soft biological tissues, is that the corresponding loss modulus keeps its maximal value over a wide range of frequencies.

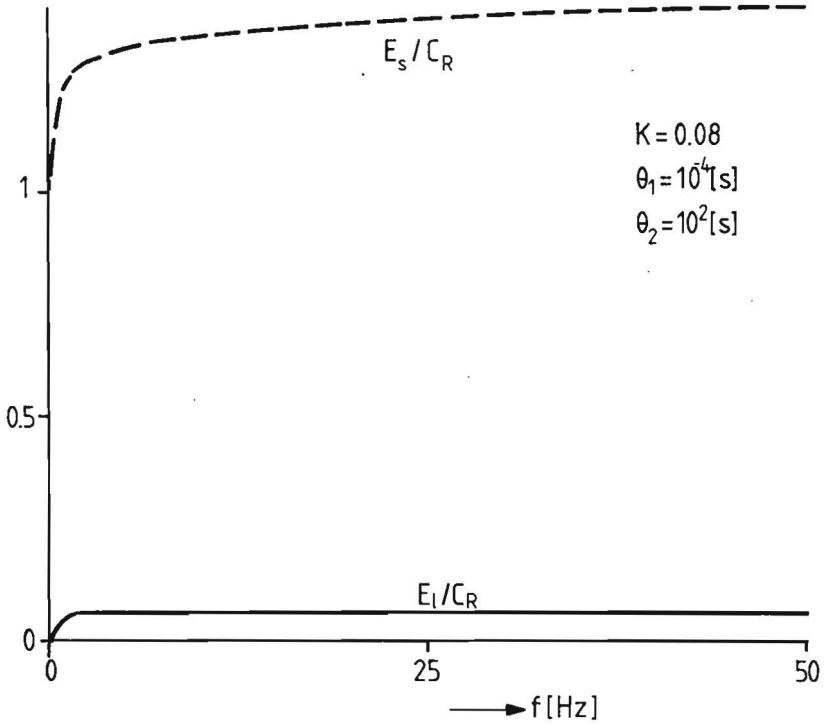

Fig. C8.
Loss and storage modulus corresponding with a relaxation spectrum $S(\theta) = K/\theta$ for $\theta_1 < \theta < \theta_2$ and equal to zero elsewhere.

APPENDIX D
A BRIEF OUTLINE OF THE THEORY OF CONTINUUM MECHANICS

Symbols:

s	scalar
$\vec{a}$	vector
$\mathbf{A}$	second-order tensor
$\mathbf{I}$	second-order unit tensor
${}^4\mathbf{L}$	fourth-order tensor
$\underset{\sim}{b}, \underset{\sim}{\vec{c}}$	column matrices, containing scalar and vector components, respectively
$\underline{I}$	unit scalar matrix
$\underline{B}, \underline{\vec{C}}$	rectangular matrices, containing scalar and vector components, respectively

Operations:

Scalar product: $\vec{a} \circ \vec{b} = c$

$\vec{a} \circ \mathbf{A} = \vec{d}$

$\mathbf{A} \circ \mathbf{B} = \mathbf{C}$

Double scalar product: $\mathbf{A} \circ\circ \mathbf{B} = c$

${}^4\mathbf{L} \circ\circ \mathbf{A} = \mathbf{C}$, $\mathbf{B} \circ\circ {}^4\mathbf{L} = \mathbf{D}$

Vector product: $\vec{a} * \vec{b} = \vec{c}$

Definitions:

Length of $\vec{a}$	$\|\vec{a}\| = (\vec{a} \circ \vec{a})^{\frac{1}{2}}$
inverse scalar matrix	$\underline{A}^{-1} \underline{A} = \underline{I}$
inverse tensor	$\mathbf{A}^{-1} \circ \mathbf{A} = \mathbf{I}$
transposed matrix	$\underset{\sim}{a}^T \underline{A} \underset{\sim}{b} = \underset{\sim}{b}^T \underline{A}^T \underset{\sim}{a}$
transposed tensor	$\vec{a} \circ \mathbf{A} \circ \vec{b} = \vec{b} \circ \mathbf{A}^T \circ \vec{a}$.

1. *Introduction*

In this appendix a brief outline is given of the theory of continuum mechanics. First, a short treatment of the geometrical and kinematical aspects involved in the description of the deformation of a continuum is given (section 2.1). After an introduction dealing with the stress tensor (section 2.2), the equations of motion (section 2.3) and their equivalent, the principle of virtual work (section 2.4) are formulated. Using standard finite element techniques, this principle is reformulated in section 2.5 in a discrete form for one element (section 2.5.2) and the incremental solution method for the discretized model of the continuum is outlined (section 2.5.3). Finally, the properties of two elements, used in modelling the aortic valve, are formulated in section 3. For an extensive treatment of the theory of nonlinear continuum mechanics the reader is referred to current textbooks (e.g. Chadwick, 1976; Sedov, 1972).

2. *General outline of the theory of continuum mechanics*

2.1 *Geometrical aspects*

2.1.1 *Some basic assumptions and definitions*

Consider a continuum B bounded by a surface A in three-dimensional space. Due to external interactions (loads, prescribed displacements etc.) its configuration has changed from a known reference configuration V_τ at time τ to the current configuration V(t) at time $t>\tau$. For the mathematical description of this transformation we choose a fixed point, the origin O, in space. The position of a point P of B in the current configuration V(t) is denoted by the vector $\vec{x}$ and in the reference configuration V_τ by the vector $\vec{x}_\tau$ (fig. D.2.1). It is assumed that every point of B is uniquely related to a particular set $\underset{\sim}{\xi}$ of material coordinates with

$$\underset{\sim}{\xi}^T = [\xi_1 \ \xi_2 \ \xi_3]. \tag{2.1.1}$$

Then $\vec{x}$ will be a function of $\underset{\sim}{\xi}$ and t, that is

$$\vec{x} = \vec{\phi}(\underset{\sim}{\xi}, t) \tag{2.1.2}$$

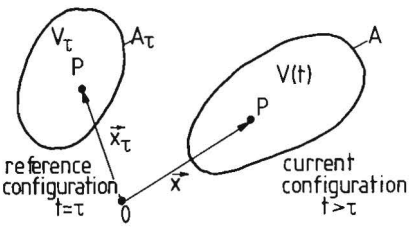

Fig. D2.1.
The reference and the current configuration of a continuum V.

and it is assumed that for each t this equation can be solved for $\underset{\sim}{\xi}$ so that

$$\underset{\sim}{\xi} = \underset{\sim}{\psi}(\vec{x},t);\ \vec{\phi}(\underset{\sim}{\psi}(\vec{x},t),t) = \vec{x} \text{ for } \forall\ \vec{x},t. \tag{2.1.3}$$

In the current configuration, the vector $d\vec{x}$ from a point P with material coordinates $\underset{\sim}{\xi}$ to a neighbouring point Q with material coordinates $\underset{\sim}{\xi}+d\underset{\sim}{\xi}$ is given by

$$d\vec{x} = \vec{x}(\underset{\sim}{\xi}+d\underset{\sim}{\xi},t) - \vec{x}(\underset{\sim}{\xi},t) = \vec{\underset{\sim}{\eta}}^{T}\, d\underset{\sim}{\xi} \tag{2.1.4}$$

where $\vec{\underset{\sim}{\eta}}$ is a column matrix with vectors $\vec{\eta}_1$, $\vec{\eta}_2$, $\vec{\eta}_3$ as components, defined by

$$\vec{\underset{\sim}{\eta}} := \underset{\sim}{\nabla}\vec{x}\ ;\ \underset{\sim}{\nabla}^{T} = \left[\frac{\partial}{\partial\xi_1}\ \frac{\partial}{\partial\xi_2}\ \frac{\partial}{\partial\xi_3}\right]. \tag{2.1.5}$$

Solving (2.1.4) for $d\underset{\sim}{\xi}$ results in

$$d\underset{\sim}{\xi} = (\vec{\underset{\sim}{\eta}}\circ\vec{\underset{\sim}{\eta}}^{T})^{-1}\ \vec{\underset{\sim}{\eta}}\circ d\vec{x}. \tag{2.1.6}$$

The square, symmetrical and regular matrix $\vec{\underset{\sim}{\eta}}\circ\vec{\underset{\sim}{\eta}}^{T}$ is called the metric matrix.

Consider a function y of $\vec{x}$ and t. Then using (2.1.2) $y = y(\vec{x},t)$ can be written as a function of $\underset{\sim}{\xi}$ and t as given below :

$$y = y(\vec{x},t) = y(\vec{\phi}(\xi,t),t). \tag{2.1.7}$$

Using (2.1.4) and (2.1.5), for the difference dy of this function in P and Q, it follows that

$$dy = y(\vec{x}+d\vec{x},t) - y(\vec{x},t) = d\underset{\sim}{\xi}^T(\underset{\sim}{\nabla}y), \tag{2.1.8}$$

and with (2.1.6) it is found that

$$dy = d\vec{x}\circ\vec{\nabla}y \tag{2.1.9}$$

where $\vec{\nabla}$ is the so-called gradient operator in the current configuration, defined by

$$\vec{\nabla} := \vec{\underset{\sim}{\Pi}}^T (\vec{\underset{\sim}{\Pi}}\circ\vec{\underset{\sim}{\Pi}}^T)^{-1} \underset{\sim}{\nabla}. \tag{2.1.10}$$

Similarly the gradient operator in the reference configuration is defined by

$$\vec{\nabla}_\tau := \vec{\underset{\sim}{\Pi}}_\tau^T(\vec{\underset{\sim}{\Pi}}_\tau\circ\vec{\underset{\sim}{\Pi}}_\tau)^{-1} \underset{\sim}{\nabla} \; ; \; \vec{\underset{\sim}{\Pi}}_\tau = \underset{\sim}{\nabla}\vec{x}_\tau \tag{2.1.11}$$

and it can be easily shown that

$$\vec{\nabla}_\tau \vec{x}_\tau = \mathbf{I} \; ; \; \vec{\nabla}\vec{x} = \mathbf{I} \tag{2.1.12}$$

where $\mathbf{I}$ is the second-order unit tensor.

2.1.2 The Lagrangian deformation tensor

The position vector $\vec{x}$ of any material point P in the current configuration V(t) can be written as a function of t and of the position vector $\vec{x}_\tau$ of P in the reference configuration V_τ. With $\vec{x} = \vec{\phi}(\xi,t)$ and $\xi = \psi(\vec{x}_\tau,\tau)$ we get

$$\vec{x} = \vec{F}(\vec{x}_\tau,t). \tag{2.1.13}$$

This is the so-called Lagrangian description of V(t). Using (2.1.9), the vector $d\vec{x}$ from a material point P, with reference vector $\vec{x}_\tau$, to a material point Q with reference vector $\vec{x}_\tau+d\vec{x}_\tau$ (fig. D.2.2) is given by

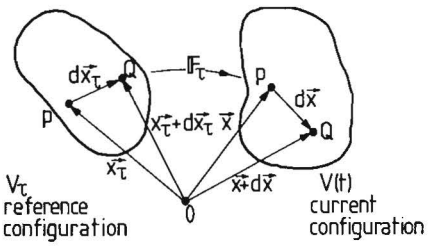

Fig. D2.2.
Transformation of a differential vector $\vec{dx}_\tau$ into $\vec{dx}$.

$$\vec{dx} = \mathbb{F}_\tau \circ \vec{dx}_\tau \tag{2.1.14}$$

where $\mathbb{F}_\tau$ is the Lagrangian deformation tensor, defined as

$$\mathbb{F}_\tau := (\vec{\nabla}_\tau \vec{F})^T = (\vec{\nabla}_\tau \vec{x})^T. \tag{2.1.15}$$

It can be shown that $\mathbb{F}_\tau$ is regular and that $\det(\mathbb{F}_\tau)$ is equal to the ratio $J_{v\tau}$ of the volume dV of a material element in the current configuration and the volume dV_τ of that element in the reference configuration [Veldpaus et al., 1980].

$$J_{v\tau} := \frac{dV}{dV_\tau} = \det(\mathbb{F}_\tau) \neq 0. \tag{2.1.16}$$

The transformation factor $J_{a\tau}$ relating the areas dA_τ and dA of a surface element is given by [Veldpaus et al., 1980].

$$J_{a\tau} := \frac{dA}{dA_\tau} = J_{v\tau} \left\| \mathbb{F}_\tau^{-T} \circ \vec{n}_\tau \right\| \tag{2.1.17}$$

where $\vec{n}_\tau$ is the outward unit normal vector on the surface element in the reference configuration. Moreover, it can be shown that $\mathbb{F}_\tau$ relates the gradient operators $\vec{\nabla}$ and $\vec{\nabla}_\tau$ so that

$$\vec{\nabla} = \mathbb{F}_\tau^{-T} \circ \vec{\nabla}_\tau. \tag{2.1.18}$$

2.1.3 The Green strain tensor

Consider the vectors $d\vec{x}$ and $d\vec{x}_\tau$ used in the preceding section (fig.2.2). On introducing unit vectors $\vec{e}$ and $\vec{e}_\tau$, we can write

$$d\vec{x} = ds\,\vec{e} \quad ; \quad ds = \|d\vec{x}\| = \|\mathbb{F} \circ d\vec{x}_\tau\| \tag{2.1.19}$$

$$d\vec{x}_\tau = ds_\tau\,\vec{e}_\tau \; ; \; ds_\tau = \|d\vec{x}_\tau\| \tag{2.1.20}$$

where ds and ds_τ represent the distance between the neighbouring material points P and Q in the current and the reference configuration, respectively. The stretch λ_τ is the ratio of these distances,

$$\lambda_\tau = \frac{ds}{ds_\tau} = \sqrt{\vec{e}_\tau \circ \mathbb{F}_\tau^T \circ \mathbb{F}_\tau \circ \vec{e}_\tau}, \tag{2.1.21}$$

while the Green strain ε_τ in the direction of $\vec{e}_\tau$ is defined as

$$\varepsilon_\tau = \frac{1}{2}(\lambda_\tau^2 - 1). \tag{2.1.22}$$

With λ_τ according to (2.1.21) and $\vec{e}_\tau \circ \vec{e}_\tau = 1$ it is easily seen that ε_τ can be written as

$$\varepsilon_\tau = \vec{e}_\tau \circ \mathbb{E}_\tau \circ \vec{e}_\tau \tag{2.1.23}$$

where $\mathbb{E}_\tau$, the symmetric Green strain tensor, is given by

$$\mathbb{E}_\tau = \frac{1}{2}(\mathbb{F}_\tau^T \circ \mathbb{F}_\tau - \mathbb{I}). \tag{2.1.24}$$

2.2 The Cauchy and the second Piola-Kirchhoff stress tensors

The stress vector $\vec{p}$ on an infinitesimally small surface element with area dA, containing the point with position vector $\vec{x}$ is defined as

$$\vec{p}(\vec{x},t) = \frac{d\vec{K}}{dA} = \lim_{\Delta A \to 0} \frac{\Delta\vec{K}}{\Delta A} \tag{2.2.1}$$

where $d\vec{K}$ is the load vector acting on the surface element.
Consider an infinitesimally small tetrahedron of the continuum in the present configuration (fig. D.2.3). The tetrahedron is bounded by

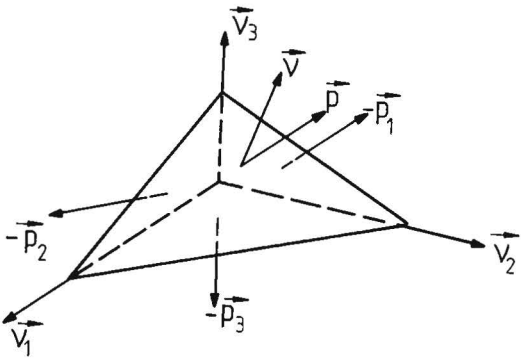

Fig. D2.3.
The stress vectors on a tetrahedron.

three mutually perpendicular surfaces with areas dA_1, dA_2 and dA_3 and outward unit normal vectors $\vec{v}_1$, $\vec{v}_2$ and $\vec{v}_3$,

$$\underset{\sim}{\vec{v}}^T = [\vec{v}_1 \ \vec{v}_2 \ \vec{v}_3], \tag{2.2.2}$$

and by an oblique surface with outward unit normal vector $\vec{v}$ and area dA. The areas dA_1, dA_2, dA_3 and dA are related by

$$dA_i = \vec{v}_i \circ \vec{v} dA. \tag{2.2.3}$$

The stress vectors on the mutually perpendicular surfaces are denoted by $\vec{p}_1$, $\vec{p}_2$ and $\vec{p}_3$,

$$\underset{\sim}{\vec{p}}^T = [\vec{p}_1 \ \vec{p}_2 \ \vec{p}_3] , \tag{2.2.4}$$

whereas the stress vector on the oblique surface is $\vec{p}$. Assuming a load vector per unit volume $\vec{k}$, force equilibrium requires

$$\vec{p} \, dA - \sum_{i=1}^{3} \vec{p}_i \, dA_i + \vec{k} \, d \, V = \vec{0} . \tag{2.2.5}$$

On diminishing the dimensions of the tetrahedron the last term tends to zero and, after dividing by dA, we find

$$\vec{p} = \sigma^T \circ \vec{v} = \vec{v} \circ \sigma \tag{2.2.6}$$

where σ is the so-called Cauchy stress tensor, defined as

$$\sigma = \underset{\sim}{\nu}^{T} \vec{p}. \tag{2.2.7}$$

This tensor is associated with the current configuration. Another stress tensor which is often used, is the second Piola-Kirchhoff stress tensor

$$\mathbb{S}_{\tau} = J_{v\tau} \; \mathbb{F}_{\tau}^{-1} \circ \sigma \circ \mathbb{F}_{\tau}^{-T} \tag{2.2.8}$$

It should be noted that $\mathbb{S}_{\tau}$ is associated with the reference configuration.

2.3 The equations of motion

The relationships between the change of motion of any part $\bar{V}(t)$ of a continuum and the external load acting on it are given by the Newtonian laws

$$\vec{K} = \frac{d\vec{I}}{dt} \tag{2.3.1}$$

and

$$\vec{M} = \frac{d\vec{L}}{dt} \; . \tag{2.3.2}$$

$\vec{K}$ and $\vec{M}$ represent the resulting external load on $\bar{V}(t)$ and the resulting external moment on V(t) with respect to the origin O. The impulse $\vec{I}$ of $\bar{V}(t)$ and the impulse moment $\vec{L}$ of $\bar{V}(t)$ with respect to the origin O are defined by

$$\vec{I}(t) = \int_{\bar{V}(t)} \rho \, \vec{v} \, d\bar{V} \tag{2.3.3}$$

and

$$\vec{L}(t) = \int_{\bar{V}(t)} \vec{x} * \rho \vec{v} \, d\bar{V} \tag{2.3.4}$$

where ρ represents the specific mass in the current configuration and $\vec{v} = \frac{d\vec{x}}{dt}$ the velocity. In general, the external load on $\bar{V}(t)$ will consist of a load per unit volume $\vec{k}(\vec{x},t)$ and a load $\vec{p} = \vec{n} \circ \sigma$ acting on the surface $\bar{A}(t)$ of $\bar{V}(t)$ with outward unit normal vector $\vec{n}$. The resulting external load is given by

$$\vec{K} = \int_{\bar{V}(t)} \vec{k} \, d\bar{V} + \int_{\bar{A}(t)} \vec{n} \circ \sigma \, d\bar{A} \tag{2.3.5}$$

whereas, for the resulting moment, it applies that

$$\vec{M} = \int_{\bar{V}(t)} \vec{x} * \vec{k} \, d\bar{V} + \int_{\bar{A}(t)} \vec{x} * (\vec{n} \circ \sigma) \, d\bar{A} \tag{2.3.6}$$

Substitution of (2.3.3) and (2.3.5) into (2.3.1) and of (2.3.4) and (2.3.6) into (2.3.2) yields after some manipulations [Veldpaus et al., 1980] the local equations of motion

$$\vec{\nabla} \circ \sigma + \vec{k} = \rho \dot{\vec{v}} \qquad \forall \vec{x} \in V(t) \wedge \forall t \tag{2.3.7}$$

$$\sigma = \sigma^T. \tag{2.3.8}$$

Here, $\dot{\vec{v}} = \dot{\vec{v}}(\vec{x},t)$ is the so-called material time derivative of the velocity and is equal to the acceleration of the material point with current position vector $\vec{x}(t)$.
Due to (2.3.8) the Cauchy stress sensor σ must be symmetrical and it is clear that the second Piola-Kirchhoff stress tensor $\$_\tau$ will be symmetrical as well, so that

$$\$_\tau = \$_\tau^T. \tag{2.3.9}$$

2.4 The principle of virtual work

An equivalent formulation of the equation of motion

$$\vec{\nabla} \circ \sigma + \vec{k} - \rho \dot{\vec{v}} = \vec{0} \qquad \forall \vec{x} \in V(t) \wedge \forall t \tag{2.4.1}$$

is given by the requirement that

$$\int_{V(t)} (\vec{\nabla} \circ \sigma + \vec{k} - \rho \dot{\vec{v}}) \circ \vec{h} \, dV = 0 \tag{2.4.2}$$

applies to each $\vec{h} = \vec{h}(\vec{x},t)$ for which the integral exists. We now interprete $\vec{h}$ as a variation of the position vector $\vec{x}$ in the current configuration V(t) giving

$$\vec{h} := \delta\vec{x}. \tag{2.4.3}$$

If $\delta\vec{x}$ is continuous and piecewise differentiable for all values of t and all $\vec{x} \in V(t)$ we say that $\delta\vec{x}$ is admissible. For such $\delta\vec{x}$ the integral in (2.4.2) can be rewritten as

$$\int_{V(t)} \sigma \circ\circ (\vec{\nabla}\delta\vec{x})^T \, dV = \int_{V(t)} (\vec{k} - \rho\dot{\vec{v}}) \circ \delta\vec{x} \, dV + \int_{A(t)} \vec{p} \circ \delta\vec{x} \, dA. \tag{2.4.4}$$

The requirement that this equation applies to each admissible $\delta\vec{x}$, represents the principle of virtual work, associated with the current configuration.

In the following we will reformulate this principle in terms of the reference configuration. With (2.1.18) the left-hand side of (2.4.4) is seen to be equal to

$$\sigma \circ\circ (\vec{\nabla}\delta\vec{x})^T = \sigma \circ\circ ((\vec{\nabla}_\tau \delta\vec{x})^T \circ \mathbb{F}_\tau^{-1}). \tag{2.4.5}$$

With the definition (2.2.8) of the second Piola-Kirchhoff stress tensor $\$_\tau$ and using some identities of tensor calculus we find

$$\sigma \circ\circ (\vec{\nabla}\delta\vec{x})^T = \frac{1}{J_{v\tau}} (\$_\tau \circ \mathbb{F}^T) \circ\circ (\vec{\nabla}_\tau \delta\vec{x})^T. \tag{2.4.6}$$

Using the integral transformations applying to a function a of $\vec{x} = \vec{F}(\vec{x}_\tau, t)$ and t:

$$\int_{V(t)} a \, dV(t) = \int_{V_\tau} J_{v\tau} a \, dV_\tau; \qquad \int_{A(t)} a \, dA(t) = \int_{A_\tau} J_{a\tau} a \, dA_\tau, \tag{2.4.7}$$

and the equivalents of $\vec{k}$, $\vec{p}$ and ρ with respect to the reference configuration

$$\vec{k}_\tau := J_{v\tau}\,\vec{k};\ \vec{p}_\tau := J_{a\tau}\vec{p}\ ;\ \rho_\tau := J_{v\tau}\rho, \tag{2.4.8}$$

it can be found from (2.4.4) and (2.4.6) that the principle of virtual work in terms of the reference configuration and the second Piola-Kirchhoff stress tensor is given by the requirement that

$$\int_{V_\tau} (\$_\tau \circ \mathbb{F}_\tau^T) \bullet\bullet (\vec{\nabla}_\tau \delta\vec{x})^T \, dV = \int_{V_\tau} \vec{w}_\tau \circ \delta\vec{x} \, dV\tau + \int_{A_\tau} \vec{p}_\tau \circ \delta\vec{x} \, dA_\tau \tag{2.4.9}$$

applies for each admissible $\delta\vec{x}$.
In this equation use has been made for the abbreviation

$$\vec{w}_\tau = \vec{k}_\tau - \rho_\tau \dot{\vec{v}}. \tag{2.4.10}$$

It should be noted that from the law of mass conservation it follows that ρ_τ does not depend on t,

$$\rho_\tau = \rho_\tau(\vec{x}_\tau). \tag{2.4.11}$$

2.5 The finite element method.

2.5.1 Introduction

On using the finite element method the continuum is divided into a - sometimes very large - number of pieces relatively simple in shape, the so-called elements. The unknown position vectors of the material points in an element in the present configuration are approximated by a linear combination of the present position vectors of a number of discrete points of the element, the so-called nodal points. The unknown quantities of state in these points are called the nodal point variables. If the relation between the quantities of state at an arbitrary point of the element and the nodal point variables is known, the element properties can be determined using the principle of virtual work. The constitutive equation, i.e. the relation between stresses and strains, must therefore also be available. Once the properties of

the elements and their mutual connections are known, they are assembled and the properties of the continuum can be approximated. For descriptions of the techniques involved in this process, the reader is referred to textbooks on the finite element method (e.g. Zienkiewicz, 1977). In the following, attention will be focussed on the formulation of the properties of a single element.

2.5.2 The principle of virtual work for one element

Consider an element e ($e \in \{1,2,.....,N^e\}$ where N^e is the number of elements) with n nodal points. The present position vector of the nodal point k is denoted by $\vec{q}^e_k(t)$ and the set of the position vectors of all nodal points of this element e is denoted by $\underset{\sim}{\vec{q}}^e(t)$ and defined as

$$(\underset{\sim}{\vec{q}}^e)^T = [\vec{q}^e_1 \ldots. \vec{q}^e_n]. \tag{2.5.1}$$

The position vectors $\vec{x}_\tau$ and $\vec{x}$ of an arbitrary point of the element in, respectively, the reference configuration and the current configuration are approximated by

$$\vec{x}_\tau(\xi) = \underset{\sim}{N}^T(\xi)\underset{\sim}{\vec{q}}^e_\tau \quad ; \quad \underset{\sim}{\vec{q}}^e_\tau = \underset{\sim}{\vec{q}}^e(t=\tau) \tag{2.5.2}$$

and

$$\vec{x}(\xi,t) = \underset{\sim}{N}^T(\xi)\ \underset{\sim}{\vec{q}}^e(t) \tag{2.5.3}$$

where $\underset{\sim}{N}^T(\xi)$ is a set of known interpolation functions:

$$\underset{\sim}{N}^T(\xi) = [\underset{\sim}{N}_1(\xi) \ldots.. N_n(\xi)]. \tag{2.5.4}$$

As stated by (2.5.2) and (2.5.3), the same interpolation functions $\underset{\sim}{N}(\xi)$ are used in both the reference configuration and the current configuration. Elements of this type are called iso-parametric. The condition to be fullfilled by the interpolation functions emanate from two requirements: these functions must be capable of representing all rigid-body motions (i.e. $\underset{\sim}{F}_\tau$ is a orthonormal tensor, not depending on $\vec{x}_\tau$) as well as all homogeneous deformation patterns (i.e. $\underset{\sim}{F}_\tau = \underset{\sim}{C}_\tau(t)$, where $\underset{\sim}{C}_\tau$ is an arbitrary tensor not depending on $\vec{x}_\tau$). In an iso-

parametric three-dimensional continuum element these requirements are met by the necessary and sufficient condition

$$\sum_{i=1}^{n} N_i(\underset{\sim}{\xi}) = 1 \tag{2.5.5}$$

for each $\underset{\sim}{\xi}$ within the element.

The discrete formulation of the principle of virtual work will be derived below. Substitution of (2.5.3) into $\mathbb{F}_\tau = (\vec{\nabla}_\tau \vec{x})^T$ yields

$$\mathbb{F}_\tau = (\vec{\underset{\sim}{\Phi}}^T \vec{\underset{\sim}{q}}^e)^T \tag{2.5.6}$$

where the column matrix $\vec{\underset{\sim}{\Phi}}$ is given by

$$\vec{\underset{\sim}{\Phi}}^T = \vec{\nabla}_\tau \underset{\sim}{N}^T. \tag{2.5.7}$$

For the variation $\delta\vec{x}$ of $\vec{x}$ it applies that

$$\delta\vec{x} = \underset{\sim}{N}^T \delta\vec{\underset{\sim}{q}}^e, \tag{2.5.8}$$

since the interpolation functions $\underset{\sim}{N}(\underset{\sim}{\xi})$ are known functions of $\underset{\sim}{\xi}$. With (2.5.6) for $\mathbb{F}_\tau$, (2.5.8) for $\delta\vec{x}$ and since $\vec{\underset{\sim}{q}}^e = \vec{\underset{\sim}{q}}^e(t)$ is a function of t alone, we obtain for (2.4.9)

$$(\delta\vec{\underset{\sim}{q}}^e)^T \circ \{\int_{V_\tau^e} \vec{\underset{\sim}{\Phi}} \circ \$_\tau \circ \vec{\underset{\sim}{\Phi}}^T \, dV_\tau^e\} \vec{\underset{\sim}{q}} = (\delta\underset{\sim}{q}^e)^T \circ \{\int_{V_\tau^e} \underset{\sim}{N} \vec{w}_\tau dV_\tau^e + \int_{A_\tau^e} \underset{\sim}{N} \vec{p}_\tau dA_\tau^e\} \tag{2.5.9}$$

or, in a condensed form

$$(\vec{\underset{\sim}{q}}^e)^T \circ (\vec{\underset{\sim}{Q}}^e - \vec{\underset{\sim}{R}}^e) = 0 \tag{2.5.10}$$

The column matrices $\vec{\underset{\sim}{Q}}^e$ and $\vec{\underset{\sim}{R}}^e$ contain the internal and external force vectors at the nodal points of the element. They are defined as

$$\vec{\underset{\sim}{Q}}^e = \{\int_{V_\tau^e} \vec{\underset{\sim}{\Phi}} \circ \$_\tau \circ \vec{\underset{\sim}{\Phi}}^T \, dV_\tau^e\} \vec{\underset{\sim}{q}}^e \; ; \; \vec{\underset{\sim}{R}}^e = \int_{V_\tau^e} \underset{\sim}{N} \vec{w}_\tau dV_\tau^e + \int_{A_\tau^e} \underset{\sim}{N} \vec{p}_\tau \, dA_\tau^e \, . \tag{2.5.11}$$

V_τ^e and A_τ^e denote, respectively, the volume and the boundary surface of the element in the original configuration. The mutual connections between the elements are accounted for by connecting the common nodal points of adjacent elements to the so-called nodes of the original system and relating the column matrices $\underset{\sim}{\vec{q}}^e$ of all elements to the column matrix $\underset{\sim}{\vec{q}}$ of the position vectors of these nodes. Using standard techniques of finite element methods, the force vectors $\underset{\sim}{\vec{Q}}^e$ and $\underset{\sim}{\vec{R}}^e$ at the nodal points of the elements can be combined to obtain the corresponding, resulting force vectors $\underset{\sim}{\vec{Q}}$ and $\underset{\sim}{\vec{R}}$ of the assembled set of elements, i.e. the discretized model of the original continuum. This assembling process is based on the fact that the virtual work of the resulting forces equals that of the elemental nodal point forces, so that

$$\sum_{e=1}^{N^e} (\delta \underset{\sim}{\vec{q}}^e)^T \circ \underset{\sim}{\vec{Q}}^e = \delta \underset{\sim}{\vec{q}}^T \circ \underset{\sim}{\vec{Q}} \; ; \quad \sum_{e=1}^{N^e} (\delta \underset{\sim}{\vec{q}}^e)^T \circ \underset{\sim}{\vec{R}}^e = \delta \underset{\sim}{\vec{q}}^T \circ \underset{\sim}{\vec{R}}$$

With these quantities the equations of motion for the discrete model of the continuum can be derived as

$$\underset{\sim}{\vec{Q}} - \underset{\sim}{\vec{R}} = \underset{\sim}{\vec{0}} \qquad (2.5.12)$$

2.5.3 The incremental solution method

In the equations of motion $\underset{\sim}{\vec{Q}} - \underset{\sim}{\vec{R}} = \underset{\sim}{\vec{0}}$ the internal and external forces $\underset{\sim}{\vec{Q}}$ and $\underset{\sim}{\vec{R}}$ can depend on t and, in general, are nonlinear functions of $\underset{\sim}{\vec{q}}$, which in turn is a function of t. Therefore, an incremental solution method has to be used for the determination of $\underset{\sim}{\vec{q}}$. Such a method consists of the computation of $\underset{\sim}{\vec{q}}(t_{i+1})$ from the known values of $\underset{\sim}{\vec{q}}$ at $t_o, t_1, \ldots t_i$. For an arbitrary function a of $\underset{\sim}{\vec{q}}(t)$ and t we define the increment Δa of a in the time interval $[t_i, t_{i+1}]$ as

$$\Delta a = a(\underset{\sim}{\vec{q}}(t_{i+1}),\ t_{i+1}) - a(\underset{\sim}{\vec{q}}(t_i),\ t_i). \qquad (2.5.13)$$

Using (2.5.11) the increments $\Delta \underset{\sim}{\vec{Q}}^e$ and $\Delta \underset{\sim}{\vec{R}}^e$ of the internal and external force vectors at the nodal points of element e can be written as:

$$\Delta\vec{\underset{\sim}{Q}}^{e} = \{\int_{V_\tau^e} \vec{\underset{\sim}{\Phi}} \circ \Delta\$_\tau \circ \vec{\underset{\sim}{\Phi}}^{T} dV_\tau^e\}\,\vec{g}^{e} + \{\int_{V_\tau^e} \vec{\underset{\sim}{\Phi}} \circ \$_\tau \circ \vec{\underset{\sim}{\Phi}}^{T}\, dV_\tau^e\}\Delta\vec{g}^{e} \tag{2.5.14}$$

$$\Delta\vec{\underset{\sim}{R}}^{e} = \int_{V_\tau^e} \underset{\sim}{N}\, \Delta\vec{w}_\tau\, dV_\tau^e + \int_{A_\tau^e} \underset{\sim}{N}\, \Delta\vec{p}_\tau\, dA_\tau^e. \tag{2.5.15}$$

Products of $\Delta\$_\tau$ and $\Delta\vec{g}^{e}$ have been omitted in the derivation of (2.5.14) assuming that the increments are very small. The second integral in (2.5.14) represents the so-called initial stiffness matrix $\underline{\Gamma}^{e}$, so that

$$\underline{\Gamma}^{e} = \int_{V_\tau^e} \vec{\underset{\sim}{\Phi}} \circ \$_\tau \circ \vec{\underset{\sim}{\Phi}}^{T}\, dV_\tau^e. \tag{2.5.16}$$

If $\$_\tau$ is known at $t=t_i$ this matrix can be determined. To elaborate the first integral, the relationship between the increments $\Delta\$_\tau$ and $\Delta\mathbb{E}_\tau$, i.e. the constitutive equation, must be known.
We assume that for this equation it applies that

$$\Delta\$_\tau = {}^{4}\mathbb{L}_\tau \circ\circ \Delta\mathbb{E}_\tau, \tag{2.5.17}$$

where ${}^{4}\mathbb{L}_\tau$ is a fourth-order tensor representing material moduli. In the case of time-independent behaviour (2.5.17) will always apply if $\Delta\mathbb{E}_\tau$ is infinitesimally small. ${}^{4}\mathbb{L}_\tau$ may be a function of $\mathbb{E}_\tau$ and in actual calculations it must be possible to compute the components of ${}^{4}\mathbb{L}_\tau$ if the components of $\mathbb{E}_\tau$ are given. Using the linearized relation

$$\Delta\mathbb{E}_\tau = \frac{1}{2}\,(\mathbb{F}_\tau^{T} \circ \Delta\mathbb{F}_\tau + \Delta\mathbb{F}_\tau^{T} \circ \mathbb{F}_\tau), \tag{2.5.18}$$

we find with (2.5.14)

$$\Delta\vec{\underset{\sim}{Q}}^{e} = \underline{\Lambda}^{e} \circ \Delta\vec{g}^{e} + \underline{\Gamma}^{e}\,\Delta\vec{g}^{e} \tag{2.5.19}$$

with

$$\underline{\Lambda}^{e} = \int_{V_\tau^e} (\vec{\underset{\sim}{\Phi}}^{T}\mathbb{F}_\tau^{T}) \circ\circ {}^{4}\mathbb{L}_\tau \circ\circ (\vec{\underset{\sim}{\Phi}}^{T}\mathbb{F}_\tau^{T})\, dV_\tau^e. \tag{2.5.20}$$

Again using standard finite element techniques, the increments $\Delta\vec{Q}^e$ for all elements can be combined to get the increment $\Delta\vec{Q}$ of the resulting force vector $\vec{Q}$. From (2.5.19) it can be seen that the relation between this increment and the increment $\Delta\vec{q}$ of the column matrix $\vec{q}$ will be linear if (and in general only if) the time increment $\Delta t = t_{i+1}-t_i$ is sufficiently small. The external force vectors $\vec{R}$ can be treated in a more or less similar way. For a special case we will discuss this in the next section. Finally we arrive at a linear set of equations for the unknown increments $\Delta\vec{q}$. Solving this set and using $\vec{q}(t_{i+1}) = \vec{q}(t_i)+\Delta\vec{q}$ gives the solution for the position vectors of the nodes at time $t=t_{i+1}$. For details of this method and the numerical aspects of the solution procedure we have to refer to text books on this subject (e.g. Zienkiewicz, 1977; Veldpaus et al., 1980).

3. Formulation of the properties of some elements

3.1 The membrane element

In formulating the properties of the membrane element it will be assumed that the stress vector in each point of the midplane of the membrane always lies in the tangent plane at that point. Furthermore, the membrane is assumed to have no bending stiffness while stresses are constant across the thickness.
The position vector of a point P in the midplane of the membrane is a function of the material coordinates ξ_1 and ξ_2 of P, so that

$$\vec{x} = \vec{x}(\xi,t) \; ; \; \vec{x}_\tau = \vec{x}_\tau(\xi) \; ; \; \xi^T = [\xi_1 \; \xi_2]. \tag{3.1.1}$$

In the current configuration two independent tangent vectors of the midplane are given by

$$\vec{n} = \underset{\sim}{\nabla}^m\vec{x} \; ; \; (\underset{\sim}{\nabla}^m)^T = [\frac{\partial}{\partial\xi_1} \quad \frac{\partial}{\partial\xi_2}] \; . \tag{3.1.2}$$

Their cross product $\vec{n}_1*\vec{n}_2$ is a vector with length $\Xi \neq 0$ and the unit normal vector $\vec{n}$ on the midplane follows from

$$\vec{n} = \frac{1}{\Xi}\vec{n}_1*\vec{n}_2 \; ; \; \Xi = \|\vec{n}_1*\vec{n}_2\| \; . \tag{3.1.3}$$

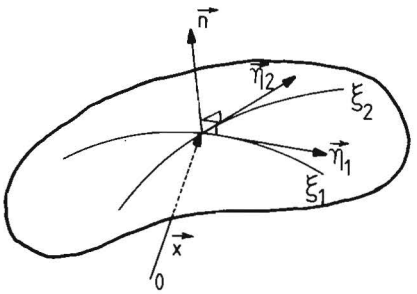

Fig. D3.1.
The membrane in the current configuration.

Let $y=y(\vec{x},t)$ be a function of t that is defined for each point in the midplane and let dy be the difference of this function in two neighbouring points P and Q with position vectors $\vec{x}(\xi,t)$ and $\vec{x}(\xi+d\xi,t) = \vec{x}(\xi,t) + d\vec{x}$, respectively. Then it is easy to show that

$$dy = (\vec{\nabla}^m \vec{x})^T \circ d\vec{x} \tag{3.1.4}$$

where $\vec{\nabla}^m$ is given by

$$\vec{\nabla}^m = \vec{\underline{D}}^T (\vec{\underline{D}} \circ \vec{\underline{D}}^T)^{-1} \underline{\nabla}^m. \tag{3.1.5}$$

In order to formulate the principle of virtual work for the membrane we start from (2.4.9)

$$\int_{V_\tau} (\$_\tau \circ \underline{F}_\tau^T) \circ\circ (\vec{\nabla}_\tau \delta\vec{x})^T \, dV_\tau = \int_{V_\tau} \vec{w}_\tau \circ \delta\vec{x} \, dV_\tau + \int_{A_\tau} \vec{p}_\tau \circ \delta\vec{x} \, dA_\tau. \tag{2.4.9}$$

With the given assumptions on the stress vector and the additional assumption that one of the principal strain directions is normal to the midplane, the second Piola-Kirchhoff stress tensor can be written as

$$\$_\tau = \vec{\underline{D}}_\tau^T \underline{S}_\tau \vec{\underline{D}}_\tau \quad ; \vec{\underline{D}}_\tau(\xi) = \vec{\underline{D}}(\xi,\tau) \tag{3.1.6}$$

A further elaboration (including the analysis of increments) of the left-hand side of (2.4.9) follows exactly the same lines as in the

preceding section. At the right-hand side of (2.4.9) especially the second term is of importance for membranes and, therefore, we concentrate on this term for the case that the surface load $\vec{p}$ is a pressure load. Using

$$\vec{p} = - p\vec{n} \; ; \; \vec{p}_\tau = J_{a\tau}\, \vec{p} \tag{3.1.7}$$

the virtual work due to the pressure load in the current configuration is given by

$$\delta W_p = \int_A \vec{p} \circ \delta\vec{x} \; dA. \tag{3.1.8}$$

For an increment $\Delta(\delta W_p)$ of δW_p it applies that [De Wilde, 1981]

$$\Delta(\delta W_p) = \int_A \frac{1}{J_{a\tau}} \Delta(J_{a\tau}\vec{p}) \circ \delta\vec{x} \; dA. \tag{3.1.9}$$

With

$$\Delta(J_{a\tau}\vec{p}) = - J_{a\tau}\vec{n} \, \Delta p - p\Delta(J_{a\tau}\vec{n}) \tag{3.1.10}$$

and

$$p\Delta(J_{a\tau}\, \vec{n}) = (\vec{\nabla}^m \circ \Delta\vec{x})\vec{p} \circ \delta\vec{x} - \vec{p} \circ (\vec{\nabla}^m \Delta\vec{x}) \circ \delta\vec{x} \tag{3.1.11}$$

it is found, after some manipulations, that

$$\Delta(\delta W_p) + \int_A \Delta p \; \vec{n} \circ \delta\vec{x} \; dA = \int_A (\vec{\nabla}^m \circ \Delta\vec{x})\vec{p} \circ \delta\vec{x} \; dA + \int_A \delta\vec{x} \; \vec{p} \circ \circ \vec{\nabla}^m \Delta\vec{x} \; dA. \tag{3.1.12}$$

The first integral at the right-hand side can be rewritten as the sum of a boundary and a surface integral, using the identity

$$\int_A \vec{\nabla}^m \circ \vec{a} \; dA = \oint_\Gamma \vec{a} \circ \vec{\eta} \; d\Gamma + \int_A (\vec{\nabla}^m \circ \vec{n})(\vec{n} \circ \vec{a}) \; dA, \tag{3.1.13}$$

where Γ and $\vec{n}$ represent the boundary of the surface A and the unit outward normal vector on the boundary, respectively. For an increment of the virtual work due to the pressure load finally this yields

$$\Delta(\delta W_p) = -\int_A \Delta p\, \vec{n}\circ\delta\vec{x}\, dA + \oint_\Gamma \Delta\vec{x}\circ\vec{n}\, \vec{p}\circ\delta\vec{x}\, d\Gamma +$$

$$+ \int_A \Delta\vec{x}\circ\{-p\vec{n}\vec{n} + (\vec{\nabla}^m p)\vec{n} + p\vec{\nabla}^m\vec{n}\}\circ\delta\vec{x}\, dA +$$

$$- \int_A [\Delta\vec{x}\circ(\vec{p}\circ\vec{\nabla}^m\delta\vec{x}) + \{(\vec{\nabla}^m\Delta\vec{x})^T\circ\vec{p}\}\circ\delta\vec{x}]dA. \qquad (3.1.14)$$

It can be shown that the tensor $p\,\vec{\nabla}^m\vec{n}$ in the third integral is symmetrical. Therefore, in the case of a constant pressure load ($\vec{\nabla}^m p=\vec{0}$) and when the boundary integral is equal to zero (e.g. fixed boundary) only a symmetric tensor, represented by the last two integrals, remains for the calculations.
The discretized formulation of the principle of virtual work (2.5.9) for a membrane element now becomes

$$(\delta\vec{\underset{\sim}{q}}^e)^T\circ\left[\int_{V_\tau^e}\vec{\underset{\sim}{\Phi}}^m\circ S_\tau\circ\vec{\underset{\sim}{\Phi}}^m\, dV_\tau^e\}\,\vec{\underset{\sim}{q}}^e - \int_{V_\tau^e}\underset{\sim}{N}^m\vec{w}_\tau\, dV_\tau^e - \int_{A_\tau^e}\underset{\sim}{N}^m\vec{p}_\tau\, dA^e\right] = 0 \qquad (3.1.15)$$

where

$$\vec{\underset{\sim}{\Phi}}^{mT} = \vec{\nabla}_\tau\underset{\sim}{N}^{mT}\ ;\ \vec{\nabla}_\tau^m = \vec{n}_\tau^T(\vec{\underset{\sim}{n}}_\tau\circ\vec{n}_\tau^T)^{-1}\,\underset{\sim}{\nabla}^m.$$

while the column matrix $\underset{\sim}{N}^m$ contains the interpolation functions chosen for the membrane element. Because the various quantities are assumed to be constant across the membrane thickness $h_\tau(\underset{\sim}{\xi})$ in the reference configuration, the volume integrals in (3.1.15) can be transformed into surface integrals by writing the volume dV_τ of an infinitesimal small element in the reference configuration as

$$dV_\tau = h_\tau(\underset{\sim}{\xi})\, dA_\tau \;;\; dA_\tau = \|\vec{\eta}_{\tau 1} * \vec{\eta}_{\tau 2}\|\, d\xi_1 d\xi_2. \qquad (3.1.16)$$

It should be noted that $dV_\tau = h_\tau(\underset{\sim}{\xi})\, dA_\tau$ is an approximation.

After discretizing (3.1.14) and using (3.1.15) the incremental formulation of the equations of motion for a pressurized membrane can be derived in the same way as in section 2.5.3.

3.2 The cable element

The cable element can be characterized by a line. For its geometrical description one material coordinate ξ suffices. It will be assumed that the element has no bending stiffness and that all stresses, except the normal stress in the tangential direction, are zero. For the position vector of a point of the cable in the reference and the current configuration it applies that

$$\vec{x}_\tau = \vec{x}_\tau(\xi) \;;\; \vec{x} = \vec{x}(\xi,t) \qquad (3.2.1)$$

and therefore the tangent vectors in the current and the reference configuration are given by

$$\vec{\eta} = \frac{d\vec{x}}{d\xi} \quad ; \quad \vec{\eta}_\tau = \frac{d\vec{x}_\tau}{d\xi} = \vec{\eta}(\xi,\tau). \qquad (3.2.2)$$

As only normal stresses in the tangential direction differ from zero, for the Cauchy stress tensor it applies that

$$\mathbf{\sigma} = \sigma\, \vec{n}\, \vec{n} \quad ; \quad \vec{n} = \frac{\vec{\eta}}{\|\vec{\eta}\|}$$

Assuming that the tangential direction is a principal strain direction, it can easily be shown that for the second Piola-Kirchhoff stress tensor we have

$$\mathbf{S}_\tau = S_\tau\, \vec{n}_\tau\, \vec{n}_\tau; \quad \vec{n}_\tau = \frac{\vec{\eta}_\tau}{\|\vec{\eta}_\tau\|}. \qquad (3.2.3)$$

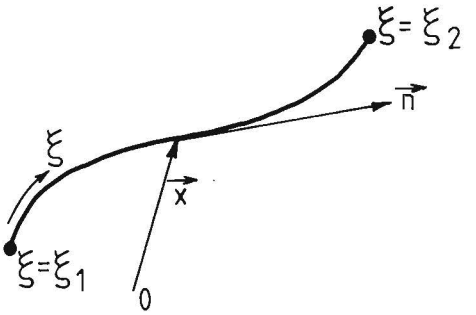

Fig. D3.2.
The cable in the current configuration.

For the principle of virtual work for the cable we obtain

$$\delta\vec{q}^{T}\circ\left[\left\{\int_{V_\tau}\underset{\sim}{\vec{\Phi}}^{c}\bullet\$_\tau\bullet\underset{\sim}{\vec{\Phi}}^{c^T}\,dV_\tau\right\}\vec{q} - \int_{V_\tau}\underset{\sim}{N}^{c}\,\vec{w}_\tau\,dV_\tau - \int_{A_\tau}\underset{\sim}{N}^{c}\,\vec{p}_\tau\,dA_\tau\right] = 0 \quad (3.2.4)$$

with

$$\underset{\sim}{\vec{\Phi}}^{c^T} = \vec{\nabla}^{c}_{\tau}\,\underset{\sim}{N}^{c^T} = \vec{\eta}_\tau\,\frac{\partial\underset{\sim}{N}^{c^T}}{\partial\xi}\Big/\|\vec{\eta}_\tau\|^{2}\,.$$

All quantities are assumed to be constant across the cross-sectional area. Therefore, for shallow curved cables the volume of an infinitesimally small element in the reference configuration can be described by

$$dV_\tau = A_\tau(\xi)\,\|d\vec{x}_\tau\| = A_\tau(\xi)\,\|\vec{\eta}_\tau\|\,d\xi \quad (3.2.5)$$

where $A_\tau(\xi)$ represents the cross-sectional area in the reference configuration. With (3.2.4) and (3.2.5) and on the assumption that $\vec{p}_\tau \neq \vec{0}$ only at the end surfaces ($\xi = \xi_1$, $\xi = \xi_2$), we find after some manipulations for the principle of virtual work that

$$\delta\vec{q}^{T}\circ\Bigg[\Bigg\{\int_{\xi=\xi_1}^{\xi_2}\frac{d\underset{\sim}{N}^{c}}{d\xi}\,S_{\tau}\,\frac{d\underset{\sim}{N}^{c^{T}}}{d\xi}\;A_{\tau}(\xi)\,\|\vec{n}_{\tau}\|^{-1}\,d\xi\Bigg\}\vec{\underset{\sim}{q}}+$$

$$-\int_{\xi=\xi_1}^{\xi_2}\underset{\sim}{N}^{c}\,\vec{w}_{\tau}\,A_{\tau}(\xi)\,\|\vec{n}_{\tau}\|\,d\xi+\{N^{c}\,\vec{p}_{\tau}\,A_{\tau}(\xi)\}\Big|_{\xi=\xi_1}+$$

$$-\{\underset{\sim}{N}^{c}\,\vec{p}_{\tau}\,A_{\tau}(\xi)\}\Big|_{\xi=\xi_2}\Bigg]=0. \qquad (3.2.6)$$

REFERENCES

Abrahams, M. (1967):
Mechanical behaviour of tendon in vitro.
Med. Biol. Engng 5, 433-443.

Apter, J.T. (1964):
Mathematical development of a physical model of some visco-elastic properties of the aorta.
Bulletin of Mathematical Biophysics 26, 367-388.

Arts, M.G.J. (1978):
A mathematical model of the dynamics of the left ventricle and the coronary circulation.
Thesis University of Limburg, Maastricht, The Netherlands.

Bellhouse, B.J. and Talbot, L. (1969):
The fluid mechanics of the aortic valve.
J. Fluid Mech. 35, 721-735.

Bingham, D.N. and DeHoff, P.H. (1979):
A constitutive equation for the canine anterior cruciate ligament.
J. Biomech. Engng 101, 15-22.

Brewer, R.J., Deck, J.D., Capati, B. and Nolan, S.P. (1976):
The dynamic aortic root: its role in aortic valve function.
J. Thorac. Cardiovasc. Surg. 72 (3), 413-417.

Brewer, R.J., Mentzer, R.M., Deck, J.D., Ritter, R.C., Trefil, J.S. and Nolan, S.P. (1977):
An *in vivo* study of the dimensional changes of the aortic valve leaflets during the cardiac cycle.
J. Thorac. Cardiovasc. Surg. 74 (4), 645-650.

Carton, R.W., Dainauskas, J. and Clark, J.W. (1962):
Elastic properties of single elastic fibres.
J. Appl. Physiol., 17 (3), 547-551.

Cataloglu, A., Gould, P.L. and Clark, R.E. (1975):
Validation of a simplified mathematical model for the stress analysis of human aortic heart valves.
J. Biomech. 8, 347-348.

Chadwick, P. (1976):
Continuum mechanics: concise theory and problems.
Ed. George Allen and Unwin, London.

Chen, Y.L. and Fung, Y.C. (1973):
Stress-strain-history relations of rabbit mesentery in simple elongation.
Biomech. Symp., AMD-2, ASME, 9-10.

Chong, K.P., Wieting, D.W., Hwang, N.H.C. and Kennedy, J.H. (1973):
Stress analysis of normal human aortic valve leaflets during diastole.
Biomat., Med. Dev., Art. Org. 1 (2), 307-321.

Chong, M. and Missirlis, Y.F. (1978):
Aortic valve mechanics-Part II: A stress analysis of the porcine aortic valve leaflets in diastole.
Biomat., Med. Dev., Art. Org. 6 (3), 225-244.

Christensen, R.M. (1971):
Theory of viscoelasticity. An introduction.
Academic Press, London.

Clark, R.E. and Butterworth, G.A.M. (1971):
Characterization of the mechanics of human aortic and mitral valve leaflets.
Surgical Forum 22, 134-136.

Clark, R.E. (1973):
Stress-strain characteristics of fresh and frozen human aortic and mitral leaflets and chordae tendineae.
J. Thorac. Cardiovasc. Surg. 66, 202-208.

Clark, R.E. and Finke, E.H. (1974):
Scanning and light microscopy of human aortic leaflets in stressed and relaxed states.
J. Thorac. Cardiovasc. Surg. 67 (5), 792-803.

Comninou, M. and Yannas, J.V. (1976):
Dependence of stress-strain nonlinearity of connective tissues on the geometry of collagen fibres.
J. Biomech. 9, 427-433.

Decraemer, W.F., Maes, M.A. and Vanhuyse, V.J. (1980a):
An elastic stress-strain relation for soft biological tissues based on a structural model.
J. Biomech. 13, 463-468.

Decraemer, W.F., Maes, M.A., Vanhuyse, V.J. and Vanpeperstraete, P. (1980b):
A non-linear viscoelastic constitutive equation for soft biological tissues, based upon a structural model.
J. Biomech. 13, 559-564.

DeHoff, P.H. (1978):
On the nonlinear viscoelastic behaviour of soft biological tissues.
J. Biomech. 11, 35-40.

Diamant, J., Keller, A., Baer, E., Litt, M. and Arridge, R.G.C. (1972):
Collagen; ultrastructure and its relation to mechanical properties as a function of ageing.
Proc. R. Soc. Lond. B. 180, 293-315.

Frisén, M., Mägi, M., Sonnerup, L. and Viidik, A. (1969):
Rheological analysis of soft collagenous tissue. Part I: Theoretical considerations.
J. Biomech. 2, 13-20.

Fung, Y.C.B. (1967):
Elasticity of soft tissues in simple elongation.
Am. J. Physiol. 213 (6), 1532-1544.

Fung, Y.C.B. (1972):
Stress-strain-history relations of soft tissues in simple elongation.
Chapter 7 in: *Biomechanics, its foundations and objectives* (edited by Fung, Y.C.B., Perrone, N. and Anliker, M.), 181-208, Prentice-Hall Inc.

Gou, P.F. (1970):
Strain energy function for biological tissues.
J. Biomech. 3, 547-550.

Gould, P.L., Cataloglu, A., Dhatt, G., Chattopadhyay, A. and Clark, R.E. (1973):
Stress analysis of the human aortic valve.
Computers and Structures 3, 377-384.

Gould, P.L., Cataloglu, A. and Clark, R.E. (1976):
Mathematical modelling of human aortic valve leaflets.
Appl. Math. Modelling 1, 33-36.

Gould, P.L., Baldini, S.E., Rossow, M.P. and Clark, R.E. (1980):
Stress analysis of aortic valves.
International Conference Proceedings on Finite Elements in Biomechanics 2, 583-604.

Gray, H. (1980):
Anatomy.
36th rev. ed. Edited by R. Warwick and P.L. Williams, London.
Churchill Livingstone.

Gross, L. and Kugel, M.A. (1931):
Topographic anatomy and histology of the valves in the human heart.
Am. J. Pathol. 7, 445-473.

Guth, E., Wack, P.E. and Anthony, R.L. (1946):
Significance of the equation of state for rubber.
J. Appl. Physics 17, 347-351.

Guyton, A.C. (1981):
Textbook of medical physiology.
6th ed., Philadelphia, W.B. Saunders Company.

Hass, G.M. (1942):
Elasticity and tensile strength of elastic tissue isolated from the human aorta.
Arch. Pathol. 34, 971.

Haut, R.C. and Little, R.W. (1972):
A constitutive equation for collagen fibres.
J. Biomech. 5, 423-430.

Heckman, J.L. and Ascanio, G. (1972):
A cinefluoroscopic recording of aortic valve motion.
Fed. Proc. 31, 817.

Jenkins, R.B. and Little, R.W. (1974):
A constitutive equation for parallel-fibred elastic tissue.
J. Biomech. 7, 397-402.

Karara, S. and Marzan, G.T. (1973):
Determination of the geometry of trileaflet aortic heart valves.
Proc. 17th Annual Technical Meeting of the Society of Photo-Optical Instrumentation Engineers, San Diego, Calif.

Kenedi, R.M. Gibson, T., Evans, J.M. and Barbenel, J.C. (1975):
Tissue mechanics.
Phys. Med. Biol. 20 (5), 699-717.

Lake, L.W. and Armeniades, C.D. (1972):
Structure-property relations of aortic tissue.
Trans. Amer. Soc. Artif. Organs 18, 202-209.

Lanir, Y. (1979):
A structural theory for the homogeneous biaxial stress-strain relationships in flat collagenous tissues.
J. Biomech. 12, 423-436.

Lim, K.O. and Boughner, D.R. (1976):
The low frequency dynamic viscoelastic properties of human aortic valve tissue.
Circ. Res. 39 (2), 209-214.

Lockett, F.J. (1972):
Nonlinear viscoelastic solids.
Academic Press. London.

Lozsádi, K. and Arvay, A. (1969):
Comparative anatómical investigations on the heterotransplantation of the aortic valve.
Acta Chir. Acad. Sci. Hung. 10 (2), 207-214.

Lyons, M.F. (1976):
Ultrastructural organization in the aortic valve of the dog.
Anat. Rec. 184 (3), 467.

Mercer, J.L. (1973):
The movements of the dog's aortic valve studied by high speed cine-angiography.
Brit. J. Radiol. 46, 344-349.

Missirlis, Y.F. (1973):
In vitro studies of human aortic valve mechanics.
Thesis Rice University, Houston, Texas.

Missirlis, Y.F. and Armeniades, C.D. (1976):
Stress analysis of the aortic valve during diastole.
J. Biomech. 9, 447-480.

Missirlis, Y.F. and Chong, M. (1978):
Aortic valve mechanics - Part I: Material properties of natural porcine aortic valves.
J. Bioengng 2, 287-300.

Mohri, H., Reichenbach, D.D. and Merendino, K.A. (1972):
Biology of homologous and heterologous aortic valves.
Biological tissue in heart valve replacement (Edited by Ionescu, M.I., Ross, D.N. and Wooler, G.H.), 137-142, Butterworths, London.

Mundth, E.D., Wright, J.E.C. and Austen, W.G. (1971):
Development of a method for stress-strain analysis of cardiac valvular tissue.
Current Topics in Surgical Research 3, 67-72.

Neubert, H.K.P. (1963):
A simple model representing internal damping in solid materials.
The Aeronautical Quarterly 14, 187-210.

Pinto, J.G. and Fung, Y.C. (1973):
Mechanical properties of the heart muscle in the passive state.
J. Biomech. 6, 597-616.

Pinto, J.G. and Patitucci, P.J. (1980):
Visco-elasticity of passive cardiac muscle.
J. Biomech. Engng 102, 57-61.

Reid, K. (1970):
The anatomy of the sinus of Valsalva.
Thorax 25, 79-85.

Renterghem, R.J. van, Steenhoven, A.A. van and Beneken, J.E.W. (1979):
The pressure-volume relationship of the aortic valve in terms of compliance.
Biomedizinische Technïek 24, 281-282.

Rigby, B.J., Hirai, N., Spikes, J.D. and Eyring, H. (1959):
The mechanical properties of rat tail tendon.
J. Gen. Physiol. 43, 265-283.

Rigby, B.J. (1964):
Effect of cyclic extension on the physical properties of tendon collagen and its possible relation to biological ageing of collagen.
Nature 202, 1072-1074.

Rousseau, E. (1980):
Onderzoek naar de mechanische eigenschappen van aortaklepweefsel.
Report WE 80.05, Eindhoven University of Technology, The Netherlands.

Sands, M.P., Rittenhouse, E.A., Mohri, H. and Merendino, K.A. (1969):
An anatomical comparison of human, pig, calf and sheep aortic valves.
Ann. Thorac. Surg. 8 (5), 407-414.

Sauren, A.A.H.J. and Hout, M.C. van (1979):
De prekonditionering van aortaklepweefsel.
Report Eindhoven Heart Valve Research Project,
Eindhoven University of Technology, The Netherlands.

Sauren, A.A.H.J., Kuijpers, W., Steenhoven, A.A. van and Veldpaus, F.E. (1980):
Aortic valve histology and its relation with mechanics-preliminary report.
J. Biomech. 13 (2), 97-104.

Schwerdt, H., Constantinesco, A. and Chambron, J. (1980):
Dynamic viscoelastic behaviour of the human tendon in vitro.
J. Biomech. 13, 913-922.

Sedov. L.J. (1972):
A course in continuum mechanics.
Ed. Wolters-Noordhoff Publishing, Groningen.

Silverman, M.E. and Schlant, R.E. (1970):
Functional anatomy of the cardiovascular system.
Chapter 3 in: The Heart, ed. Hurst, J.W. and Logue, R.B.; New York, McGraw-Hill.

Smith, R.B. and Taylor, J.M. (1971):
Vascularization of atrioventricular and semilunar valves in cattle, pigs and sheep.
Cardiovasc. Res. 5, 194-200.

Snyder, R.W. (1972):
Large deformation of isotropic biological tissue.
J. Biomech. 5, 601-606.

Soong, T.T. and Huang, W.N. (1973):
A stochastic model for biological tissue elasticity in simple elongation.
J. Biomech. 6, 451-458.

Steenhoven, A.A. van (1979):
The closing behaviour of the aortic valve.
Thesis Eindhoven University of Technology, Eindhoven, The Netherlands.

Steenhoven, A.A. van and Dongen, M.E.H. van (1979):
Model studies of the closing behaviour of the aortic valve.
J. Fluid Mech. 90 (1), 21-32.

Steenhoven, A.A. van , Liu, S.H. and Veenstra, P.C. (1979a):
Application of the natural aortic valve closing mechanism to the design of heart valve prostheses.
Proc. Eur. Soc. Artif. Organs 6, 263-267.

Steenhoven, A.A. van, Verlaan, C.W.J., Veenstra, P.C. and Reneman, R.S. (1981):
An in-vivo cinematographic analysis of the behaviour of the aortic valve.
Am. J. Physiol. 240, H286-H292.

Swanson, M.E. and Clark, R.E. (1973):
Aortic valve leaflet motion during systole.
Circ. Res. 23, 42-48.

Swanson, W.M. and Clark, R.E. (1974):
Dimensions and geometric relationships of the human aortic valve as a function of pressure.
Circ. Res. 35, 871-882.

Tanaka, T.T. and Fung, Y.C. (1974):
Elastic and inelastic properties of the canine aorta and their variation along the aortic tree.
J. Biomech. 7, 357-370.

Thubrikar, M., Harry, R. and Nolan, S.P. (1977):
Normal aortic valve function in dogs.
Am. J. Cardiol. 40, 563-568.

Thubrikar, M., Piepgrass, W.C., Deck, J.D. and Nolan, S.P. (1978):
Stresses of natural vs prosthetic aortic valve leaflets.
Proc. 31st ACEMB, Atlanta, Georgia, 34.7, 291.

Thubrikar, M., Piepgrass, W.C., Bosher, L.P. and Nolan, S.P. (1980):
The elastic modulus of canine aortic valve leaflets *in vivo* and *in vitro*.
Circ. Res. 47 (5), 792-800.

Trenkner, M., Raczyński, S. and Gutkowski, R. (1976):
Optimal diameter of the stent for aortic valvular grafts.
J. Thor. Cardiovasc. Surg. 72 (4), 613-617.

Veldpaus, F.E., Brekelmans, W.A.M., Schreurs, P.J.G. and Hulsen, M. (1980):
Geometrically nonlinear mechanics (Dutch).
PATO course material, Eindhoven University of Technology, The Netherlands.

Viidik, A. (1968):
A rheological model for uncalcified parallel-fibred collagenous tissue.
J. Biomech. 1, 3-11.

Wainwright, S.A., Biggs, W.D., Currey, J.D. and Gosline, J.M. (1976):
Mechanical design in organisms.
Edited by Arnold, E., London.

Wijn, P.F.F. (1980):
The alinear viscoelastic properties of human skin *in vivo* for small deformations.
Thesis University of Nijmegen, Nijmegen, The Netherlands.

Wilde, M. de (1981):
Een bijdrage tot de mechanische modelvorming van de aortaklep.
Report WE 81.04, Eindhoven University of Technology, The Netherlands.

Wismans, J.S.H.M. (1980):
A three-dimensional mathematical model of the human knee joint.
Thesis Eindhoven University of Technology, Eindhoven, The Netherlands.

Woo, S.L.-Y., Simon, B.R., Kuei, S.C. and Akeson, W.H. (1980):
Quasi-linear viscoelastic properties of normal articular cartilage.
J. Biomech. Engng 102, 85-90.

Wright, J.E.C. and Ng, Y.L. (1974):
Elasticity of human aortic valve cusps.
Cardiovasc. Res. 8, 384-390.

Yamada, H. (1970):
Strength of biological materials.
Baltimore, Williams and Wilkins, 110-111.

Zienkiewicz, O.C. (1977):
The finite element method.
Third edition. McGraw-Hill, London.

Zimmerman, J. (1969):
The functional and surgical anatomy of the aortic valve.
Am. J. Med. Sci. 5, 862-866.

samenvatting

Het in dit proefschrift beschreven onderzoek heeft tot doel het inzicht te vergroten in het mechanisch gedrag van de natuurlijke aortaklep. Met name de factoren, die de mechanische spanningstoestand in de klepvliezen bij gesloten klep bepalen, zijn onderzocht middels analyses met een speciaal daartoe ontwikkeld numeriek model. Bepalend bij de ontwikkeling van dit model waren de inzichten, verkregen uit histologisch onderzoek, alsmede experimenteel bepaalde gegevens met betrekking tot de mechanische weefseleigenschappen.

De weefselstructuur werd langs lichtmicroscopische weg onderzocht. De klepvliezen blijken een gelaagde structuur te bezitten welke globaal als volgt is opgebouwd: aan de aortazijde een laag dicht opeengepakte collageenbundels die voornamelijk in omtreksrichting verlopen, aan ventrikelzijde een netwerk van willekeurig georiënteerde elastinevezels welke lagen gescheiden worden door een losmazige structuur. De wand van de holte achter ieder vlies (de sinus van Valsalva) bestaat voornamelijk uit in omtreksrichting verlopende gladde spiervezels die zijn ingebed in elastine-weefsel zonder duidelijke vezeloriëntatie. De aortaring, een kraakbeenachtige structuur die rijk is aan collagene vezels, vormt de overgang tussen de vliezen en de sinusholten.

Middels *in vitro* experimenten werden de mechanische eigenschappen van strookjes uit de vliezen, de wanden van de sinusholten en het aangrenzende gedeelte van de aorta onderzocht. In één-assige trekproeven werden de strookjes met constante reksnelheid opgerekt en vervolgens op constante lengte gehouden. De aanzienlijke verschillen tussen de spannings-rek krommen voor vliesweefsel enerzijds en die voor sinus- en aortaweefsel anderzijds, zijn kwalitatief te verklaren op basis van de histologische verschillen tussen deze weefsels. De collageenbundels in de vliezen blijken een verstevigend effect te hebben en uitgesproken anisotropie te veroorzaken. Het weefsel van de sinus- en aortawanden is nagenoeg isotroop en vertoont een veel grotere compliantie dan het vliesweefsel. De spannings-rek krommen van de diverse klepweefsels zijn slechts in geringe mate gevoelig voor de reksnelheid. De spanningsrelaxatie, die in alle onderzochte

strookjes optrad, werd geanalyseerd met behulp van een wiskundig model. In de vliezen treedt meer spanningsrelaxatie op dan in de sinus- en aortawanden. Op het mathematisch model gebaseerde voorspellingen geven aan dat de visceuze verliezen bij cyclisch belasten in de vliezen groter zullen zijn dan in de sinus- en aortawanden.

In een numeriek model is de invloed van de bundelstructuur op het mechanisch gedrag van de vliezen bij gesloten klep bestudeerd. De bundels werden geschematiseerd als kabels terwijl de elastinelaag werd gerepresenteerd door membranen. Met en zonder bundels vallen de hoofdspanningsrichtingen in de membranen nagenoeg samen met de omtreks- en radiale richting. In de situatie zonder bundels treden de grootste hoofdspanningen op in omtreksrichting. Het effect van de bundels is tweeledig. Zij leiden de op de membraangedeelten werkende drukbelasting door naar de aortawand. Daarnaast bewerkstelligen zij een meer homogene spanningsverdeling in de membranen door de waarden van de maximale hoofdspanningen te reduceren tot het niveau van de minimale hoofdspanningen. De waarden van de minimale hoofdspanningen zijn in beide situaties, met en zonder bundels, nagenoeg gelijk. Bij aanwezigheid van de bundels zijn de schuifspanningen verwaarloosbaar klein omdat de spanningen in de hoofdrichtingen nagenoeg gelijk zijn.

nawoord

Zowel aan de uitvoering van het onderzoek als aan het samenstellen van dit proefschrift hebben velen bijgedragen. De gastvrijheid en de collegialiteit in de Vakgroep Technische Mechanica hebben in belangrijke mate bijgedragen aan de prettige sfeer waarin ik de afgelopen jaren kon werken. Met name aan Frans Veldpaus ben ik zeer veel dank verschuldigd voor de uitermate prettige en inspirerende samenwerking. In woord en daad heeft hij vele essentiële bijdragen geleverd, zowel aan het onderzoek als aan het samenstellen van dit proefschrift.

Velen droegen bij aan het experimentele gedeelte. In de eerste plaats bedank ik in dit verband Tini van Hout. In de ontwikkeling van de meetopstelling en in de uitvoering van de experimenten heeft hij een wezenlijk aandeel gehad. Voor de vervaardiging van talloze onderdelen van de opstelling droeg Frans v.d. Broek op nauwgezette wijze zorg. De vakkundigheid en behulpzaamheid van Jules IJzermans stonden er borg voor dat eventuele storingen in de opstelling snel werden verholpen en dat de benodigde randapparatuur altijd beschikbaar was. De uitvoering van de in dit proefschrift beschreven snelle trekproeven zou niet mogelijk zijn geweest zonder de inventiviteit en de spontane medewerking van Karel Koekkoek. De heren Van Loon en Paulussen zorgden ervoor dat het materiaal, waarmee proeven werden uitgevoerd, als het ware op afroep beschikbaar was. Jos Banens en Lambert van Beukering bedank ik voor hun hulp bij het geschikt maken van de meetgegevens voor de uiteindelijke verwerking. Dankzij Thijs Sluiter is er een wel zeer gebruikersvriendelijk programma voor de verwerking en de analyse van de meetgegevens tot stand gekomen.

Het geduld en de behulpzaamheid waarmee Dr. W. Kuijpers mij inwijdde in de beginselen van de histologie en de zorg die hij en zijn medewerkers besteedden aan de vervaardiging van de talloze preparaten, hebben de waardevolle bijdrage vanuit de histologie aan dit onderzoek mogelijk gemaakt. Dhr. J. van Dijck ben ik bijzondere dank verschuldigd, zowel voor het feit dat ik naar behoeven beslag mocht leggen op zijn microscopische en fotografische apparatuur alsook voor de zorg-

vuldigheid waarmee hij de in dit proefschrift opgenomen foto's heeft vervaardigd.

Anton van Steenhoven, Rob van Renterghem en Ed Rousseau waren fijne collega's wier steun, zowel bij de uitvoering van het onderzoek als bij het samenstellen van dit proefschrift, van groot belang was.

In het kader van een afstudeerwerk zijn aan dit onderzoek bijdragen geleverd door Jan Wuite, Frans Hoekstra, Toon Peerboom en Ed Rousseau. Maurits de Wilde ben ik zeer erkentelijk voor het extra werk dat hij verzette bij de berekeningen met het klepmodel. Huub Sluijsmans bedank ik voor de volharding waarmee hij werkte aan het oplossen van computerproblemen.

Ton Hamer, Willem Hupjé, Toon Manders, Hans Rensema en Harry Sonnemans werkten mee aan het tot stand komen van de figuren in het proefschrift. Els van Bommel ben ik veel dank verschuldigd voor de snelle en accurate wijze waarop zij het grootste gedeelte van het type-werk verzorgde. De spontane hulp van Mieke Barts, Ineke Borg en Meta Okken heb ik zeer op prijs gesteld. Wilhelmien en Anton van Steenhoven bedank ik voor de nauwgezetheid waarmee zij grote delen van de tekst van het proefschrift hebben gecorrigeerd. Ton Geeraedts ben ik zeer erkentelijk voor de moeite die hij besteedde aan de uiteindelijke vormgeving van dit proefschrift.

Levensbericht.

11-09-1951	Geboren te Kerkrade.
1969	Eindexamen Gymnasium-β, Gymnasium Rolduc te Kerkrade.
1969 - 1974	Studie aan de Technische Hogeschool Eindhoven, Afdeling der Werktuigbouwkunde.
1974 - 1976	Militaire dienst.
1976 - 1981	Wetenschappelijk ambtenaar aan de Technische Hogeschool Eindhoven, Afdeling der Werktuigbouwkunde, in het kader van het Interafdelingsproject Hartklepprothesen.

STELLINGEN

behorende bij het proefschrift

THE MECHANICAL BEHAVIOUR OF THE AORTIC VALVE

1. Het analyseren van aortaklepvliezen m.b.v. schalen-theorieën leidt voorspelbaar tot niet-realistische resultaten.

   Cataloglu, A., Gould, P.L. en Clark, R.E. [1975]: Validation of a simplified mathematical model for the stress analysis of human aortic heart valves. J. Biomech. 8, 347-348.
   Gould, P.L., Baldini, S.E., Rossow, M.P. en Clark, R.E. [1980]: Stress analysis of aortic valves. International Conference Proceedings on Finite Elements in Biomechanics 2, 583-604.

2. De glutaraldehyde-behandeling van vliesweefsel uit varkensaorta-kleppen, zoals toegepast bij de fabricage van bioprothesen, verandert de visceuze eigenschappen van het vliesweefsel. Het effect hiervan op de levensduur van bioprothesen dient nader onderzocht te worden.

3. De mogelijkheden van gepolariseerd licht bij het zichtbaar maken van vezelpatronen in dunne biologische structuren zijn onvoldoende onderzocht.

4. Decraemer e.a. [1980] gebruikt ten onrechte de term "steady state" met betrekking tot de respons van biologisch weefsel op een cyclisch belastingspatroon.

   Decraemer, W.F., Maes, M.A. en Vanhuyse, V.J. [1980]: An elastic stress-strain relation for soft biological tissues based on a structural model. J. Biomech. 13, 463-468.

5. Het ontbreken van een experimenteel onderbouwde mogelijkheid om spanningstoestanden in een biologische structuur onderling te vergelijken, vormt een belangrijke leemte bij biomechanica-onderzoek.

6. Het bij veel onderzoekers ontbreken van inzicht in het cyclisch gedrag van visco-elastische materialen, heeft geleid tot overdreven veel aandacht voor zogenaamde preconditioneringsprocedures voor biologische weefsels.

7. Veel onderzoeken op het terrein van de gewrichtskinematica tonen gebrek aan inzicht in de relatie tussen de wiskundige beschrijving en de experimentele bepaling van rotaties van starre lichamen.

8. Coördinaat-vrije formulering van o.a. mechanica-theorieën bevordert de overzichtelijkheid en is daardoor uitermate geschikt voor algemene beschouwingen.

9. Een onderzoeker op het gebied van de biomechanica anno 1981 moet niet-lineaire mechanicatheorieën kunnen toepassen en derhalve de snelle ontwikkelingen op dit gebied (kunnen) volgen.

10. Biomechanica is heel moeilijke technische mechanica.

11. Het dynamisch gedrag van een wegvoertuig wordt mede bepaald door niet-lineaire effecten. Desondanks kan een analyse op grond van lineaire stochastische technieken leiden tot praktisch bruikbare resultaten.

12. Het afronden van een onderzoek met een publicatie of een proefschrift doet in veel gevallen meer een beroep op het vermogen van de onderzoeker om alle tijd-limieten te halen dan op zijn onderzoek-kwaliteiten.

13. De wet van de "afnemende meeropbrengsten" geldt in ieder geval voor de rapportage van onderzoekresultaten.

Dit proefschrift, pag. 1-142.

19 juni 1981 A.A.H.J. Sauren